

Three Magnon Excitations in One Dimensional Quantum Spin Chains

by

Richard John Lee

A Thesis Submitted to the
Faculty of Graduate Studies
in Partial Fulfilment of the
Requirements for the Degree of

MASTER OF SCIENCE

Department of Physics
University of Manitoba
Winnipeg, Manitoba

©December 1992



National Library
of Canada

Bibliothèque nationale
du Canada

Acquisitions and
Bibliographic Services Branch

Direction des acquisitions et
des services bibliographiques

395 Wellington Street
Ottawa, Ontario
K1A 0N4

395, rue Wellington
Ottawa (Ontario)
K1A 0N4

Your file *Votre référence*

Our file *Notre référence*

The author has granted an irrevocable non-exclusive licence allowing the National Library of Canada to reproduce, loan, distribute or sell copies of his/her thesis by any means and in any form or format, making this thesis available to interested persons.

L'auteur a accordé une licence irrévocable et non exclusive permettant à la Bibliothèque nationale du Canada de reproduire, prêter, distribuer ou vendre des copies de sa thèse de quelque manière et sous quelque forme que ce soit pour mettre des exemplaires de cette thèse à la disposition des personnes intéressées.

The author retains ownership of the copyright in his/her thesis. Neither the thesis nor substantial extracts from it may be printed or otherwise reproduced without his/her permission.

L'auteur conserve la propriété du droit d'auteur qui protège sa thèse. Ni la thèse ni des extraits substantiels de celle-ci ne doivent être imprimés ou autrement reproduits sans son autorisation.

ISBN 0-315-81735-6

Canada

Name _____

Dissertation Abstracts International is arranged by broad, general subject categories. Please select the one subject which most nearly describes the content of your dissertation. Enter the corresponding four-digit code in the spaces provided.

3 Magnon Excitations

SUBJECT TERM

0611

U·M·I

SUBJECT CODE

Subject Categories

THE HUMANITIES AND SOCIAL SCIENCES

COMMUNICATIONS AND THE ARTS

Architecture 0729
 Art History 0377
 Cinema 0900
 Dance 0378
 Fine Arts 0357
 Information Science 0723
 Journalism 0391
 Library Science 0399
 Mass Communications 0708
 Music 0413
 Speech Communication 0459
 Theater 0465

EDUCATION

General 0515
 Administration 0514
 Adult and Continuing 0516
 Agricultural 0517
 Art 0273
 Bilingual and Multicultural 0282
 Business 0688
 Community College 0275
 Curriculum and Instruction 0727
 Early Childhood 0518
 Elementary 0524
 Finance 0277
 Guidance and Counseling 0519
 Health 0680
 Higher 0745
 History of 0520
 Home Economics 0278
 Industrial 0521
 Language and Literature 0279
 Mathematics 0280
 Music 0522
 Philosophy of 0998
 Physical 0523

Psychology 0525
 Reading 0535
 Religious 0527
 Sciences 0714
 Secondary 0533
 Social Sciences 0534
 Sociology of 0340
 Special 0529
 Teacher Training 0530
 Technology 0710
 Tests and Measurements 0288
 Vocational 0747

LANGUAGE, LITERATURE AND LINGUISTICS

Language
 General 0679
 Ancient 0289
 Linguistics 0290
 Modern 0291
 Literature
 General 0401
 Classical 0294
 Comparative 0295
 Medieval 0297
 Modern 0298
 African 0316
 American 0591
 Asian 0305
 Canadian (English) 0352
 Canadian (French) 0355
 English 0593
 Germanic 0311
 Latin American 0312
 Middle Eastern 0315
 Romance 0313
 Slavic and East European 0314

PHILOSOPHY, RELIGION AND THEOLOGY

Philosophy 0422
 Religion
 General 0318
 Biblical Studies 0321
 Clergy 0319
 History of 0320
 Philosophy of 0322
 Theology 0469

SOCIAL SCIENCES

American Studies 0323
 Anthropology
 Archaeology 0324
 Cultural 0326
 Physical 0327
 Business Administration
 General 0310
 Accounting 0272
 Banking 0770
 Management 0454
 Marketing 0338
 Canadian Studies 0385
 Economics
 General 0501
 Agricultural 0503
 Commerce-Business 0505
 Finance 0508
 History 0509
 Labor 0510
 Theory 0511
 Folklore 0358
 Geography 0366
 Gerontology 0351
 History
 General 0578

Ancient 0579
 Medieval 0581
 Modern 0582
 Black 0328
 African 0331
 Asia, Australia and Oceania 0332
 Canadian 0334
 European 0335
 Latin American 0336
 Middle Eastern 0333
 United States 0337
 History of Science 0585
 Law 0398
 Political Science
 General 0615
 International Law and Relations 0616
 Public Administration 0617
 Recreation 0814
 Social Work 0452
 Sociology
 General 0626
 Criminology and Penology 0627
 Demography 0938
 Ethnic and Racial Studies 0631
 Individual and Family Studies 0628
 Industrial and Labor Relations 0629
 Public and Social Welfare 0630
 Social Structure and Development 0700
 Theory and Methods 0344
 Transportation 0709
 Urban and Regional Planning 0999
 Women's Studies 0453

THE SCIENCES AND ENGINEERING

BIOLOGICAL SCIENCES

Agriculture
 General 0473
 Agronomy 0285
 Animal Culture and Nutrition 0475
 Animal Pathology 0476
 Food Science and Technology 0359
 Forestry and Wildlife 0478
 Plant Culture 0479
 Plant Pathology 0480
 Plant Physiology 0817
 Range Management 0777
 Wood Technology 0746
 Biology
 General 0306
 Anatomy 0287
 Biostatistics 0308
 Botany 0309
 Cell 0379
 Ecology 0329
 Entomology 0353
 Genetics 0369
 Limnology 0793
 Microbiology 0410
 Molecular 0307
 Neuroscience 0317
 Oceanography 0416
 Physiology 0433
 Radiation 0821
 Veterinary Science 0778
 Zoology 0472
 Biophysics
 General 0786
 Medical 0760

Geodesy 0370
 Geology 0372
 Geophysics 0373
 Hydrology 0388
 Mineralogy 0411
 Paleobotany 0345
 Paleocology 0426
 Paleontology 0418
 Paleozoology 0985
 Palynology 0427
 Physical Geography 0368
 Physical Oceanography 0415

HEALTH AND ENVIRONMENTAL SCIENCES

Environmental Sciences 0768
 Health Sciences
 General 0566
 Audiology 0300
 Chemotherapy 0992
 Dentistry 0567
 Education 0350
 Hospital Management 0769
 Human Development 0758
 Immunology 0982
 Medicine and Surgery 0564
 Mental Health 0347
 Nursing 0569
 Nutrition 0570
 Obstetrics and Gynecology 0380
 Occupational Health and Therapy 0354
 Ophthalmology 0381
 Pathology 0571
 Pharmacology 0419
 Pharmacy 0572
 Physical Therapy 0382
 Public Health 0573
 Radiology 0574
 Recreation 0575

Speech Pathology 0460
 Toxicology 0383
 Home Economics 0386

PHYSICAL SCIENCES

Pure Sciences

Chemistry
 General 0485
 Agricultural 0749
 Analytical 0486
 Biochemistry 0487
 Inorganic 0488
 Nuclear 0738
 Organic 0490
 Pharmaceutical 0491
 Physical 0494
 Polymer 0495
 Radiation 0754
 Mathematics 0405
 Physics
 General 0605
 Acoustics 0986
 Astronomy and Astrophysics 0606
 Atmospheric Science 0608
 Atomic 0748
 Electronics and Electricity 0607
 Elementary Particles and High Energy 0798
 Fluid and Plasma 0759
 Molecular 0609
 Nuclear 0610
 Optics 0752
 Radiation 0756
 Solid State 0611
 Statistics 0463

Applied Sciences

Applied Mechanics 0346
 Computer Science 0984

Engineering
 General 0537
 Aerospace 0538
 Agricultural 0539
 Automotive 0540
 Biomedical 0541
 Chemical 0542
 Civil 0543
 Electronics and Electrical 0544
 Heat and Thermodynamics 0348
 Hydraulic 0545
 Industrial 0546
 Marine 0547
 Materials Science 0794
 Mechanical 0548
 Metallurgy 0743
 Mining 0551
 Nuclear 0552
 Packaging 0549
 Petroleum 0765
 Sanitary and Municipal System Science 0554
 System Science 0790
 Geotechnology 0428
 Operations Research 0796
 Plastics Technology 0795
 Textile Technology 0994

PSYCHOLOGY

General 0621
 Behavioral 0384
 Clinical 0622
 Developmental 0620
 Experimental 0623
 Industrial 0624
 Personality 0625
 Physiological 0989
 Psychobiology 0349
 Psychometrics 0632
 Social 0451



Nom _____

Dissertation Abstracts International est organisé en catégories de sujets. Veuillez s.v.p. choisir le sujet qui décrit le mieux votre thèse et inscrivez le code numérique approprié dans l'espace réservé ci-dessous.



SUJET

CODE DE SUJET

Catégories par sujets

HUMANITÉS ET SCIENCES SOCIALES

COMMUNICATIONS ET LES ARTS

Architecture	0729
Beaux-arts	0357
Bibliothéconomie	0399
Cinéma	0900
Communication verbale	0459
Communications	0708
Danse	0378
Histoire de l'art	0377
Journalisme	0391
Musique	0413
Sciences de l'information	0723
Théâtre	0465

ÉDUCATION

Généralités	515
Administration	0514
Art	0273
Collèges communautaires	0275
Commerce	0688
Économie domestique	0278
Éducation permanente	0516
Éducation préscolaire	0518
Éducation sanitaire	0680
Enseignement agricole	0517
Enseignement bilingue et multiculturel	0282
Enseignement industriel	0521
Enseignement primaire	0524
Enseignement professionnel	0747
Enseignement religieux	0527
Enseignement secondaire	0533
Enseignement spécial	0529
Enseignement supérieur	0745
Évaluation	0288
Finances	0277
Formation des enseignants	0530
Histoire de l'éducation	0520
Langues et littérature	0279

Lecture	0535
Mathématiques	0280
Musique	0522
Orientalisation et consultation	0519
Philosophie de l'éducation	0998
Physique	0523
Programmes d'études et enseignement	0727
Psychologie	0525
Sciences	0714
Sciences sociales	0534
Sociologie de l'éducation	0340
Technologie	0710

LANGUE, LITTÉRATURE ET LINGUISTIQUE

Langues	
Généralités	0679
Anciennes	0289
Linguistique	0290
Modernes	0291
Littérature	
Généralités	0401
Anciennes	0294
Comparée	0295
Médiévale	0297
Moderne	0298
Africaine	0316
Américaine	0591
Anglaise	0593
Asiatique	0305
Canadienne (Anglaise)	0352
Canadienne (Française)	0355
Germanique	0311
Latino-américaine	0312
Moyen-orientale	0315
Romane	0313
Slave et est-européenne	0314

PHILOSOPHIE, RELIGION ET THÉOLOGIE

Philosophie	0422
Religion	
Généralités	0318
Clergé	0319
Études bibliques	0321
Histoire des religions	0320
Philosophie de la religion	0322
Théologie	0469

SCIENCES SOCIALES

Anthropologie	
Archéologie	0324
Culturelle	0326
Physique	0327
Droit	0398
Économie	
Généralités	0501
Commerce-Affaires	0505
Économie agricole	0503
Économie du travail	0510
Finances	0508
Histoire	0509
Théorie	0511
Études américaines	0323
Études canadiennes	0385
Études féministes	0453
Folklore	0358
Géographie	0366
Gérontologie	0351
Gestion des affaires	
Généralités	0310
Administration	0454
Banques	0770
Comptabilité	0272
Marketing	0338
Histoire	
Histoire générale	0578

Ancienne	0579
Médiévale	0581
Moderne	0582
Histoire des noirs	0328
Africaine	0331
Canadienne	0334
États-Unis	0337
Européenne	0335
Moyen-orientale	0333
Latino-américaine	0336
Asie, Australie et Océanie	0332
Histoire des sciences	0585
Loisirs	0814
Planification urbaine et régionale	0999
Science politique	
Généralités	0615
Administration publique	0617
Droit et relations internationales	0616
Sociologie	
Généralités	0626
Aide et bien-être social	0630
Criminologie et établissements pénitentiaires	0627
Démographie	0938
Études de l'individu et de la famille	0628
Études des relations interethniques et des relations raciales	0631
Structure et développement social	0700
Théorie et méthodes	0344
Travail et relations industrielles	0629
Transports	0709
Travail social	0452

SCIENCES ET INGÉNIERIE

SCIENCES BIOLOGIQUES

Agriculture	
Généralités	0473
Agronomie	0285
Alimentation et technologie alimentaire	0359
Culture	0479
Élevage et alimentation	0475
Exploitation des pâturages	0777
Pathologie animale	0476
Pathologie végétale	0480
Physiologie végétale	0817
Sylviculture et taune	0478
Technologie du bois	0746
Biologie	
Généralités	0306
Anatomie	0287
Biologie (Statistiques)	0308
Biologie moléculaire	0307
Botanique	0309
Cellule	0379
Écologie	0329
Entomologie	0353
Génétique	0369
Limnologie	0793
Microbiologie	0410
Neurologie	0317
Océanographie	0416
Physiologie	0433
Radiation	0821
Science vétérinaire	0778
Zoologie	0472
Biophysique	
Généralités	0786
Médicale	0760

Géologie	0372
Géophysique	0373
Hydrologie	0388
Minéralogie	0411
Océanographie physique	0415
Paléobotanique	0345
Paléocologie	0426
Paléontologie	0418
Paléozoologie	0985
Palynologie	0427

SCIENCES DE LA SANTÉ ET DE L'ENVIRONNEMENT

Économie domestique	0386
Sciences de l'environnement	0768
Sciences de la santé	
Généralités	0566
Administration des hôpitaux	0769
Alimentation et nutrition	0570
Audiologie	0300
Chimiothérapie	0992
Dentisterie	0567
Développement humain	0758
Enseignement	0350
Immunologie	0982
Loisirs	0575
Médecine du travail et thérapie	0354
Médecine et chirurgie	0564
Obstétrique et gynécologie	0380
Ophtalmologie	0381
Orthophonie	0460
Pathologie	0571
Pharmacie	0572
Pharmacologie	0419
Physiothérapie	0382
Radiologie	0574
Santé mentale	0347
Santé publique	0573
Soins infirmiers	0569
Toxicologie	0383

SCIENCES PHYSIQUES

Sciences Pures	
Chimie	
Généralités	0485
Biochimie	487
Chimie agricole	0749
Chimie analytique	0486
Chimie minérale	0488
Chimie nucléaire	0738
Chimie organique	0490
Chimie pharmaceutique	0491
Physique	0494
Polymères	0495
Radiation	0754
Mathématiques	0405
Physique	
Généralités	0605
Acoustique	0986
Astronomie et astrophysique	0606
Électromagnétique et électricité	0607
Fluides et plasma	0759
Météorologie	0608
Optique	0752
Particules (Physique nucléaire)	0798
Physique atomique	0748
Physique de l'état solide	0611
Physique moléculaire	0609
Physique nucléaire	0610
Radiation	0756
Statistiques	0463

Sciences Appliquées Et Technologie

Informatique	0984
Ingénierie	
Généralités	0537
Agricole	0539
Automobile	0540

Biomédicale	0541
Chaleur et thermodynamique	0348
Conditionnement (Emballage)	0549
Génie aérospatial	0538
Génie chimique	0542
Génie civil	0543
Génie électronique et électrique	0544
Génie industriel	0546
Génie mécanique	0548
Génie nucléaire	0552
Ingénierie des systèmes	0790
Mécanique navale	0547
Métallurgie	0743
Science des matériaux	0794
Technique du pétrole	0765
Technique minière	0551
Techniques sanitaires et municipales	0554
Technologie hydraulique	0545
Mécanique appliquée	0346
Géotechnologie	0428
Matériaux plastiques (Technologie)	0795
Recherche opérationnelle	0796
Textiles et tissus (Technologie)	0794

PSYCHOLOGIE

Généralités	0621
Personnalité	0625
Psychobiologie	0349
Psychologie clinique	0622
Psychologie du comportement	0384
Psychologie du développement	0620
Psychologie expérimentale	0623
Psychologie industrielle	0624
Psychologie physiologique	0989
Psychologie sociale	0451
Psychométrie	0632



THREE MAGNON EXCITATIONS IN ONE DIMENSIONAL
QUANTUM SPIN CHAINS

BY

RICHARD JOHN LEE

A Thesis submitted to the Faculty of Graduate Studies of the University of Manitoba in partial fulfillment of the requirements of the degree of

MASTER OF SCIENCE

(c) 1993

Permission has been granted to the LIBRARY OF THE UNIVERSITY OF MANITOBA to lend or sell copies of this Thesis, to the NATIONAL LIBRARY OF CANADA to microfilm this Thesis and to lend or sell copies of the film, and UNIVERSITY MICROFILM to publish an abstract of this Thesis.

The author reserves other publication rights, and neither the Thesis nor extensive extracts from it may be printed or otherwise reproduced without the author's written permission.

Abstract

The three magnon excitation spectra of a one dimensional chain of quantum spins is analysed using the recursion method. A number of different integrable models are studied as well as a number of Hamiltonians “close” to the integrable model of L. A. Takhtajan [10] and H. M. Babujian [11]. The bound states are studied across the entire Brillouin zone and complete agreement is found with the known integrable results as well as support for a conjecture put forward by F. D. M. Haldane [12, 13].

Acknowledgements

I wish to express my sincerest thanks to Dr. B. W. Southern for his guidance, kindness and particularly his patience in supervising this research and through the endless revisions of my thesis.

Contents

Abstract	i
Acknowledgements	ii
1 Introduction	1
2 Magnetic Excitations	12
2.1 One-Magnon Excitations	12
2.2 Two-Magnon Excitations	15
3 Three-Magnon Excitations	28
3.1 Formalism and Equations	29
3.2 Three Magnon Continuum	36
3.3 Bound States and Integrable Models	41
4 The Recursion Method	46
4.1 Green's Function	46
4.2 Recursion	50
4.3 Termination of the Continued Fraction	52
4.3.1 Constant Coefficients	52
4.3.2 Oscillating Coefficients	57
4.4 Spin 1/2	63

5	Non-Integrable Models	75
5.1	Spin 1	79
5.2	Spin 3/2	90
6	Summary	103
	Appendix: Three Magnon Excitation Equations	106
	Bibliography	117

List of Figures

Fig. 2.1:	One Magnon Excitation Energy	14
Fig. 2.2:	Semi-Infinite Mass-Spring Chain With Defects	20
Fig. 2.3:	Dispersion Diagram for 2-magnon, $S = \frac{3}{2}$, Integrable Model	22
Fig. 2.4:	Dispersion Diagram for 2-magnon, $S = 1$, Parkinson Model	24
Fig. 2.5:	Dispersion Diagram for 2-magnon, $S = \frac{3}{2}$, Heisenberg Model	25
Fig. 2.6:	Dispersion Diagram for 2-magnon, $S \geq 1$, Lai-Sutherland Model	26
Fig. 3.1:	Graphical Representation of 3-magnon Hamiltonian	33
Fig. 3.2:	3-Free Continuum	37
Fig. 3.3:	2-Bound, 1-Free Continuum	39
Fig. 3.4:	Hamiltonian for 3-magnon, Lai-Sutherland Model	41
Fig. 3.5:	Hamiltonian for 3-magnon, $S = 1$, Temperley-Lieb Model	42
Fig. 3.6:	Hamiltonian for 3-magnon, $S = \frac{3}{2}$, Temperley-Lieb Model	43
Fig. 3.7:	Dispersion Diagram for 3-magnon, $S = \frac{3}{2}$, Temperley-Lieb Model	45
Fig. 4.1:	$\text{Re}(G)$ for an Infinite Chain With Single Magnon Excitations	54
Fig. 4.2:	$\text{Im}(G)$ for an Infinite Chain With Single Magnon Excitations	55
Fig. 4.3:	$\text{Re}(G)$ of Square Root Terminator	56
Fig. 4.4:	$\text{Im}(G)$ of Square Root Terminator	57
Fig. 4.5:	$\text{Re}(G)$ for Alternating Coefficients	60
Fig. 4.6:	$\text{Im}(G)$ for Alternating Coefficients	61
Fig. 4.7:	Hamiltonian for the Unphysical $S = 1$ States	63
Fig. 4.8:	Single Precision, $S = \frac{1}{2}$, a_i Coefficients	65

Fig. 4.9:	Double Precision, $S = \frac{1}{2}$, a_i Coefficients	66
Fig. 4.10:	Quadruple Precision, $S = \frac{1}{2}$, a_i Coefficients	67
Fig. 4.11:	Phase Space Relation for the Double Precision Coefficient Pairs	73
Fig. 5.1:	Dispersion Diagram for 3-magnon, $S = 1$, Integrable Model .	77
Fig. 5.2:	Dispersion Diagram for 3-magnon, $S = \frac{3}{2}$, Integrable Model .	78
Fig. 5.3:	$\text{Im}(G)$ for 3-magnon, $S = 1$, Heisenberg Model at $K = 0$. . .	80
Fig. 5.4:	$\text{Im}(G)$ for 3-magnon, $S = 1$, Heisenberg Model at $K = \frac{\pi}{4a}$. .	81
Fig. 5.5:	$\text{Im}(G)$ of a Bound State for 3-magnon, $S = 1$, Heisenberg Model at $K = \frac{\pi}{4a}$	81
Fig. 5.6:	$\text{Im}(G)$ for 3-magnon, $S = 1$, Heisenberg Model at $K = \frac{\pi}{2a}$. .	82
Fig. 5.7:	$\text{Im}(G)$ of a Bound State for 3-magnon, $S = 1$, Heisenberg Model at $K = \frac{\pi}{2a}$	82
Fig. 5.8:	$\text{Im}(G)$ for 3-magnon, $S = 1$, Heisenberg Model at $K = \frac{3\pi}{4a}$. .	82
Fig. 5.9:	$\text{Im}(G)$ of a Bound State for 3-magnon, $S = 1$, Heisenberg Model at $K = \frac{3\pi}{4a}$	82
Fig. 5.10:	$\text{Im}(G)$ for 3-magnon, $S = 1$, Heisenberg Model at $K = \frac{\pi}{a}$. . .	83
Fig. 5.11:	$\text{Im}(G)$ of the Bound States for 3-magnon, $S = 1$, Heisenberg Model at $K = \frac{\pi}{a}$	83
Fig. 5.12:	Double Precision Coefficients for $S = 1$ Heisenberg Model at $K = \frac{\pi}{a}$	84
Fig. 5.13:	Double Precision Coefficients for $S = 1$ Heisenberg Model at $K = \frac{3\pi}{4a}$	85
Fig. 5.14:	Double Precision Coefficients for $S = 1$ Heisenberg Model at $K = \frac{\pi}{2a}$	85
Fig. 5.15:	Double Precision Coefficients for $S = 1$ Heisenberg Model at $K = \frac{\pi}{4a}$	86
Fig. 5.16:	Dispersion Diagram for 3-magnon, $S = 1$, Heisenberg Model .	87
Fig. 5.17:	Dispersion Diagram for 3-magnon, $S = 1$, $g_2 = 2.25$	88

Fig. 5.18:	Dispersion Diagram for 3-magnon, $S = 1, g_2 = 4.5$ 89
Fig. 5.19:	Dispersion Diagram for 3-magnon, $S = \frac{3}{2}, g_2 = 1, g_3 = 5.5$ 91
Fig. 5.20:	Dispersion Diagram for 3-magnon, $S = \frac{3}{2}, g_2 = 5, g_3 = 5.5$ 92
Fig. 5.21:	Dispersion Diagram for 3-magnon, $S = \frac{3}{2}, g_2 = 2.5, g_3 = 1$ 95
Fig. 5.22:	Dispersion Diagram for 3-magnon, $S = \frac{3}{2}, g_2 = 2.5, g_3 = 11$ 96
Fig. 5.23:	Dispersion Diagram for 3-magnon, $S = \frac{3}{2}$, Heisenberg Model 97
Fig. 5.24:	Im(G) for 3-magnon, $S = \frac{3}{2}$, Heisenberg Model at $K = \frac{\pi}{a}$ and Using a Symmetric Initial Ket 98
Fig. 5.25:	Im(G) for 3-magnon, $S = \frac{3}{2}$, Heisenberg Model at $K = \frac{\pi}{a}$ and Using an Arbitrary Initial Ket 99
Fig. 5.26:	Dispersion Diagram for 3-magnon, $S = \frac{3}{2}, g_2 = 5, g_3 = 11$ 100
Fig. 5.27:	Dispersion Diagram for 3-magnon, $S = \frac{3}{2}, g_2 = 1, g_3 = 11$ 101
Fig. 5.28:	Dispersion Diagram for 3-magnon, $S = \frac{3}{2}, g_2 = 5, g_3 = 1$ 102

Chapter 1

Introduction

During the last century great strides have been made in our understanding of nature and magnetism has not been an exception. Once associated with mysticism and the occult, it is now understood as some of the residual effects of the electromagnetic interaction. Due to the constraints of the Pauli principle for the electrons of atoms in a lattice, the wavefunction of a collection of atoms is more than the superposition of single particle wavefunctions. Since the total wavefunction must be antisymmetric under particle exchange for fermions, a symmetric spin wavefunction and an antisymmetric spin wavefunction are associated with different spatial wavefunctions. In general, these wavefunctions will have different energies. This energy difference for the case of two hydrogen-like atoms can be characterized by the Hamiltonian,

$$\widehat{\mathcal{H}}_{12} = -J\tilde{\mathcal{S}}_1 \cdot \tilde{\mathcal{S}}_2 \quad (1.1)$$

where $\tilde{\mathcal{S}}_i$ is a three component quantum spin operator and J is known as the exchange integral. When $J > 0$ parallel alignment of the spins is favoured (ferromagnetism) and $J < 0$ favours anti-parallel alignment (anti-ferromagnetism).

A Hamiltonian with the form above but extended to include all interactions between all pairs in a lattice, was described in detail by Heisenberg in 1928 [1].

$$\widehat{\mathcal{H}} = - \sum_{ij} J_{ij} (\tilde{\mathcal{S}}_i \cdot \tilde{\mathcal{S}}_j) \quad (1.2)$$

This Hamiltonian was proposed as a model for strongly magnetic phenomenon (ferromagnetism, anti-ferromagnetism and ferrimagnetism) and a number of assumptions were made to construct the simplest model that still exhibits the most significant characteristics of these magnetic materials. For example, it was known that the macroscopic magnetic moments that are observed in these types of materials were due primarily to the magnetic moments of the electrons and that the magnetic moment due to the orbital motion can be ignored. As only changes in energy due to magnetic degrees of freedom are significant for strong magnetic effects, the contribution from factors such as the direct Coulomb force and the spin-orbit or spin-spin interactions can be ignored [2].

The exchange interaction itself, $\tilde{\mathcal{S}}_i \cdot \tilde{\mathcal{S}}_j$, is due to the Coulomb interaction but, as shown by PAM Dirac (1929) [6], it is strictly a quantum mechanical effect. The exchange interaction arises from the form the lattice wavefunction must have due to interchange of particles on different sites (ie. the Pauli principle) and although there is a direct interaction between electrons, the symmetry properties of the wavefunction result in a spin dependent exchange term. The magnitude of the exchange interaction will be influenced by the amount of overlap of the electronic wavefunctions.

It is also possible to obtain the Heisenberg Hamiltonian by performing a perturbation on a lattice of non-interacting spins, using the Coulomb potential as the perturbation. If higher order perturbations are considered, the Hamiltonian can be written as a linear combination of powers of the pair exchange operator, $\tilde{\mathcal{S}}_i \cdot \tilde{\mathcal{S}}_j$, giving

$$\hat{\mathcal{H}} = - \sum_{ij} \sum_{n=1}^{2S} J_{ij}^{(n)} (\tilde{\mathcal{S}}_i \cdot \tilde{\mathcal{S}}_j)^n \quad (1.3)$$

The range of interactions will depend upon the details of the particular solid and in this thesis only insulators are considered. We will only consider the exchange

integral ($J_{ij}^{(n)}$) to be non-zero for those sites, i and j , which are within a small, arbitrarily chosen, region of each other. The simplest choice is nearest neighbours. The lattice will be restricted further by only considering a one dimensional lattice with identical spins on each site and uniform nearest neighbour interactions. The Hamiltonian can be expressed as

$$\widehat{\mathcal{H}} = - \sum_i \sum_{n=1}^{2S} J^{(n)} (\tilde{\mathcal{S}}_i \cdot \tilde{\mathcal{S}}_{i+1})^n \quad (1.4)$$

The $n = 0$ term is omitted as it can be absorbed into the zero of energy.

A more general form for the Hamiltonian can be considered by taking into account such factors as anisotropic spin exchange (ie. replacing $\tilde{\mathcal{S}}_i \cdot \tilde{\mathcal{S}}_j$ by $\alpha \mathcal{S}_i^x \mathcal{S}_j^x + \beta \mathcal{S}_i^y \mathcal{S}_j^y + \gamma \mathcal{S}_i^z \mathcal{S}_j^z$, $\alpha \neq \beta \neq \gamma$) or single ion effects (ie. adding term of the form $\alpha \sum_i (\mathcal{S}_i^z)^2$), but these will not be considered here. However, the extensions necessary to account for these effects could be integrated into our formalism without serious difficulty.

Since the system under consideration consists of a linear chain of N ($N \rightarrow \infty$) quantum spins with periodic boundary conditions, we have the following commutation relation

$$[\widehat{\mathcal{T}}_a, \widehat{\mathcal{H}}] = 0 \quad (1.5)$$

where $\widehat{\mathcal{T}}_a$ is the discrete translation operator over intervals equal to the lattice spacing, a . The Hamiltonian (1.4) also has the properties

$$[\tilde{\mathcal{S}}^2, \widehat{\mathcal{H}}] = 0 \quad (1.6)$$

$$[\mathcal{S}^z, \widehat{\mathcal{H}}] = 0 \quad (1.7)$$

where (1.6) follows from the fact that the total spin operator can be expressed as

$$\begin{aligned}\tilde{S}^2 &= \left(\sum_{i=1}^N \tilde{S}_i \right)^2 \\ &= \sum_i \tilde{S}_i^2 + \sum_i \tilde{S}_i \cdot \tilde{S}_{i+1} + \sum_{j \neq i, i+1} \tilde{S}_i \cdot \tilde{S}_j\end{aligned}\quad (1.8)$$

and

$$\left[(\tilde{S}_i \cdot \tilde{S}_j + \tilde{S}_{i+1} \cdot \tilde{S}_j), (\tilde{S}_i \cdot \tilde{S}_{i+1}) \right] = 0 \quad (1.9)$$

The term, $\sum_i \tilde{S}_i^2$, is a constant and the term, $\sum_i \tilde{S}_i \cdot \tilde{S}_{i+1}$, is identical to the exchange operator in $\widehat{\mathcal{H}}$, therefore both of these commute with the Hamiltonian. Similarly, (1.7) follows from the identity

$$\left[(\mathcal{S}_i^z + \mathcal{S}_{i+1}^z), (\tilde{S}_i \cdot \tilde{S}_{i+1}) \right] = 0 \quad (1.10)$$

A convenient and complete orthonormal set of states which describes the Hamiltonian is given by the simultaneous eigenkets of \tilde{S}_i^2 and \mathcal{S}_i^z . These states are represented, in the Dirac bra-ket notation, as $|S, m\rangle_i$, where

$$\tilde{S}_i^2 |S, m\rangle_i = \hbar^2 S(S+1) |S, m\rangle_i \quad (1.11)$$

$$\mathcal{S}_i^z |S, m\rangle_i = \hbar m |S, m\rangle_i \quad (1.12)$$

for the i^{th} site. For convenience, the units for all subsequent equations are chosen such that $\hbar \equiv 1$. The Hamiltonian can be rewritten in terms of the usual ladder operators, $\mathcal{S}_i^\pm = \mathcal{S}_i^x \pm i\mathcal{S}_i^y$ which have the properties

$$\mathcal{S}_i^+ |S, m\rangle_i = \sqrt{S(S+1) - m(m+1)} |S, m+1\rangle_i \quad (1.13)$$

$$\mathcal{S}_i^- |S, m\rangle_i = \sqrt{S(S+1) - m(m-1)} |S, m-1\rangle_i \quad (1.14)$$

$$\begin{aligned}
[\mathcal{S}_i^+, \mathcal{S}_j^-] &= 2\mathcal{S}_j^z \delta_{ij} \\
[\mathcal{S}_i^z, \mathcal{S}_j^\pm] &= \pm \mathcal{S}_j^\pm \delta_{ij}
\end{aligned}
\tag{1.15}$$

Equations (1.13) and (1.14) have the property that the z -component of a spin can only be raised or lowered $2S$ times from its minimum or maximum value.

$$\mathcal{S}_i^- |S, -S\rangle_i = 0 \tag{1.16}$$

$$\mathcal{S}_i^+ |S, S\rangle_i = 0 \tag{1.17}$$

In terms of these operators, the Hamiltonian becomes

$$\widehat{\mathcal{H}} = - \sum_i \sum_{n=1}^{2S} J^{(n)} \left[\frac{1}{2} (\mathcal{S}_i^+ \mathcal{S}_{i+1}^- + \mathcal{S}_i^- \mathcal{S}_{i+1}^+) + \mathcal{S}_i^z \mathcal{S}_{i+1}^z \right]^n \tag{1.18}$$

The vanishing commutators in (1.5)-(1.7) are a result of the symmetries of $\widehat{\mathcal{H}}$. Therefore the eigenstates of $\widehat{\mathcal{H}}$ can be labelled by quantum numbers corresponding to these symmetries. These are the eigenvalues of the translation operator ($\widehat{\mathcal{T}}_a$), total angular momentum ($\widehat{\mathcal{S}}^2$) and the total z -component angular momentum (\mathcal{S}^z). The state of maximum total S has the spin aligned along some arbitrary direction. If we take this direction to be the $-z$ axis, then, an exact eigenstate of $\widehat{\mathcal{H}}$ can be constructed by taking a direct product of these single spin basis states.

$$|0\rangle = |S, -S\rangle_1 |S, -S\rangle_2 |S, -S\rangle_3 \cdots |S, -S\rangle_N \tag{1.19}$$

where the 0 is a collective index. This is clearly an eigenstate of $\widehat{\mathcal{H}}$ as can be shown from (1.16) and (1.17). The state given above, (1.19), has an extremum in the eigenvalue of the \mathcal{S}^z operator and is known as the ferromagnetic state. In the Heisenberg model ($n = 1$) and when $J > 0$ this is also the ground state but for the more general Hamiltonian(1.4) this may not be true depending on the values of $J^{(n)}$. The models which we consider are restricted to those for which $|0\rangle$ is the

ground state.

The Hamiltonian is rotationally invariant in the absence of an external magnetic field. A very weak magnetic field can be assumed in the $-z$ direction, say, to remove the rotational degeneracy and hence define a single unique ground state. The ground state energy per site is given by $E_0 = -\sum_{n=1}^{2S} J^{(n)} S^{2n}$. The Hamiltonian(1.4) can be written as a sum of pair Hamiltonians

$$\widehat{\mathcal{H}}_l = -\sum_{n=1}^{2S} J^{(n)} \tilde{\mathcal{P}}_l^n \quad (1.20)$$

where

$$\begin{aligned} \tilde{\mathcal{P}}_l &= \tilde{\mathcal{S}}_l \cdot \tilde{\mathcal{S}}_{l+1} \\ &= \frac{1}{2} (\mathcal{S}_l^+ \mathcal{S}_{l+1}^- + \mathcal{S}_l^- \mathcal{S}_{l+1}^+) + \mathcal{S}_l^z \mathcal{S}_{l+1}^z \end{aligned} \quad (1.21)$$

A convenient choice of variables to describe the Hamiltonian is defined as follows:

$$\lambda_j = -\sum_{n=1}^{2S} J^{(n)} \left[\frac{j(j+1)}{2} - S(S+1) \right]^n, \quad j = 0, 1, 2, \dots, 2S \quad (1.22)$$

The λ_j are the eigenvalues of each pair Hamiltonian and j is the total angular momentum quantum number of the pair. Differences between these eigenvalues and the ground state eigenvalue λ_{2S} are defined by

$$\alpha_m(S) = \lambda_{2S-m} - \lambda_{2S}, \quad m \in \{1, 2, 3, \dots, 2S\} \quad (1.23)$$

and the corresponding ratios of these differences are denoted by

$$g_m(S) = \frac{\alpha_m(S)}{\alpha_1(S)} \quad (1.24)$$

The quantities, $\alpha_m(S)$, represent the energy difference when the total spin quantum

number of a pair is decreased by m . The ferromagnetic state, (1.19), is stable provided all $\alpha_m(S) \geq 0$.

We now consider excitations of this system. These can be labelled by the eigenvalues of the total S_z operator, \mathcal{S}^z , of the system. The smallest change in \mathcal{S}^z for this system occurs when the z -component of a single spin on the lattice, j say, is raised by one quantum. This state is represented by

$$|j\rangle = \frac{1}{\sqrt{2S}} \mathcal{S}_j^+ |0\rangle \quad (1.25)$$

where $\frac{1}{\sqrt{2S}}$ is a normalization factor. The $\{|j\rangle\}$ form a complete orthonormal set of single deviation, excitation states or the $m = 1$ states. Unfortunately, these states are not eigenstates of the Hamiltonian. A new basis can be constructed by taking the following linear combinations of $|j\rangle$.

$$|k\rangle = \sum_j \frac{e^{ikr_j}}{\sqrt{N}} |j\rangle, \quad r_j = ja \quad (1.26)$$

where k is a wavevector defined by $k = \frac{2\pi n}{Na}$, $n = -\frac{N}{2}, -\frac{N}{2}+1, \dots, \frac{N}{2}$. By applying the Hamiltonian to these states, it can be shown that these are eigenstates of $\widehat{\mathcal{H}}$ with energy eigenvalues $E(k) = NE_0 + \alpha_1(1 - \cos ka)$. These $m = 1$ eigenstates have real wavevectors and are known as magnons. In the semi-classical limit, when the spins can be treated as classical vectors, the solutions can also be interpreted as waves propagating through the lattice of spins, hence they are also known as spin waves. Since the Hamiltonian is simply a mathematical model for magnetic materials and many approximations have been made in its construction, it is possible that these eigenstates are simply mathematical artifacts and not present in real materials. However, magnons have been observed using such methods as infra-red absorption and neutron scattering. As well they may be observed indirectly by microwave

absorption. As examples, magnons have been observed by Hoogenbeets et. al. [4] as well as by Haines and Drumheller [5] for a $S = \frac{1}{2}$ nearly Heisenberg quasi-one dimensional compound $(C_8H_{11}NH_3)CuCl_3$. Further, magnon bound states have been observed by Torrance and Tinkham in $CoCl_2 \cdot 2H_2O$ [3] which is a $S = \frac{1}{2}$ quasi-one dimensional compound but is more closely approximated by an Ising model. Although the thermodynamics of the observed magnons do not completely agree with theory (which would not be expected from such a simple model) the fit is empirically accurate.

For other subspaces corresponding to $m > 1$, we have more than one magnon present and the solution to the Schrödinger equation is not nearly so simple or straightforward. In fact, a general solution for a general class of Hamiltonians, with an arbitrary number of magnons has yet to be found. There are, however, some notable exceptions: a set of models which are grouped together because of the form of the solution rather than the form of their Hamiltonians. These specific Hamiltonians are generally known as integrable models and they can be solved exactly with their solutions represented in closed form using the Bethe Ansatz [7].

The Bethe Ansatz was a method which H. Bethe introduced in 1931 to solve the m magnon system for the $S = \frac{1}{2}$ Heisenberg Hamiltonian. The Hamiltonian has a sufficient number of symmetry properties, and hence conserved quantities, to completely define the system. For the case of an infinite linear chain, there must be an infinite number of these symmetries. Some of these are global and familiar, such as the total momentum, K , but most are far from obvious. In the special Hamiltonians where this property is found, it is possible to find a set of eigenstates which are simultaneous eigenstates of all the conserved quantities and completely diagonalize the Hamiltonian. These are the integrable models and the Bethe Ansatz uses one of the Hamiltonian's symmetries, permutation symmetry, to generate a set of states which are such simultaneous eigenstates. The solutions of the integrable models belong to two classifications: scattering state solutions and

bound state solutions. The scattering state solutions are associated with a real wavevectors whereas the bound state solutions are states where all the magnons are bound together as a single entity and are associated with complex wavevectors. These solutions and their properties will be described in more detail in Chapter 2.

A relatively well known integrable model is the Sutherland-Lai model [15] which corresponds to $g_m = \frac{1 - (-1)^m}{2}$. This model includes the $S = \frac{1}{2}$ Heisenberg model, which was considered by Bethe, but generalizes the permutation symmetry to general S . As will be shown in Chapters 2 and 3, the effect of the Hamiltonian on a complete set of states can be represented using a small number of these α_m or g_m . Other examples of integrable models are the Parkinson model [8] and is also known as the Temperley-Lieb model [9]. The Temperley-Lieb model has all $\alpha_m = 0$ except one. The integrable Hamiltonian which has received considerable attention is that found by Takhtajan [10] and Babujian [11], using a method known as the quantum inverse scattering method. In this method, the magnons are treated as a scattering problem where there are incoming beams which interact and the scattered beam is studied to try and reconstruct the scattering potential. These models can be characterized by special values of the g_m . Specifically, $g_m = 2S [\psi(2S + 1) - \psi(2S + 1 - m)]$, where $\psi(x) = \frac{\partial}{\partial x} \{\ln [\Gamma(x)]\}$ and $\Gamma(x)$ is the usual gamma function.

It has been observed by Haldane [12, 13] that for these integrable models, the excitations have some special features. For example, the solution to the m magnon problem has a single bound state branch which is real and continuous across the minimum of m or $2S$ Brillouin zones when using the extended zone representation for the total wavevector K . Here m is the number of magnons under consideration and S is the total spin on each site. In the reduced zone representation, which is the form we will use, the bound state has several branches which exactly meet at the Brillouin zone boundaries and are completely decoupled from a continuum of scattering states. Haldane conjectured that the non-integrable models will have gaps at these boundaries and the bound states will couple to the continua. This

conjecture has been verified for the case of two magnon excitations by Southern et. al. [14].

In the next chapter the current situation of known results for elementary excitations will be discussed. Specifically the one and two magnon cases will be discussed in detail. For one and two magnon excitations, the problem can be solved exactly, for all dimensions, regardless of whether the Hamiltonian is integrable or not. For $m > 2$ excitations, this is no longer true and it will be necessary to use a different method to solve such a system. Some of the possible methods of solution are the Bethe Ansatz or the Quantum Inverse Scattering Method as mentioned above but these can only be used when the Hamiltonian is integrable. It is also possible to solve the problem by using methods based on transfer matrix methods or real space rescaling techniques or by simply applying sheer computational power to diagonalize the Hamiltonian. However, there is a method which can provide considerable information about the system and is more computationally convenient. This method is known as the Recursion Method. This approach was introduced by R. Haydock [16] for electronic problems and does not present the solution in closed form (which is not possible for the non-integrable models), but rather it is a procedure to reduce the Hamiltonian to a tridiagonal form which can then be used to easily calculate other quantities of interest. Since a matrix representation of the Hamiltonian is used, the generated tridiagonal matrix is closely linked to the basis used in the generation of the Hamiltonian. The manipulation of the Hamiltonian to simplify the use of this method will be treated in Chapter 3 and an explanation of how the method is applied will be given in Chapter 4 as well as some difficulties which are associated with the method and their solutions. The results from this method when used on the lattices with different values of S and with different Hamiltonians will be presented in Chapter 5. Finally, a summary and conclusions are given in Chapter 6. The literature on a three magnon system is sparse but, where possible, the results are compared to previously calculated results as well as

the exact results for the appropriate integrable cases.

Chapter 2

Magnetic Excitations

In this chapter, the solutions for the one and two magnon ferromagnetic excitations will be described in detail since the initial formalism necessary for the three magnon excitations (treated in Chapter 3) follows a similar procedure.

2.1 One-Magnon Excitations

The normalized single spin deviation states are

$$|i\rangle = \frac{1}{\sqrt{2S}} S_i^+ |0\rangle, \quad i = 1, 2, 3, \dots, N \quad (2.1)$$

The effect of the operator, $\tilde{\mathcal{P}}_l$, on $|i\rangle$ is given by

$$\begin{aligned} \tilde{\mathcal{P}}_l |i\rangle &= S^2 |i\rangle, & i \neq l, l+1 \\ \tilde{\mathcal{P}}_l |l\rangle &= S(S-1)|l\rangle + S|l+1\rangle \\ \tilde{\mathcal{P}}_l |l+1\rangle &= S|l\rangle + S(S-1)|l+1\rangle \end{aligned} \quad (2.2)$$

The non-diagonal equations from the set (2.2) can also be expressed in matrix form

$$\tilde{\mathcal{P}}_l \begin{bmatrix} |l\rangle \\ |l+1\rangle \end{bmatrix} = \begin{bmatrix} S(S-1) & S \\ S & S(S-1) \end{bmatrix} \begin{bmatrix} |l\rangle \\ |l+1\rangle \end{bmatrix} \quad (2.3)$$

and hence

$$\begin{aligned}\tilde{\mathcal{P}}_l^n \begin{bmatrix} |l\rangle \\ |l+1\rangle \end{bmatrix} &= S^n \begin{bmatrix} S-1 & 1 \\ 1 & S-1 \end{bmatrix}^n \begin{bmatrix} |l\rangle \\ |l+1\rangle \end{bmatrix} \\ &= \frac{S^n}{2} \begin{bmatrix} S^n + (S-2)^n & S^n - (S-2)^n \\ S^n - (S-2)^n & S^n + (S-2)^n \end{bmatrix} \begin{bmatrix} |l\rangle \\ |l+1\rangle \end{bmatrix}\end{aligned}\quad (2.4)$$

From (1.20) and (1.23) we obtain

$$\widehat{\mathcal{H}}_l |i\rangle = \begin{cases} E_0 |i\rangle & , i \neq l, l+1 \\ E_0 |l\rangle + \frac{\alpha_1(S)}{2} |l\rangle - \frac{\alpha_1(S)}{2} |l+1\rangle & , i = l \\ E_0 |l\rangle + \frac{\alpha_1(S)}{2} |l\rangle - \frac{\alpha_1(S)}{2} |l-1\rangle & , i = l+1 \end{cases}\quad (2.5)$$

Therefore,

$$\widehat{\mathcal{H}} |i\rangle = NE_0 |i\rangle + \alpha_1(S) |i\rangle - \frac{\alpha_1(S)}{2} |i+1\rangle - \frac{\alpha_1(S)}{2} |i-1\rangle\quad (2.6)$$

The equation (2.6) has a tight binding form and can be mapped directly to other tight binding systems, such as mass-spring systems, by taking an infinite one dimensional chain of masses and springs with $NE_0 + \alpha_1$ as related to the “mass” and $\frac{\alpha_1}{2}$ as the “spring constant”. The solution to this system of equations can be found by taking linear combinations of the $|j\rangle$

$$|k\rangle = \frac{1}{\sqrt{N}} \sum_j e^{i(jka)} |j\rangle\quad (2.7)$$

where k is the total wavevector and is restricted to the values $-\frac{\pi}{a} < k \leq \frac{\pi}{a}$. The Hamiltonian, when applied to this set of states, gives

$$\begin{aligned}\widehat{\mathcal{H}} |k\rangle &= NE_0 |k\rangle + \frac{1}{2} \sum_j \alpha_1(S) e^{i(jka)} (2|j\rangle - |j-1\rangle - |j+1\rangle) \\ &= NE_0 |k\rangle + \alpha_1(S) (1 - \cos ka) |k\rangle\end{aligned}\quad (2.8)$$

Hence the $\{|k\rangle\}$ diagonalizes $\widehat{\mathcal{H}}$ and the dispersion relation can be found

$$\begin{aligned} E(k) &= \langle k | \widehat{\mathcal{H}} | k \rangle \\ &= NE_0 + \alpha_1(S)(1 - \cos ka) \end{aligned} \quad (2.9)$$

The one-magnon excitation energy $E_1(k) = \alpha_1(S)(1 - \cos ka)$ is plotted in Fig. 2.1.

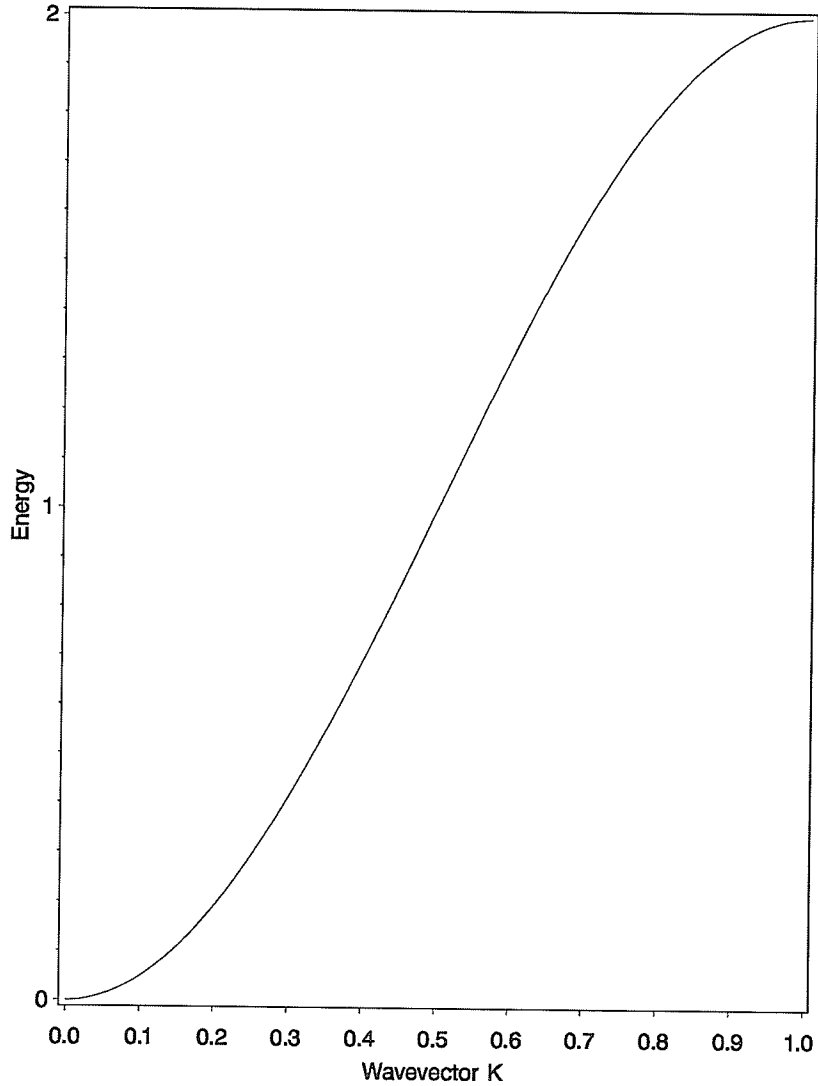


Figure 2.1: One magnon excitation energy. The wavevector is in units of $\frac{\pi}{a}$ and the energy is in units of α_1 .

The solutions to the $m = 1$ magnon excitations are characterized by real wavevectors and correspond to the extended modes for a mass-spring system. Note that the solution is independent of the choice of $J^{(n)}$ except for changes in the value of α_1 . The form of the solution is a direct consequence of translational invariance. The analogue of this behaviour in a mass-spring system is that the extended modes are essentially independent of the size of the masses and the strength of the springs (as long as they are all uniform). A restriction which must be applied to the magnon solutions is $\alpha_1 \geq 0$, to keep the solutions stable.

2.2 Two-Magnon Excitations

An orthonormal set of two spin deviation states can be defined as

$$\begin{aligned} |i, j\rangle &= \frac{1}{2S} \mathcal{S}_i^+ \mathcal{S}_j^+ |0\rangle, \quad i \neq j \\ |i, i\rangle &= \frac{1}{2\sqrt{S(2S-1)}} \mathcal{S}_i^+ \mathcal{S}_i^+ |0\rangle \end{aligned} \quad (2.10)$$

where the labels i and j are taken such that $i \leq j$. Following a similar approach to that used for the one magnon excitations, the effect of the operator, $\tilde{\mathcal{P}}_l = \tilde{\mathcal{S}}_l \cdot \tilde{\mathcal{S}}_{l+1}$, on the given set of states yields

$$\tilde{\mathcal{P}}_l |i, j\rangle = S^2 |i, j\rangle, \quad i \neq l, l+1; j \neq l, l+1 \quad (2.11)$$

$$\tilde{\mathcal{P}}_l |i, i\rangle = S^2 |i, i\rangle, \quad i \neq l \quad (2.12)$$

$$\tilde{\mathcal{P}}_l |l, i\rangle = S |l+1, i\rangle + S(S-1) |l, i\rangle, \quad i \neq l, l+1 \quad (2.13)$$

$$\tilde{\mathcal{P}}_l |l+1, i\rangle = S |l, i\rangle + S(S-1) |l+1, i\rangle, \quad i \neq l, l+1 \quad (2.14)$$

$$\tilde{\mathcal{P}}_l |l, l+1\rangle = \sqrt{S(2S-1)} (|l, l\rangle + |l+1, l+1\rangle) + (1-S)^2 |l, l+1\rangle \quad (2.15)$$

$$\tilde{\mathcal{P}}_l |l, l\rangle = \sqrt{S(2S-1)} |l, l+1\rangle + S(S-2) |l, l\rangle \quad (2.16)$$

The $\tilde{\mathcal{P}}_l$ operator is symmetric, therefore

$$\tilde{\mathcal{P}}_l |i, l\rangle = S(S-1)|i, l\rangle + S|i, l+1\rangle, \quad i \neq l, l+1 \quad (2.17)$$

$$\tilde{\mathcal{P}}_l |i, l+1\rangle = S|i, l\rangle + S(S-1)|i, l+1\rangle, \quad i \neq l, l+1 \quad (2.18)$$

The non-diagonal equations, (2.13) – (2.16), can be written in matrix form as follows

$$\tilde{\mathcal{P}}_l \begin{pmatrix} |l, i\rangle \\ |l+1, i\rangle \\ |l, l\rangle \\ |l, l+1\rangle \\ |l+1, l+1\rangle \end{pmatrix} = \begin{bmatrix} S(S-1) & S & 0 & 0 & 0 \\ S & S(S-1) & 0 & 0 & 0 \\ 0 & 0 & S(S-2) & \sqrt{S(2S-1)} & 0 \\ 0 & 0 & \sqrt{S(2S-1)} & S(S-2)+1 & \sqrt{S(2S-1)} \\ 0 & 0 & 0 & \sqrt{S(2S-1)} & S(S-2) \end{bmatrix} \begin{pmatrix} |l, i\rangle \\ |l+1, i\rangle \\ |l, l\rangle \\ |l, l+1\rangle \\ |l+1, l+1\rangle \end{pmatrix} \quad (2.19)$$

This matrix is block diagonal so to find $\tilde{\mathcal{P}}_l^n$ it is sufficient to find the n^{th} power of

$$A = S \begin{bmatrix} S-1 & 1 \\ 1 & S-1 \end{bmatrix} \quad (2.20)$$

and

$$B = \sqrt{S(2S-1)} \begin{bmatrix} \frac{S(S-2)}{\sqrt{S(2S-1)}} & 1 & 0 \\ 1 & \frac{S(S-2)+1}{\sqrt{S(2S-1)}} & 1 \\ 0 & 1 & \frac{S(S-2)}{\sqrt{S(2S-1)}} \end{bmatrix} \quad (2.21)$$

The matrix, A , is identical to the matrix given in (2.3) for a one magnon excitation. Therefore, A^n has the same form as the matrix in (2.4). B^n can be expressed as

$$B^n = \frac{1}{2(4S-1)} \begin{bmatrix} \varphi + \psi & \rho & \varphi - \psi \\ \rho & 2\varphi + \frac{\rho}{\sqrt{S(2S-1)}} & \rho \\ \varphi - \psi & \rho & \varphi + \psi \end{bmatrix} \quad (2.22)$$

where

$$\varphi = S^{2n}(2S-1) + 2S(S^2 - 4S + 1)^n \quad (2.23)$$

$$\psi = S^n(4S-1)(S-2)^n \quad (2.24)$$

$$\rho = 2\sqrt{S(2S-1)} [S^{2n} - (S^2 - 4S + 1)^n] \quad (2.25)$$

Then, the effect of the pair Hamiltonian, $\widehat{\mathcal{H}}_l$, on the two magnon basis states is given by

$$i < j-1, \quad \widehat{\mathcal{H}}_l |i, j\rangle = \begin{cases} E_0 |i, j\rangle, & i \neq l, l+1; j \neq l, l+1 \\ E_0 |i, j\rangle + \frac{\alpha_1(S)}{2} |i, j\rangle - \frac{\alpha_1(S)}{2} |i-1, j\rangle, & i = l+1 \\ E_0 |i, j\rangle + \frac{\alpha_1(S)}{2} |i, j\rangle - \frac{\alpha_1(S)}{2} |i+1, j\rangle, & i = l \\ E_0 |i, j\rangle + \frac{\alpha_1(S)}{2} |i, j\rangle - \frac{\alpha_1(S)}{2} |i, j-1\rangle, & j = l+1 \\ E_0 |i, j\rangle + \frac{\alpha_1(S)}{2} |i, j\rangle - \frac{\alpha_1(S)}{2} |i, j+1\rangle, & j = l \end{cases} \quad (2.26)$$

$$\widehat{\mathcal{H}}_l |i, i+1\rangle = \begin{cases} E_0 |i, i+1\rangle & , i \neq l-1, l, l+1 \\ E_0 |i, i+1\rangle + \frac{\alpha_1(S)}{2} |i, i+1\rangle - \frac{\alpha_1(S)}{2} |i, i+2\rangle & , i = l-1 \\ E_0 |i, i+1\rangle + \frac{2S-1}{4S-1} \alpha_2(S) |i, i+1\rangle - \frac{\sqrt{S(2S-1)}}{4S-1} \alpha_2(S) |i, i\rangle \\ \quad - \frac{\sqrt{S(2S-1)}}{4S-1} \alpha_2(S) |i+1, i+1\rangle & , i = l \\ E_0 |i, i+1\rangle + \frac{\alpha_1(S)}{2} |i, i+1\rangle - \frac{\alpha_1(S)}{2} |i-1, i+1\rangle & , i = l+1 \end{cases} \quad (2.27)$$

$$\widehat{\mathcal{H}}_l |i, i\rangle = \begin{cases} E_0 |i, i\rangle & , i \neq l, l+1 \\ E_0 |i, i\rangle + \frac{1}{2} \left[\alpha_1(S) + \frac{2S\alpha_2(S)}{4S-1} \right] |i, i\rangle - \frac{\sqrt{S(2S-1)}}{4S-1} \alpha_2(S) |i, i+1\rangle \\ \quad - \frac{1}{2} \left[\alpha_1(S) - \frac{2S\alpha_2(S)}{4S-1} \right] |i+1, i+1\rangle & , i = l \\ E_0 |i, i\rangle + \frac{1}{2} \left[\alpha_1(S) + \frac{2S\alpha_2(S)}{4S-1} \right] |i, i\rangle - \frac{\sqrt{S(2S-1)}}{4S-1} \alpha_2(S) |i-1, i\rangle \\ \quad - \frac{1}{2} \left[\alpha_1(S) - \frac{2S\alpha_2(S)}{4S-1} \right] |i-1, i-1\rangle & , i = l+1 \end{cases} \quad (2.28)$$

Each state has two indices which label the sites with spins flipped. Since the Hamiltonian only depends upon the relative position of the spin flips, we will use the centre of mass, $\left(\frac{i+j}{2}\right)$, and relative coordinate $r = j - i$. In addition, Bloch's theorem allows us to perform a Fourier transform with respect to the centre of mass coordinate as follows

$$|K; r\rangle = \frac{1}{\sqrt{N}} \sum_{j=1}^N e^{-Kai(j-\frac{r}{2})} |j-r, j\rangle \quad (2.29)$$

where K is the total wavevector and

$$|i, j\rangle = \frac{1}{\sqrt{N}} \sum_{\{K\}} e^{Kai(j-\frac{r}{2})} |K; r\rangle \quad (2.30)$$

The effect of the Hamiltonian on $\{|K; r\rangle\}$ is given by

$$\begin{aligned}\widehat{\mathcal{H}}|K; r\rangle &= NE_0|K; r\rangle + 2\alpha_1(S)|K; r\rangle - \alpha_1(S)\cos\left(\frac{Ka}{2}\right)|K; r-1\rangle \\ &\quad - \alpha_1(S)\cos\left(\frac{Ka}{2}\right)|K; r+1\rangle, \quad r \neq 0, 1\end{aligned}\quad (2.31)$$

$$\begin{aligned}\widehat{\mathcal{H}}|K; 1\rangle &= NE_0|K; 1\rangle + \left[\alpha_1(S) + \frac{(2S-1)\alpha_2(S)}{4S-1}\right]|K; 1\rangle - \\ &\quad \frac{2\sqrt{S(2S-1)}}{4S-1}\alpha_2(S)\cos\left(\frac{Ka}{2}\right)|K; 0\rangle - \\ &\quad \alpha_1(S)\cos\left(\frac{Ka}{2}\right)|K; 2\rangle\end{aligned}\quad (2.32)$$

$$\begin{aligned}\widehat{\mathcal{H}}|K; 0\rangle &= NE_0|K; 0\rangle + \left[\alpha_1(S)(1 - \cos Ka) + \frac{2S\alpha_2(S)}{4S-1}(1 + \cos Ka)\right]|K; 0\rangle \\ &\quad - \frac{2\sqrt{S(2S-1)}}{4S-1}\alpha_2(S)\cos\left(\frac{Ka}{2}\right)|K; 1\rangle\end{aligned}\quad (2.33)$$

For each value of K these equations are equivalent to a one dimensional, semi-infinite, tight-binding form and can be mapped to the equations for any other problem with similar characteristics. Specifically, the equations of motion for a semi-infinite linear chain of masses and springs has this form. However, the equations for a uniform mass-spring chain has the form given in (2.6). By including defects in the chain, a direct analogy can be made to the $m = 2$ spin equations, (2.31) – (2.33). Consider a mass-spring system with defects as given below (Fig. 2.2).

system the minimum and maximum of the continuum is given by

$$E_{min}(K) = 2\alpha_1(S) \left[1 - \cos\left(\frac{Ka}{2}\right) \right] \quad (2.40)$$

$$E_{max}(K) = 2\alpha_1(S) \left[1 + \cos\left(\frac{Ka}{2}\right) \right] \quad (2.41)$$

The other 2-magnon equations, (2.32) and (2.33), describe interactions between the two magnons and are responsible for the bound state solutions, or the localized modes in a mass-spring chain. The true bound states, ie. the solutions which lie outside the scattering state continuum, can be obtained as the solution of the following cubic equation ([14])

$$\begin{aligned} & \left[\frac{(2S-1)g_2}{4S-1} - 1 \right] [E(K) + 2\alpha_1]^3 - \\ & \left\{ \left[\frac{(2S-1)g_2}{4S-1} - 1 \right]^2 + \left[\frac{4S(2S-1)g_2^2}{(4S-1)^2} - 4g_2 + 5 \right] \cos^2 \left[\frac{Ka}{2} \right] \right\} [E(K) + 2\alpha_1]^2 \\ & - 4 \left\{ \left[\frac{2Sg_2^2 - (8S-1)g_2}{4S-1} + 2 \right] \cos^4 \left[\frac{Ka}{2} \right] + [g_2 - 1] \left[\frac{(2S-1)g_2}{4S-1} - 1 \right] \cos^2 \left[\frac{Ka}{2} \right] \right\} [E(K) + 2\alpha_1] \\ & - 4 \left[(g_2 - 1)^2 + \left(\frac{2Sg_2}{4S-1} - 1 \right)^2 \cos^2 \left(\frac{Ka}{2} \right) \right] \cos^4 \left(\frac{Ka}{2} \right) \\ & = 0 \end{aligned} \quad (2.42)$$

When a bound state enters a scattering state continuum, it interacts with the continuum to produce a resonance.

For a one magnon excitation, much of the variation which is possible on the Hamiltonian does not affect the solution since the excitation energy only depends on $\alpha_1(S)$ hence, the solutions for integrable and non-integrable models are qualitatively the same. However, for the two magnon excitations, there is a noticeable difference between the integrable and non-integrable models. The primary integrable model of interest for this system is the Hamiltonian due to Takhtajan and Babujian or when $\alpha_2 = \frac{4S-1}{2S-1}\alpha_1$. This model has two bound state branches which lie completely outside the scattering state continuum and meet exactly at the Brillouin zone boundary.

An example of this case for $S = \frac{3}{2}$ is shown Fig. 2.3. Due to the limitations on the maximum size of the graphs and the proximity of the lower bound state branch to the minimum edge of the scattering state continuum, the lower branch is not visible in the diagram (Fig. 2.3).

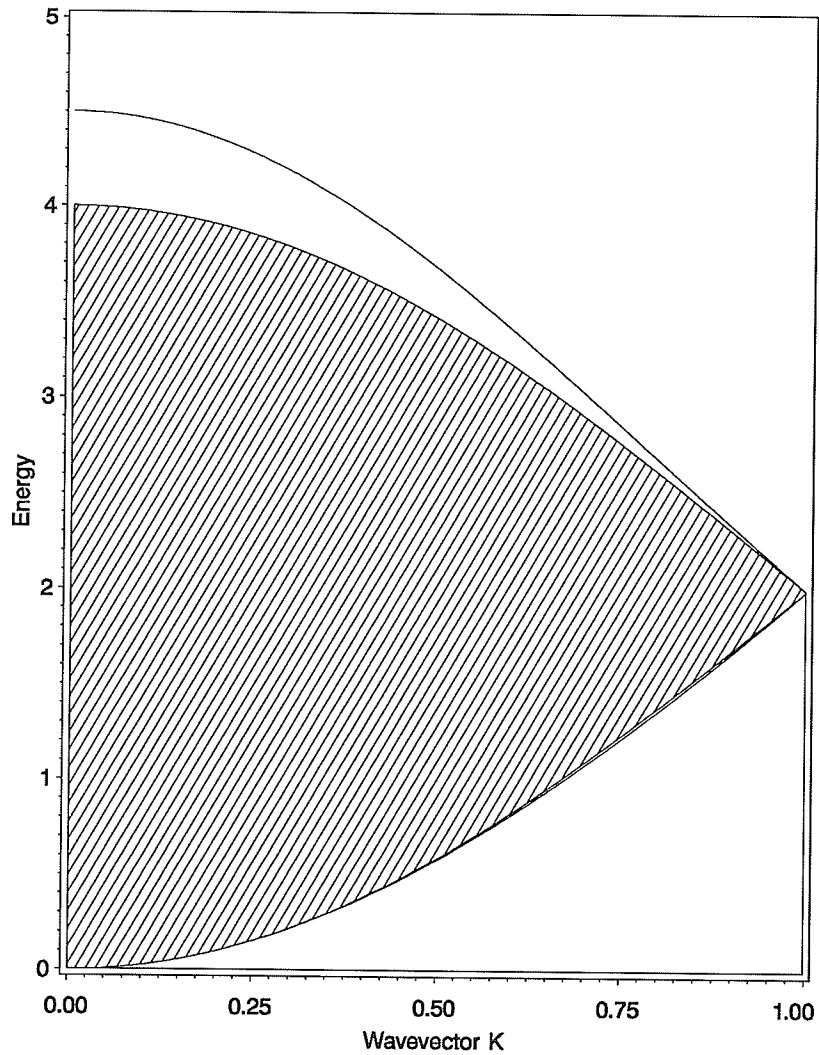


Figure 2.3: Two magnon bound state branches (solid line) and scattering state continuum (shaded region) for $S = \frac{3}{2}$ Integrable model. Wavevector in units of $\frac{\pi}{a}$ and energy in units of α_1

The two bound state branches can be described by the curves (See [14].)

$$E = \frac{2\alpha_1}{4S^2 - 1} \left\{ \left[4S^2 + \cos^2 \left(\frac{Ka}{2} \right) - 1 \right] \pm 2S \cos \left(\frac{Ka}{2} \right) \sqrt{4S^2 + \cos^2 \left(\frac{Ka}{2} \right) - 1} \right\} \quad (2.43)$$

The special integrable model identified by Parkinson has only the α_{2S} non-zero so for $S = \frac{3}{2}$, the two magnon equations reduce to simply the constant NE_0 term. When $S = 1$, $\alpha_1 = 0$ and $\alpha_2 \neq 0$. This can be viewed as removing all the springs with spring constant k from the mass-spring chain, Fig. 2.2. The equations, (2.31) – (2.33), now give exactly two solutions

$$E(K) = 0 \quad (2.44)$$

$$E(K) = \frac{\alpha_2}{4S - 1} \left[4S - 1 + \left(4 \cos^2 \frac{Ka}{2} \right) \right] \quad (2.45)$$

These are plotted in Fig. 2.4 (below)

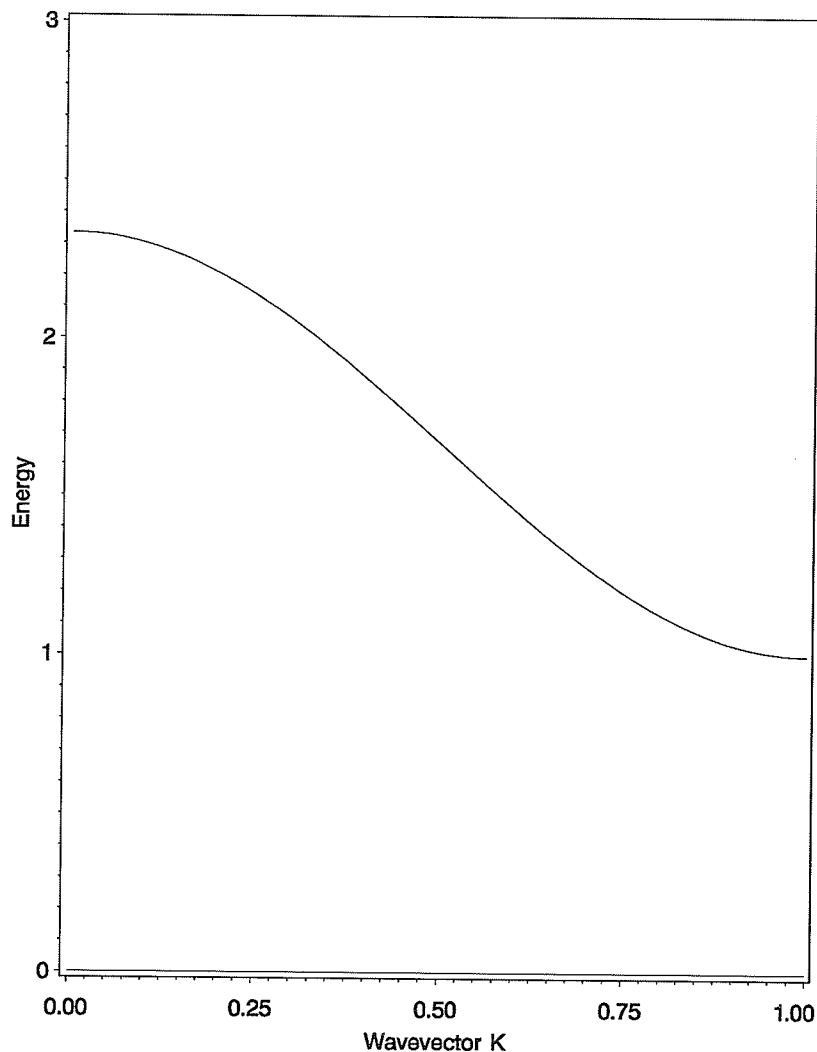


Figure 2.4: Parkinson model of two magnon excitations for $S = 1$. Wavevector in units of $\frac{\pi}{a}$ and energy in units of α_2 .

For $S = \frac{1}{2}$, $\alpha_2 = 0$ and this is equivalent to $g_2 = 0$. This case is discussed later along with the Lai-Sutherland model, which also is characterized by this value of g_2 . For now, a small digression will be made to describe what occurs when the Hamiltonian deviates from integrability.

As α_2 deviates from the integrable value, $\left(\frac{4S-1}{2S-1}\alpha_1\right)$, the bound state branches no longer meet at the Brillouin zone boundary, forming a gap. This gap increases as $\left|\frac{4S-1}{2S-1}\alpha_1 - \alpha_2\right|$ increases. When $\alpha_2 < 2\alpha_1 \forall S$ the upper branch moves entirely

within the continuum and only the lower branch remains. The Heisenberg model, Fig. 2.5, is such an example.

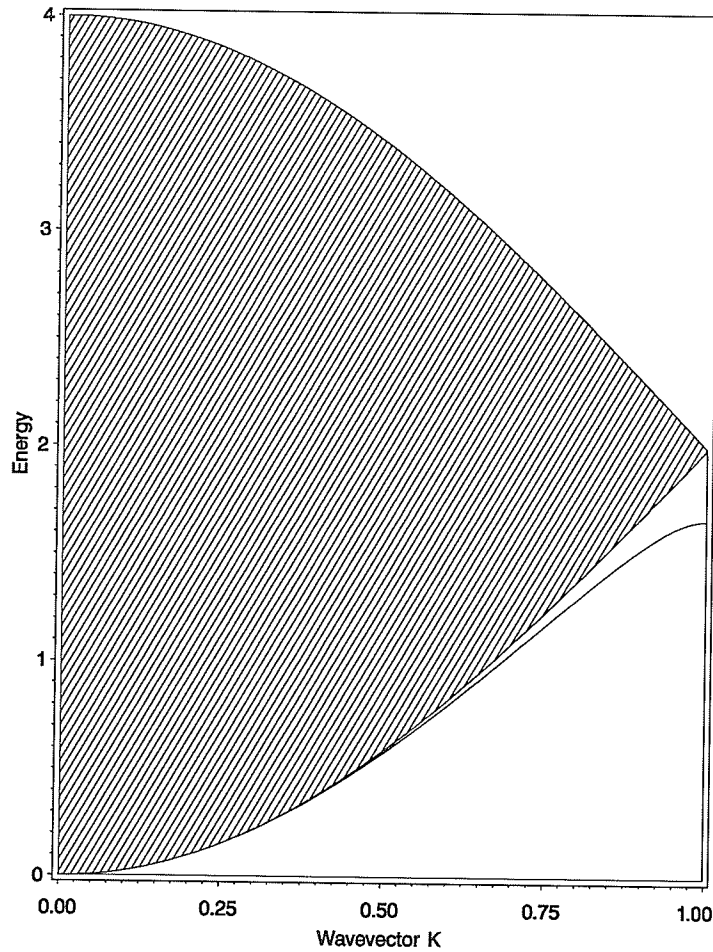


Figure 2.5: Two magnon bound state (solid line) and continuum (shaded region) for $S = \frac{3}{2}$ Heisenberg model. Energy in units of α_1 .

When $\alpha_2 > \frac{4S-1}{2S-1}$, it is the lower branch which moves into the continuum eventually leaving only the upper branch.

Returning to the discussion of the special integrable models, (the Parkinson, $S = \frac{1}{2}$ and the Lai-Sutherland models) recall that these models have $g_2 = 0$. Referring back to Fig. 2.2, this is equivalent to removing the first spring (the k' spring). The solutions now consist of two parts, one solution corresponding to the main part

of the chain (to the right) and the solution for the site at the left. The solution for the right half is similar to the general case of the two magnon excitations when $g_2 < 2$, except that there is no resonance from the upper branch and the lower branch is the only bound state solution. But, if $S \geq 1$ (When $S = 1$ the model is equivalent to the Lai-Sutherland model) the $|K; 0\rangle$ state (or the solitary mass at the very left of the chain) is not physically forbidden. (This site corresponds to two magnons on the same lattice site.) The solution is given by $E(K) = \alpha_1(1 - \cos Ka)$. Both of these bound state energy curves have been plotted in Fig. 2.6, below

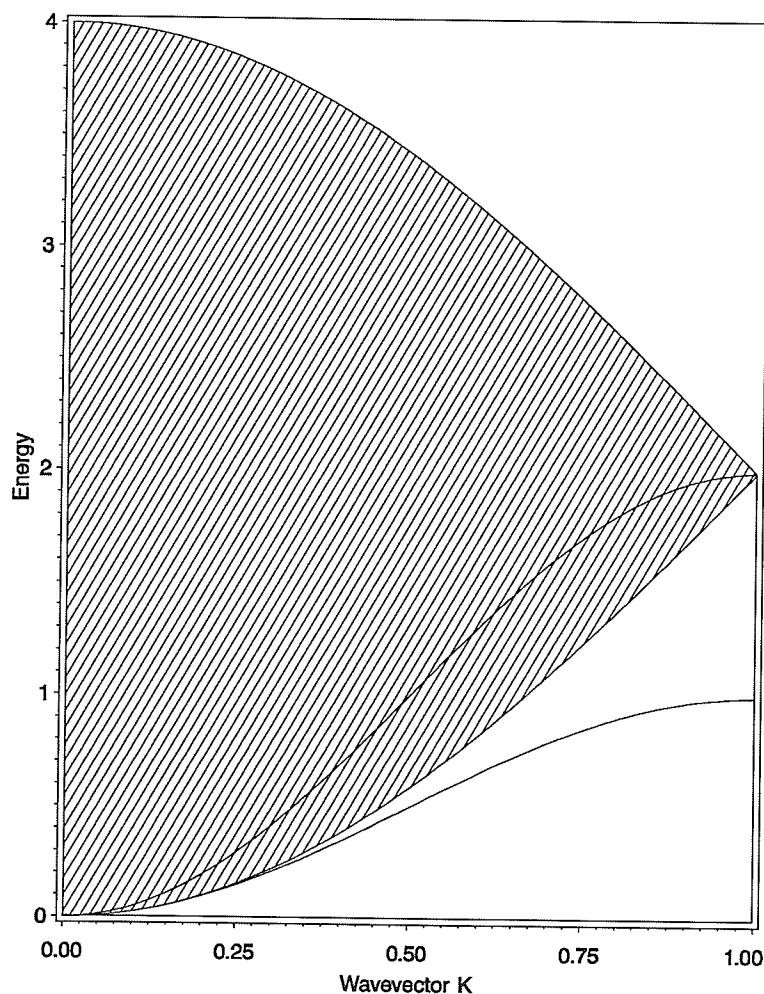


Figure 2.6: Integrable model of Lai-Sutherland for two magnon excitations. Wavevectors in units of $\frac{\pi}{a}$ and energy in units of α_1 .

In the integrable models, the excitations have special features. Either, the equation decouples as in the Lai-Sutherland and Parkinson models, or the bound states form one branch which is continuous across two Brillouin zones. These branches form gaps when the Hamiltonian deviates from integrability and the gaps vary in size as the Hamiltonian moves further from the integrable point. This is in accordance with the Haldane conjecture ([12],[13]). Whether this conjecture is valid for three magnon excitations as well as the general behaviour of the system will be investigated further in the rest of the thesis. Three magnon excitations are somewhat more difficult than one and/or two magnon excitations and Chapter 3 is entirely devoted to the necessary formalism.

Chapter 3

Three-Magnon Excitations

There have been a number of papers which have been devoted to three magnon excitations in the past. The first was H. Bethe (1931, [7]) who actually solved a system with m -magnon excitations, but his analysis only applies for integrable Hamiltonians. However, some years ago there were a series of papers which dealt specifically with three magnons such as C. Majumdar (1970, [17]; 1972, [18]) ; S. Mukhopadhyay and C. Majumdar (1976), [19]; and J. Van Himbergen (1977) [20]. These were based on the formalism developed by L. Faddeev (1961) [21], which treats the system as a system of magnons which can scatter off one another or bind together to form a stable complex. In the above references the approach to the problem is very general but detailed solutions are given only for a one dimensional spin $\frac{1}{2}$ chain. Generally, the procedure used was to transform to a magnon basis labelled by wavevectors and to perform all calculations within this space. In this basis it is difficult to identify non-physical states such as those which correspond to raising a single spin by more than $2S$. The papers describe the various methods which were used to find and eliminate these unphysical states. The techniques involved the identification of a number of constraints based on some simple physical arguments. The problem was compounded, in some of the papers, by the use of an approximate Hamiltonian (to the Heisenberg model) which has some spurious solutions. A paper which posed the problem in a slightly different form (but using a similar method of solution) was that by P. J. Millet and H. Kaplan (1974) [22].

These authors also encountered spurious solutions but only for $S = \frac{1}{2}$. Systems with $S > \frac{1}{2}$ were studied without such difficulties.

The approach to solve the three magnon system in this thesis is somewhat different. A Fourier transform of only the centre of mass is performed, which gives a good quantum number for the translationally invariant general Hamiltonian, (1.4). The other two coordinates which are required to describe the relative positions of the magnons are kept in coordinate space. Because of this, the unphysical states are easily identified. We used completely numerical methods to solve the system, whereas the papers cited above mainly attempted to obtain analytic expressions of the solutions. Only the formalism needed to describe the system is given in this chapter. However, solutions to a restricted class of Hamiltonians which can be obtained without the complete solution to the general set of equations are also described. The method of solution to the full interacting equations will be described in Chapter 4.

3.1 Formalism and Equations

An orthonormal set of three spin deviations are

$$|i, j, k\rangle = C_{ijk} \mathcal{S}_i^+ \mathcal{S}_j^+ \mathcal{S}_k^+ |0\rangle \quad (3.1)$$

where C_{ijk} is a normalization constant satisfying

$$C_{ijk} = \begin{cases} \frac{1}{\sqrt{8S^3}}, & i \neq j \neq k \\ \frac{1}{\sqrt{8S^2(2S-1)}}, & 2 \text{ of } \{i, j, k\} \text{ the same} \\ \frac{1}{\sqrt{24S(2S-1)(S-1)}}, & i = j = k \end{cases} \quad (3.2)$$

and with the indices $i \leq j \leq k$ for the entire set of states. The general procedure to establish the effect of $\widehat{\mathcal{H}}$ on these states follows that used for the one and two magnon excitations. When $\widetilde{\mathcal{P}}_l$ operates on these states, above, the resulting matrix

is block diagonal. The two smallest blocks are of the same form as for free magnons and for two magnons which are bound together (with the remaining magnon not interacting with the others), respectively. The effect of $\tilde{\mathcal{P}}_l^n$ on the states which generates these submatrices are already known from previous chapters, (2.2) and (2.13)–(2.16). The last block to consider corresponds to the case when the three magnons are on the same or neighbouring sites. The resulting matrix, which is given in the appendix, is transformed to a diagonal matrix to facilitate the calculation of raising it to the n^{th} power.

The combination of all these matrices were sufficient to obtain the effect of $\widehat{\mathcal{H}}$ on the complete set of states, in coordinate space and the details of these derivations are also given in the appendix. The translational invariance of the Hamiltonian enables a transformation to be made to a centre of mass coordinate (R) and two relative coordinates (x, y). Specifically, the transformation

$$|i, j, k\rangle \Rightarrow |R, x, y\rangle, \begin{cases} R &= \frac{1}{3}(i + j + k) \\ x &= j - i \\ y &= k - j \end{cases} \quad (3.3)$$

can be used. The coordinates were labelled such that $i \leq j \leq k$ so that $x, y \geq 0$. Representing these states as linear combinations of the eigenstates of the translation operator gives,

$$|R, x, y\rangle = \frac{1}{\sqrt{N}} \sum_{\{K\}} e^{iRKa} |K; x = j - i, y = k - j\rangle \quad (3.4)$$

or

$$|K; x, y\rangle = \frac{1}{\sqrt{N}} \sum_R e^{-iRKa} |R, x, y\rangle \quad (3.5)$$

where K is the wavevector of the centre of mass and $Ka = \frac{2\pi n}{N}$, $n \in \mathcal{Z}$. The

Hamiltonian can be expressed using the following quantities

$$\varepsilon = 3\alpha_1(S) \quad (3.6)$$

$$\varepsilon_0 = 3S(S-1) \left[\frac{\alpha_1(S)(1 - \cos Ka)}{S(4S-3)} + \frac{\alpha_2(S)(1 + \cos Ka)}{(S-1)(4S-1)} + \frac{\alpha_3(S)(1 - \cos Ka)}{3(S-1)(4S-3)} \right] \quad (3.7)$$

$$\varepsilon_1 = \frac{1}{2} \left[\frac{3(3S-2)}{4S-3} \alpha_1(S) + \frac{3S-1}{4S-1} \alpha_2(S) - \frac{3(1-S)}{4S-3} \alpha_3(S) \right] \quad (3.8)$$

$$\varepsilon_2 = \alpha_1(S) + 2 \left(\frac{2S-1}{4S-1} \right) \alpha_2(S) \quad (3.9)$$

$$\varepsilon_3 = 2 \left[\alpha_1(S) + \frac{S}{4S-1} \alpha_2(S) \right] \quad (3.10)$$

$$\varepsilon_4 = 2\alpha_1(S) + \left(\frac{2S-1}{4S-1} \right) \alpha_2(S) \quad (3.11)$$

$$u = -\frac{\zeta}{2} \left[\frac{S\alpha_1(S)}{4S-3} + \frac{(1-S)\alpha_2(S)}{4S-1} - \frac{3(1-S)\alpha_3(S)}{4S-3} \right] \quad (3.12)$$

$$v = -\frac{\zeta}{2} \alpha_1(S) \quad (3.13)$$

$$v_0 = \frac{\zeta}{2} \sqrt{3S(S-1)} \left[\frac{\alpha_1(S)(1 - \zeta^{*3})}{4S-3} - \frac{\alpha_2(S)(1 + \zeta^{*3})}{4S-1} - \frac{\alpha_3(S)(1 - \zeta^{*3})}{4S-3} \right] \quad (3.14)$$

$$v_1 = -\frac{\zeta}{2} \left\{ \alpha_1(S) + \zeta^{*3} \left[\alpha_1(S) - \frac{2S\alpha_2(S)}{4S-1} \right] \right\} \quad (3.15)$$

$$w = -\frac{\zeta \alpha_2(S) \sqrt{S(2S-1)}}{4S-1} \quad (3.16)$$

where * represents the operation of complex conjugation and $\zeta = e^{\frac{Kai}{3}}$. The effect of the Hamiltonian on the transformed set of kets, $\{|K; x, y\rangle\}$, is as follows

$$\widehat{\mathcal{H}}|K; 0, 0\rangle = \varepsilon_0|K; 0, 0\rangle + v_0|K; 0, 1\rangle + v_0^*|K; 1, 0\rangle \quad (3.17)$$

$$\begin{aligned} \widehat{\mathcal{H}}|K; 0, 1\rangle &= \varepsilon_1|K; 0, 1\rangle + u|K; 1, 0\rangle + v_1|K; 0, 2\rangle + w^*|K; 1, 1\rangle \\ &\quad + v_0^*|K; 0, 0\rangle \end{aligned} \quad (3.18)$$

$$\begin{aligned}\widehat{\mathcal{H}}|K;1,0\rangle &= \varepsilon_1|K;1,0\rangle + u^*|K;0,1\rangle + v_1^*|K;2,0\rangle + w|K;1,1\rangle \\ &\quad + v_0|K;0,0\rangle\end{aligned}\quad (3.19)$$

$$\begin{aligned}\widehat{\mathcal{H}}|K;1,1\rangle &= \varepsilon_2|K;1,1\rangle + w|K;0,1\rangle + w^*|K;1,0\rangle + w^*|K;0,2\rangle \\ &\quad + w|K;2,0\rangle + v|K;1,2\rangle + v^*|K;2,1\rangle\end{aligned}\quad (3.20)$$

and for $x, y > 1$

$$\begin{aligned}\widehat{\mathcal{H}}|K;0,y\rangle &= \varepsilon_3|K;0,y\rangle + v_1^*|K;0,y-1\rangle + v_1|K;0,y+1\rangle \\ &\quad + w|K;1,y-1\rangle + w^*|K;1,y\rangle\end{aligned}\quad (3.21)$$

$$\begin{aligned}\widehat{\mathcal{H}}|K;x,0\rangle &= \varepsilon_3|K;x,0\rangle + v_1|K;x-1,0\rangle + v_1^*|K;x+1,0\rangle \\ &\quad + w^*|K;x-1,1\rangle + w|K;x,1\rangle\end{aligned}\quad (3.22)$$

$$\begin{aligned}\widehat{\mathcal{H}}|K;1,y\rangle &= \varepsilon_4|K;1,y\rangle + v^*|K;1,y-1\rangle + v|K;1,y+1\rangle \\ &\quad + v^*|K;2,y\rangle + v|K;2,y-1\rangle + w^*|K;0,y+1\rangle + \\ &\quad w|K;0,y\rangle\end{aligned}\quad (3.23)$$

$$\begin{aligned}\widehat{\mathcal{H}}|K;x,1\rangle &= \varepsilon_4|K;x,1\rangle + v|K;x-1,1\rangle + v^*|K;x+1,1\rangle \\ &\quad + v|K;x,2\rangle + v^*|K;x-1,2\rangle + w^*|K;x,0\rangle + \\ &\quad w|K;x+1,0\rangle\end{aligned}\quad (3.24)$$

$$\begin{aligned}\widehat{\mathcal{H}}|K;x,y\rangle &= \varepsilon|K;x,y\rangle + v^*|K;x+1,y\rangle + v|K;x-1,y\rangle \\ &\quad + v^*|K;x-1,y+1\rangle + v|K;x+1,y-1\rangle + v^*|K;x,y-1\rangle \\ &\quad + v|K;x,y+1\rangle\end{aligned}\quad (3.25)$$

The quantum number, K – the total wavevector, is common to all the equations and should be understood implicitly for all that follows. Also, the ground state was taken as the zero of energy.

Note that equation (3.25), by itself, describes the behaviour of the system when the magnons are separated by more than nearest neighbours and depend solely on $\alpha_1(S)$. Also, when one of the magnons is further than nearest neighbours from the

other two, (3.21)–(3.24), or when all three are exactly nearest neighbours, (3.20), the equations depend on $\alpha_1(S)$ and $\alpha_2(S)$ only. When two magnons are on the same site and the other is also on that site, (3.17), or a nearest neighbour to the other two, (3.18) and (3.20), the equations depend on $\alpha_1(S)$, $\alpha_2(S)$, and $\alpha_3(S)$. All $\alpha_n(S)$, $n > 3$, do not appear for this system and are only necessary when considering four or more magnons. The equations, above, can be represented graphically as

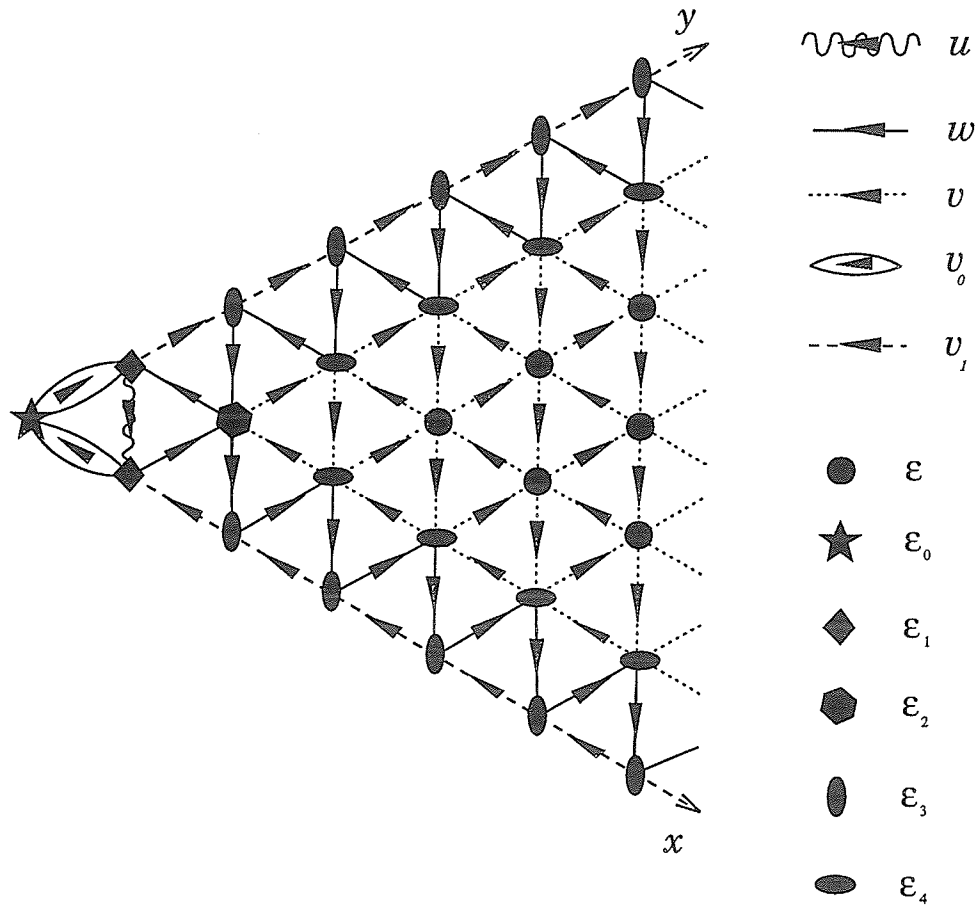


Figure 3.1: Graphical representation of the effect of the general Hamiltonian on states of the form $|K; x, y\rangle$.

The grid coordinates label the values of x and y in the ket $|x, y\rangle$ and the lines on the diagram represent the interaction between kets. The different types of lines correspond to different interactions. The arrows point to states which are generated

by the Hamiltonian when acting on the kets at the base of the arrows. But the Hamiltonian can operate on any site and, for any nearest neighbour pair of sites, if the Hamiltonian is made to act on the state which the arrow is directed toward, the coupling which results is related to the appropriate interaction (u, w, v, v_0, v_1) but the complex conjugate must be taken. In other words, the direction of all the arrows can be reversed if the complex conjugate of u, w, v, v_0 and v_1 is used. The different site markers indicate the coefficients which are associated with the self interaction of the ket that the Hamiltonian is acting on. Finally, the Hamiltonian is a nearest neighbour model so exactly one bond on the diagram can be taken in any direction from any node.

A simple example can be read off as follows: Suppose, the effect of $\widehat{\mathcal{H}}$ on $|0,0\rangle$ is desired. $|0,0\rangle$ is equivalent to $(x,y) = (0,0)$ on the diagram so, starting at the leftmost site, there is a line to $(x,y) = (0,1)$, hence the Hamiltonian produces the ket $|0,1\rangle$ and the bond corresponds to v_0 so the entire term is $v_0|0,1\rangle$. Similarly, there is an interaction to $|1,0\rangle$ but this is in the opposite direction of the arrow, so the interaction has the form $v_0^*|1,0\rangle$. The nearest neighbour model prohibits following two interactions to get to $|1,1\rangle$ and there is no direct connection so this state cannot be reached from $|0,0\rangle$. Finally, there is the symbol on the $(x,y) = (0,0)$ site which indicates there is also a $\varepsilon_0|0,0\rangle$ term. Therefore, the entire effect is $\widehat{\mathcal{H}}|0,0\rangle = \varepsilon_0|0,0\rangle + v_0|0,1\rangle + v_0^*|1,0\rangle$, as given in (3.17).

In general, the Hamiltonian will generate seven terms when it acts on any state of the form $|K; x, y\rangle$ and although the resulting equation does not resemble the two-magnon equations, (2.31)–(2.33), these equations are of a tight binding form. This becomes more apparent by considering a tight binding two dimensional triangular lattice, for example a net of masses and springs. The Hamiltonian of Fig. 3.1 can be mapped directly to such a net, if allowance is made for an edge in both the x and y directions. The mapping is accomplished by taking the site quantities $(\varepsilon_i, i = 0, 1, 2, 3, 4)$ as related to the size of the masses and the connections (u, w, v, v_0, v_1)

as the strength of the springs. The existence of such a mapping indicates that the formalism is not restricted to describing quantum spins on a chain. The formalism can be applied to any system which is characterized by two coordinates (and satisfies the condition of nearest neighbour interactions on a semi-infinite triangular lattice) such as multiple particles on a one dimensional chain, which is the case we are considering, or a single particle on a two dimensional net.

This system is similar to having defects in a linear mass-spring chain in that the outer two surface layers are inherently different from the bulk of the net and the four sites in the corner $[(x, y) = (0, 0), (1, 0), (0, 1), (1, 1)]$ are different from both the rest of the surface and the bulk. (These are the equivalents of the defects.) Thus, the equation can be separated into three groups and the general solution for each group can be obtained independently. However, the complete solution to the three magnon equations requires these general solutions to change smoothly across the boundaries between the groups. Because the Hamiltonian is mapped to a two dimensional net, some differences from the solutions to a simple system of masses and chains are to be expected but there are still two types of solutions, scattering and bound states. The scattering states can be further divided into two more classifications. First, there are those scattering states which propagate in the uniform part of the net. These are described by equation (3.25), by itself. But there are other states described by equations (3.21)–(3.24). These are states which form travelling modes that propagate along the surface and can couple with the other travelling modes described above. Finally, there are solutions corresponding to localized modes and these states are solutions to (3.17)–(3.20). Both types of scattering states are discussed in the next section (Section 3.2). While the discussion of the bound state solutions is deferred to Chapter 4.

3.2 Three Magnon Continuum

The scattering states which propagate in the uniform part of the net are equivalent to three non-interacting magnons on an infinite triangular lattice. This is apparent in the form of the equation which describes these states, (3.25). Then, the energies of the solutions must be bounded by the min/max of

$$\begin{aligned} E_1(k_1) + E_1(k_2) + E_1(k_3) &= \alpha_1(1 - \cos k_1 a) + \alpha_1(1 - \cos k_2 a) + \alpha_1(1 - \cos k_3 a) , \\ k_1 + k_2 + k_3 &= K \end{aligned} \tag{3.26}$$

These extrema are given by

$$E_{min}(K) = 3\alpha_1(S) \left(1 - \cos \frac{Ka}{3} \right) \tag{3.27}$$

$$E_{max}(K) = 3\alpha_1(S) \left[1 - \cos \left(\frac{Ka + 2\pi}{3} \right) \right] \tag{3.28}$$

and are plotted in Fig. 3.2.

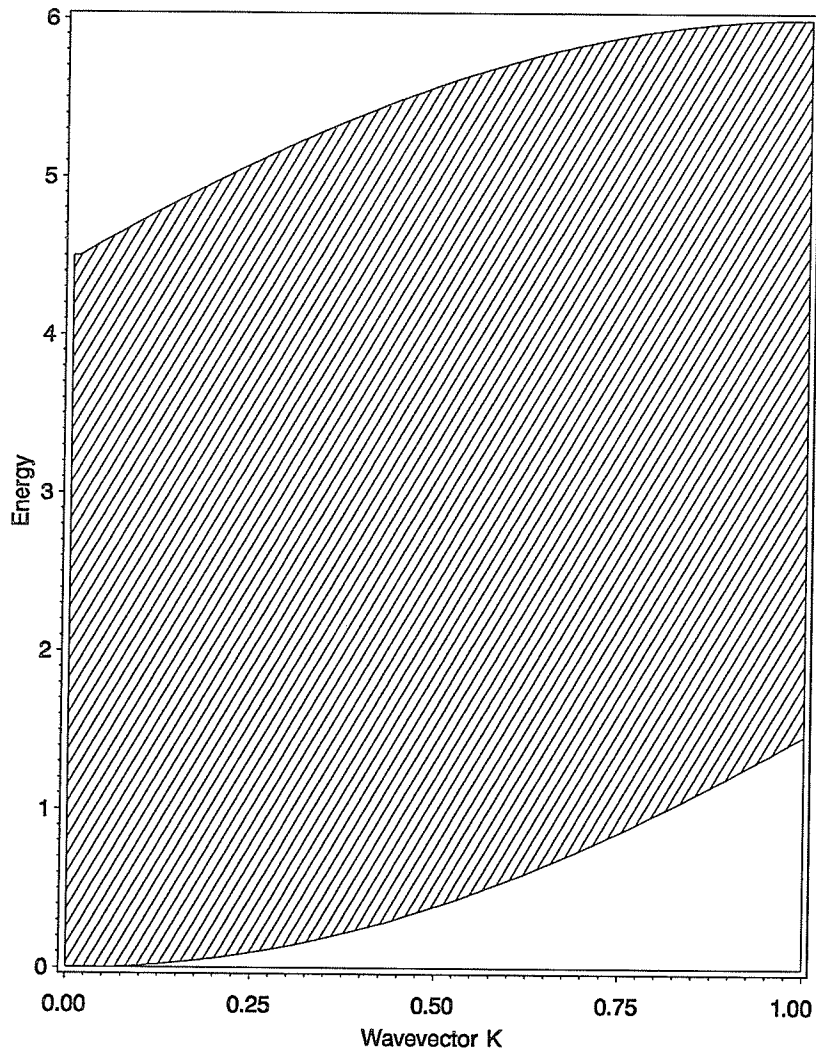


Figure 3.2: Extent of the three free magnon scattering state continuum. Energy in units of α_1 . Wavevector in units of $\frac{\pi}{a}$.

The above argument gives no information on the detailed form of the state. This would depend upon the conditions which must be imposed upon the equation to match the solutions between the region which is described by (3.25) and the region described by (3.17)–(3.24). Referring to Fig. 3.1, the boundaries to these types of scattering states are along $x = 2$ and/or $y = 2$. Each of the sites along these axes would have two constraints imposed upon it from the equations corresponding to the Hamiltonian acting on the sites along $x, y = 1$. (ie. The constraints necessary to keep the wavefunction continuous when crossing the region where the masses and

springs are uniform, $x, y \geq 2$, and the region near the edges, $x, y < 2$.) The particular site at $(x, y) = (2, 2)$ appears to have four constraints but, due to the symmetry of the net, two are not independent. Further, in the equations above there are four degrees of freedom (two for each k_1, k_2, k_3 minus two for the constraint on the total wavevector). With more degrees of freedom in equation (3.26) than constraints, a solution can always be found with an energy which lies in the shaded region of Fig. 3.2. The boundary conditions which demand a smooth transition between the regions are dependent upon the derivative of the functions used to enforce continuity of the wavefunction and would simply double the number of degrees of freedom as well as the constraints.

Whereas the equation for the previous continuum has the form of three free magnons, the second scattering state continuum includes some interactions between them. The equations which describe these scattering states, (3.21)–(3.25), define travelling modes which can propagate along most of the edges but decay into the uniform part of the net. These equations do not describe states which are represented by the sites at the leftmost corner in Fig. 3.1. [ie. sites: $(0, 0), (1, 0), (0, 1), (1, 1)$]. The form of the equations for this second scattering state continuum is the same as for a travelling two magnon bound state combined with a single free magnon. Therefore, this continuum must be bounded by the minimum and maximum of

$$E_1(k_1) + E_2(k_b), \quad k_1 + k_b = K \quad (3.29)$$

where we define E_2 as the excitation energy of a two magnon bound state and k_b is the total wavevector for the bound state. The form of E_2 varies tremendously depending upon the value of $g_2 = \frac{\alpha_2(S)}{\alpha_1(S)}$ in the Hamiltonian. For example, in the specific case of $g_2 = \frac{4S-1}{2S-1}$ there are two continua, one from each bound state branch, which exactly meet over the entire Brillouin zone as shown in Fig. 3.3.



Figure 3.3: Extent of the two-bound one-free magnon scattering state continuum. Energy in units of α_1 . Wavevector in units of $\frac{\pi}{a}$.

If g_2 deviates from $\frac{4S-1}{2S-1}$, the two bands no longer meet over the whole Brillouin zone and if g_2 is sufficiently different from this value there is only one bound state branch and hence only one of these continua is present. For example the Heisenberg model, $g_2 = \frac{4S-1}{2S}$, has only the lower continuum. As the analysis for these continua follow a similar argument as the three free continuum, these results also contain no information on the detailed form of the states. However, there are still more degrees of freedom than constraints (from the conditions to match the solutions

between regions) so a solution can always be found. To be specific, the boundaries of this region are between the sites $(0, 1) - (0, 2)$, $(1, 1) - (0, 2)$ and $(1, 1) - (1, 2)$. There are also boundaries between $(1, 0) - (2, 0)$, $(1, 1) - (2, 0)$ and $(1, 1) - (2, 1)$ but these do not give constraints independent from the first three. As for the degrees of freedom, consider the bound state first. The component wavevectors for the bound state, k_{b1} and k_{b2} satisfy

$$k_{b1} + k_{b2} = k_b \quad (3.30)$$

These component wavevectors are inherently complex, so there are four degrees of freedom for each constituent wavevector, but the total wavevector of the bound state, k_b , is real so the number of degrees of freedom decreases from eight to six. The constraint on the sum of the wavevectors, (3.30), further reduces this to four. Now consider the free magnon. This contributes two more degrees of freedom but with the constraint on the total wavevector, equation (3.29), the final total of the degrees of freedom is four with only three remaining constraints. Therefore, a solution can always be found with the energy of the solutions within the continua described above.

These different continua (the two-bound one-free continua and the three free continuum) overlap to a large degree with no gaps so that the scattering continuum for a three magnon excitation can be taken as a single band which extends from the continuum which attains the minimum energy to the continuum which achieves the maximum energy. The band edges which are internal to this single continuum band generate Van Hove singularities in the band. The scattering state continuum is important when identifying the bound states which arise from the solutions to the few remaining equations, (3.17)–(3.20). A method of solution for these bound states is described in the next chapter, Chapter 4. However, there are a number of models which can be considered without resorting to special methods of solution. These are the special integrable models introduced in Chapter 1. The Hamiltonians

for these models have certain simplifying features which enable most of the models to be solved directly from (3.17)–(3.25). The models and solution are given in the next section.

3.3 Bound States and Integrable Models

Consider, initially, the Lai-Sutherland model where $\alpha_2(S) \equiv 0$ and $\alpha_1(S) = \alpha_3(S)$. This gives $w \equiv 0 \equiv v_0$, completely decoupling the site corresponding to $|0, 0\rangle$, three magnons on the same site. This also has the effect of isolating the region with $x, y \geq 1$ from the rest of the sites as shown in Fig. 3.4, below.

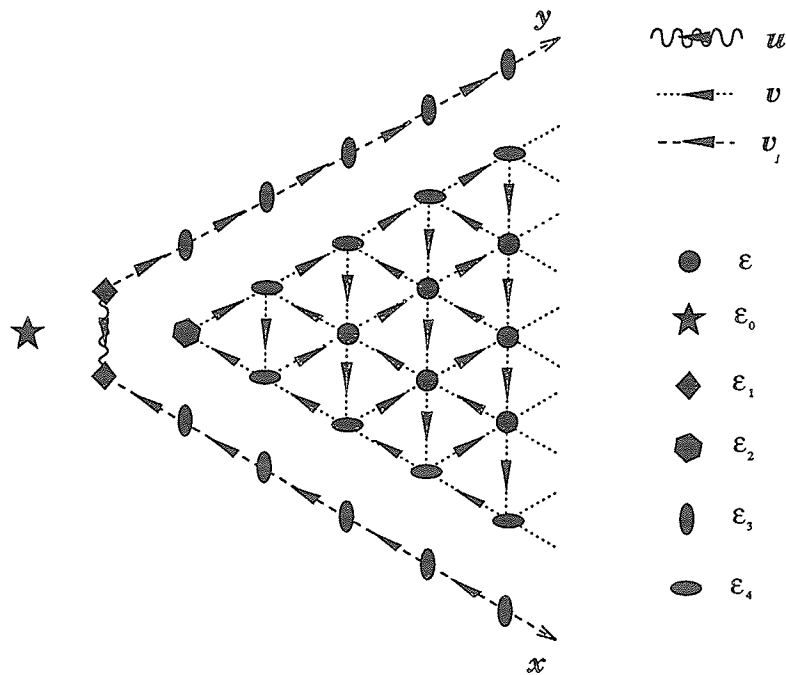


Figure 3.4: Diagram of the Hamiltonian for the Lai-Sutherland model.

For the latter region the equations reduce to the form of an integrable $S = \frac{1}{2}$ system of three magnons. The solutions, therefore, have the form as those given by Bethe and consist of two scattering state bands, as described in the previous section, and a single bound state branch with energy $\frac{\alpha_1(S)}{3} [1 - \cos(Ka)]$. The former region

has only the one site which implies the state is an eigenstate with energy $\varepsilon_0 = \alpha_1(S) [1 - \cos(Ka)]$. Therefore, this state behaves as a single free magnon. The middle region, consisting of the surface layer along with the interaction between $|1, 0\rangle$ and $|0, 1\rangle$, contain states with two magnons on the same site combined with one free magnon. If the part of the Hamiltonian which defines the behaviour of these states, only, is transformed to a tridiagonal form, the Hamiltonian takes the form of a semi-infinite mass-spring chain with one defect at one end. This is the same as was found for a two magnon excitation in Chapter 2 for $S = \frac{1}{2}$. In Chapter 2 the system was treated generally, but if the resulting equations are restricted to $S = \frac{1}{2}$, the size of S prevents raising the spin of any one site by more than one, which removes the first mass (m'') and spring (k') from Fig. 2.2. This gives a single mass defect at the beginning, with the remaining masses and springs uniform. Therefore the solutions must also have the same form as the two magnon equations, namely a band of scattering states bounded by $E_{\text{Cont}} = 2\alpha_1(S) \left[1 \pm \cos\left(\frac{Ka}{2}\right)\right]$ and a bound state of energy $E_B = \frac{\alpha_1(S)}{2} \left[1 - \cos\left(\frac{Ka}{2}\right)\right]$ (as given by Bethe).

The other special integrable model is the Temperley-Lieb Hamiltonian. These models have $\alpha_i = 0$, $i \neq 2S$. When $S = 1$, ε_0 , ε , v_0 and v are all 0, decoupling the first two layers, excluding $|0, 0\rangle$, from the rest. For any of the states in the uniform part of the net in Fig. 3.1 (ie. $x, y \geq 2$) and $|0, 0\rangle$, $\widehat{\mathcal{H}}|x, y\rangle = 0$ and $E = 0$ is the only solution. The remaining part (Fig. 3.5, below) is more easily treated using a method described in the following chapter, so that the solutions to this model will be given along with the results for the more general Hamiltonian, later. The diagram of the Hamiltonian follow the same conventions used for the diagram of the general Hamiltonian, Fig. 3.1.

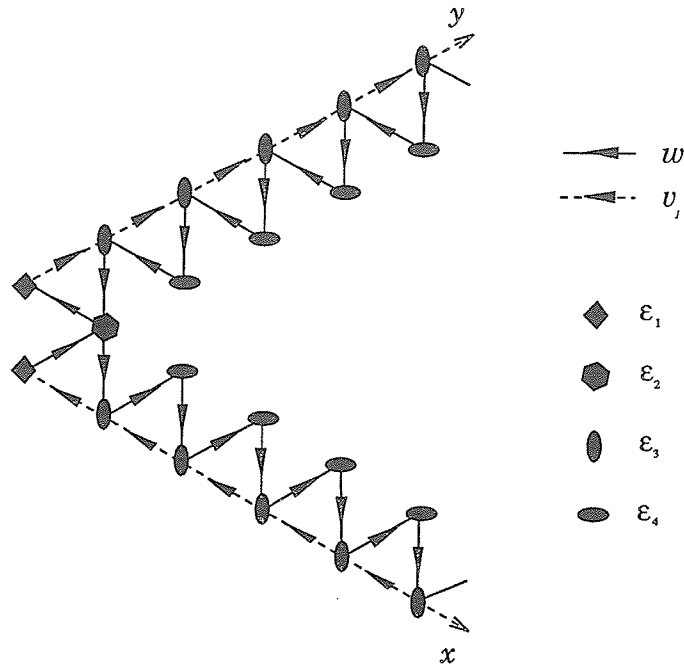


Figure 3.5: Diagram of the Hamiltonian for a $S = 1$ Temperley-Lieb model.

Quite different from the $S = 1$ case, the $S = \frac{3}{2}$ Temperley-Lieb model can be treated quite simply. The Hamiltonian has only $\epsilon_0, \epsilon_1, v_0, u$ non-zero. Explicitly,

$$\epsilon_0 = \frac{\alpha}{2} [1 - \cos(Ka)] \quad (3.31)$$

$$\epsilon_1 = \frac{\alpha}{4} \quad (3.32)$$

$$v_0 = \frac{-\alpha\zeta}{4} (1 - \zeta^{*3}) \quad (3.33)$$

$$u = \frac{-\alpha\zeta}{4} \quad (3.34)$$

taking $\alpha_3(S) \equiv \alpha$. Graphically,

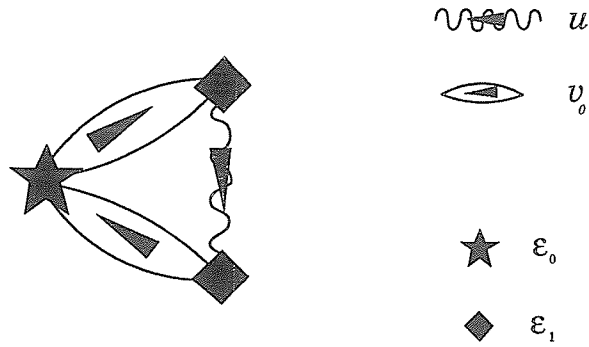


Figure 3.6: Diagram of the Hamiltonian for a $S = \frac{3}{2}$ Temperley-Lieb model.

As for the $S = 1$ case, the only solution to any of the states outside the region shown in Fig. 3.6 has $E = 0$. Using this restricted number of states, the Schrödinger equation gives

$$(E - \varepsilon_0)|0,0\rangle - v^*|1,0\rangle - v|0,1\rangle = 0 \quad (3.35)$$

$$-v|0,0\rangle + (E - \varepsilon_1)|1,0\rangle - u^*|0,1\rangle = 0 \quad (3.36)$$

$$-v^*|0,0\rangle - u|1,0\rangle + (E - \varepsilon_1)|0,1\rangle = 0 \quad (3.37)$$

which have solutions given by $E = 0, \alpha \left[1 - \frac{1}{2} \cos(Ka)\right]$. These are plotted below.

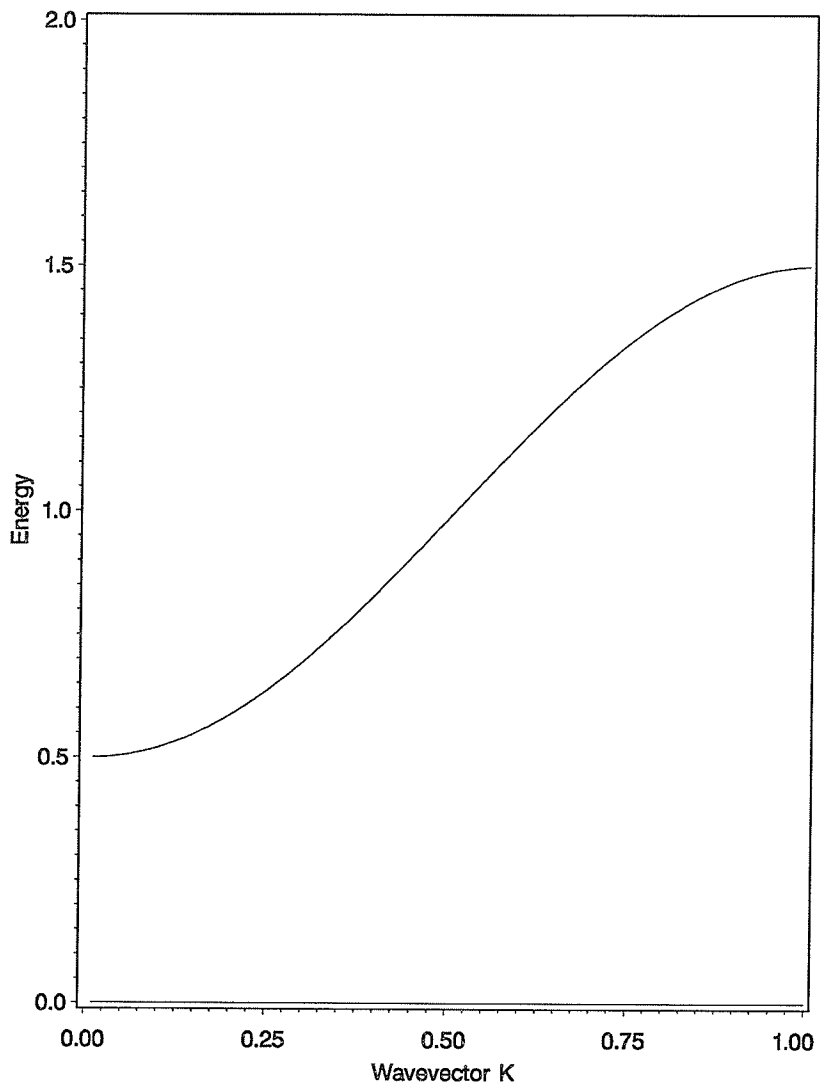


Figure 3.7: Bound state solutions of the $S = \frac{3}{2}$ Temperley-Lieb model. The energy is in units of α and the wavevector in units of $\frac{\pi}{a}$.

Chapter 4

The Recursion Method

4.1 Green's Function

If all the eigenvalues and eigenvectors can be found for the Hamiltonian then the complete solution to the equations (3.17)–(3.25) has been obtained. Unfortunately, the calculation of the eigenvectors and eigenvalues for this system, requires methods which are very complicated and/or computationally expensive. However a modest, but important, amount of information can be obtained from the equations without resorting to such complex methods. Consider the density of states for this lattice. When the three magnons are bound together as a single entity there would be a non-zero number of states over some infinitesimally small region of energy. Hence, these would appear as delta functions in the density of states. Also, some configurations may have a significant number of states over a small but finite energy range, giving a peak rather than a delta-function. These peaks can be resonances or possibly Van Hove singularities. Finally, states which are infinitesimally close to each other in energy (as in the continuum bands) would have wide ranges of energy where the density of states would be non-zero. Although we would not have the precise eigenstates, by studying the density of states we could obtain the energies which each different type of state could possess. Also, the formalism to this point has identified one good quantum number, the total wavevector K , which can be incorporated to further enhance the amount of knowledge about the system.

As a brief aside, consider an arbitrary ket, $|j\rangle$, in the three-magnon basis which can be expanded as follows

$$|j\rangle = \sum_{\lambda} c_{\lambda} |\lambda\rangle \quad (4.1)$$

where $\{|\lambda\rangle\}$ is a complete orthonormal set of states such that $\widehat{\mathcal{H}}|\lambda\rangle = E_{\lambda}|\lambda\rangle$, and E_{λ} are the energy eigenvalues of $\widehat{\mathcal{H}}$. The local Green's function is defined as

$$\begin{aligned} G_j(E_c) &= \langle j | (E_c - \widehat{\mathcal{H}})^{-1} | j \rangle, \quad E_c \in \mathcal{C} \\ &= \sum_{\lambda} \frac{|c_{\lambda}|^2}{E_c - E_{\lambda}} \end{aligned} \quad (4.2)$$

The poles of G_j occur on the real axis at the energy eigenvalues E_{λ} . The energy E_c is a complex quantity, but if we restrict ourselves to energies near the real axis, we can take $E_c = E + i\varepsilon$, $|\varepsilon| \ll 1$. Then

$$G_j = \sum_{\lambda} |c_{\lambda}|^2 \left[\frac{(E - E_{\lambda})}{(E - E_{\lambda})^2 + \varepsilon^2} - i \frac{\varepsilon}{(E - E_{\lambda})^2 + \varepsilon^2} \right] \quad (4.3)$$

and in the limit

$$\lim_{\varepsilon \rightarrow 0} [\text{Im}(G_j)] = -\pi \sum_{\lambda} |c_{\lambda}|^2 \delta(E - E_{\lambda}) \quad (4.4)$$

(See, for example, R. M. White [23] or E. N. Economou [24].) Thus, the imaginary part of the local Green's function is proportional to a sum of delta functions and is non-zero only at energies where eigenstates exist. The density of states local to $|j\rangle$ (not an eigenstate) can be defined as

$$n_j = -\frac{1}{\pi} \text{Im} [G_j(E + i\varepsilon)] \quad (4.5)$$

and the total density of states, n , is obtained by a sum over all the kets in the basis

$$\begin{aligned} n &= \sum_j n_j \\ &= -\frac{1}{\pi} \sum_{\{|j\rangle\}} \text{Im} [G_j(E + i\varepsilon)] \end{aligned} \quad (4.6)$$

The real part of the Green's function can be related to the Hilbert transform of the density of states and gives an indication of the difficulty of exciting the system at an energy, E [16]. If the chosen state, $|j\rangle$, has some special symmetries with respect to the Hamiltonian then some of the coefficients $c_{\lambda'} = 0$ for $\{\lambda'\} \subset \{\lambda\}$, and there will be no contribution from these states to the local density of states for $|j\rangle$. In practice it is very unlikely that a state would be accidentally chosen which has a significant number of the $c_{\lambda'} = 0$ to be problematic. However, there are two classes of states which may accidentally be chosen; states which are completely symmetric or completely antisymmetric. In fact it was observed that for the $S = \frac{3}{2}$ Heisenberg case, one of the bound states has no symmetric components, but this was not common and fortunately kets with either of these types of symmetries are easily identified.

When using a matrix representation, the local Green's function can be taken as a single matrix element of the operator $(E - \widehat{\mathcal{H}})^{-1}$ and without loss of generality, we can choose the G_{00} element which gives

$$G_{00} = \frac{\text{Mi}_{00}([E - \widehat{\mathcal{H}}])}{\text{Det}([E - \widehat{\mathcal{H}}])} \quad (4.7)$$

where $\text{Mi}_{ij}([E - \widehat{\mathcal{H}}])$ is the minor of element i, j for the matrix $[E - \widehat{\mathcal{H}}]$. But the Green's function would be of little value if it was difficult to calculate, and for some choices of sets of bases the calculation is trivial, such as a basis where the Hamiltonian is diagonal. In general, the appropriate basis which diagonalizes the

There is still a difficulty in that the basis which tridiagonalizes the Hamiltonian needs to be found. There is a method which can be used to easily find the tridiagonal form of the Hamiltonian and it will also generate the basis states which would produce the transformation as well, but it is the elements of the tridiagonal Hamiltonian which are the useful quantities in our case. This procedure is known as the Recursion Method and it is described in the following section.

4.2 Recursion

Although there are some standard routines for tridiagonalizing a matrix, the most efficient method, in this case, is the Recursion Method. This procedure has been extensively documented with the most complete treatment given by R. Haydock [16] for electronic systems. The method relies extensively on a three-term recursion relation of the form

$$\widehat{\mathcal{H}}u_i = a_i u_i + b_{i+1} u_{i+1} + b_i u_{i-1} \quad (4.11)$$

where $a_i, b_i \in \mathcal{R}$ and u_i is the i^{th} state of an arbitrary complete orthonormal set of states. To start the procedure, define $u_{-1} \equiv 0$ and some arbitrary state u_0 , then define a normalized state, u_1 , from

$$\widehat{\mathcal{H}}u_0 = a_0 u_0 + b_1 u_1 \quad (4.12)$$

Taking u_1 as some presently unknown state but presumed to be orthogonal to u_0 . It follows that

$$a_0 = u_0^\dagger \widehat{\mathcal{H}}u_0 \quad (4.13)$$

$$b_1 u_1 = \widehat{\mathcal{H}}u_0 - a_0 u_0 \quad (4.14)$$

In general, there will be a third term in (4.14), ie. (4.14) becomes $b_{i+1} u_{i+1} = \widehat{\mathcal{H}}u_i - a_i u_i - b_i u_{i-1}$. We can take $b_1 (b_{i+1})$ as the normalization factor for $u_1 (u_{i+1})$.

By iterating this procedure, the set of states $\{u_i\}$, can be found which will transform the Hamiltonian to the desired canonical form and the resulting tridiagonal matrix will contain the a_i and b_i as its elements. To be explicit, if a vector in the new basis

with the form $\begin{pmatrix} u_0 \\ u_1 \\ u_2 \\ \vdots \end{pmatrix}$ is used, the Hamiltonian becomes

$$\widehat{\mathcal{H}} \begin{pmatrix} u_0 \\ u_1 \\ u_2 \\ \vdots \end{pmatrix} = \begin{bmatrix} a_0 & b_1 & & & \\ b_1 & a_1 & b_2 & & 0 \\ & b_2 & a_2 & b_3 & \\ & & 0 & & \ddots \end{bmatrix} \begin{pmatrix} u_0 \\ u_1 \\ u_2 \\ \vdots \end{pmatrix} \quad (4.15)$$

For some choice of initial ket in the three-magnon basis, $u_0 = |x, y\rangle$, each successive application of the above procedure with the nearest neighbour Hamiltonian, represented in Fig. 3.1, can only couple to the kets in neighbouring columns. For example, if $u_0 = |0, 0\rangle$, then after the first iteration, u_1 involves the kets $|1, 0\rangle$ and $|0, 1\rangle$. The second iteration yields a u_2 which can involve some combination of $|1, 0\rangle$ and $|0, 1\rangle$, which is linearly independent from u_1 , as well as terms involving $|2, 0\rangle$, $|0, 2\rangle$ and $|1, 1\rangle$. The new state formed at each iteration is constructed to be orthogonal to the previous two states, thus to find the next basis state only these two states need be known, along with the Hamiltonian which connects them. This process will map the system onto an effective tight binding chain which is inhomogeneous, and for any initial choice of u_0 , there is a one to one correspondence between the a_i and b_i to the masses and strength of the springs, for a mass-spring chain. However, the precise values will change depending upon the choice of initial ket.

For this semi-infinite chain, the recursion process continues indefinitely, which creates a difficulty: when and how to stop the procedure. There are a number of important possibilities for the behaviour of the a_i and b_i coefficients for large i . The coefficients may approach constants, form some kind of periodic oscillations or

simply vary randomly. The last case, random values of a_i and b_i , correspond to a random net of masses and springs. This would not be expected for the Hamiltonian given in Fig. 3.1. As the number of iterations increases (ie. moving further to the right of the diagram) the columns become longer, and locally, it more closely approximates a uniform net. Therefore, we expect that the coefficients would approach constant values.

4.3 Termination of the Continued Fraction

4.3.1 Constant Coefficients

The easiest case to treat is when the coefficients a_i and b_i converge to constant values. The asymptotic “tail” of the continued fraction for the Green’s function can be easily evaluated exactly. To show this, let

$$\left. \begin{array}{l} a_i = a \\ b_i = b \end{array} \right\} \text{ for } i > i_{\max} \quad (4.16)$$

or the a_i and b_i are constant for all recursive iterations after the $(i_{\max})^{\text{th}}$ iteration then

$$G(E_c) = \frac{1}{E_c - a_0 - \frac{b_1^2}{E_c - a_1 - \frac{b_2^2}{\vdots \frac{b_{i_{\max}}^2}{E_c - a_{i_{\max}} - \frac{b_{i_{\max}}^2}{G_\infty}}}}} \quad (4.17)$$

where we represent the infinite tail of the continued fraction by

$$\begin{aligned} G_\infty(E_c) &= \frac{b^2}{E_c - a - \frac{b^2}{E_c - a - \frac{b^2}{\ddots}}} \\ &= \frac{b^2}{E_c - a - G_\infty(E_c)} \end{aligned}$$

$$= \frac{1}{2} \left[E_c - a \pm \sqrt{(E_c - a)^2 - 4b^2} \right] \quad (4.18)$$

This is known as the square root terminator and the choice of the positive or negative square root depends upon whether the energy was initially taken in the upper or lower half of the complex plane, or equivalently if $E - a$ is positive or negative. As examples, we will consider the case of a uniform semi-infinite chain and one magnon excitations on a uniform infinite chain, which corresponds to a semi-infinite chain with only the first spring different. The one magnon excitations give coefficients

$$a_i = a \quad \forall i \quad \text{and} \quad b_i = \begin{cases} \sqrt{2}b & i = 1 \\ b & i \neq 1 \end{cases} \quad \text{so that}$$

$$\begin{aligned} G(E) &= \frac{1}{E - a - \frac{2b^2}{E - a - G_\infty}} \\ &= \frac{E - a \mp \sqrt{(E - a)^2 - 4b^2}}{(E - a)^2 - 4b^2 \mp (E - a)\sqrt{(E - a)^2 - 4b^2}} \\ &= \frac{\pm 1}{\sqrt{(E - a)^2 - 4b^2}} \end{aligned} \quad (4.19)$$

For single magnon excitations there cannot be any bound states, and there is a continuum which can be found by calculating the (real) energies where G contains an imaginary term, or when

$$\begin{aligned} (E - a)^2 - 4b^2 &< 0 \\ a - 2b &\leq E \leq a + 2b \end{aligned} \quad (4.20)$$

Therefore, the imaginary part of G is non-zero when $E_1 = a - 2b \leq E \leq E_2 = a + 2b$. The asymptotic values of a_i and b_i are related to the minimum energy, E_1 , and the maximum energy, E_2 , by

$$a = \frac{1}{2}(E_1 + E_2) \quad (4.21)$$

$$b = \frac{1}{4}(E_2 - E_1) \quad (4.22)$$

These are merely the edges of the band and the behaviour of the density of states within the band can only be obtained by considering the Green's function with complex energies. The real and imaginary parts of (4.19) for complex energies are shown below (Fig. 4.1 and Fig. 4.2, respectively).

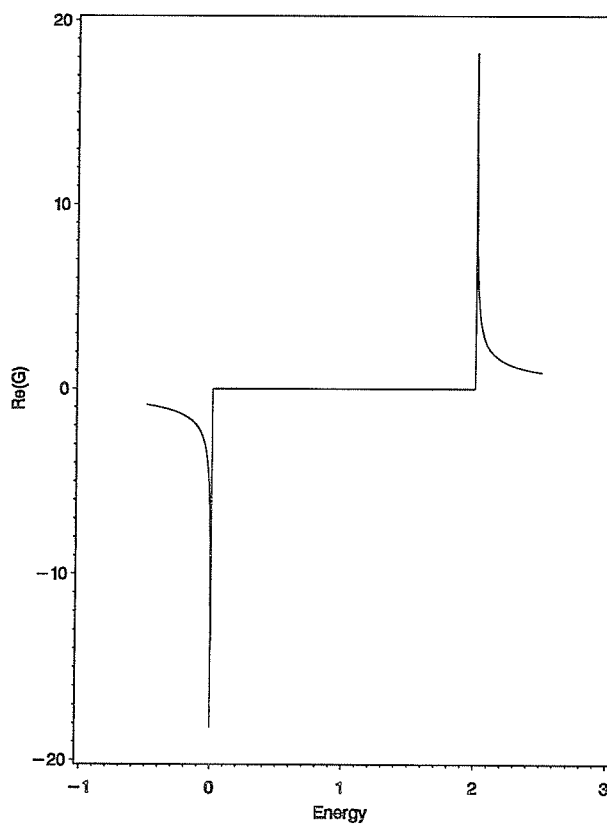


Figure 4.1: Real part of the Green's function for one magnon excitations on an infinite chain. Energy in units of α_1 .

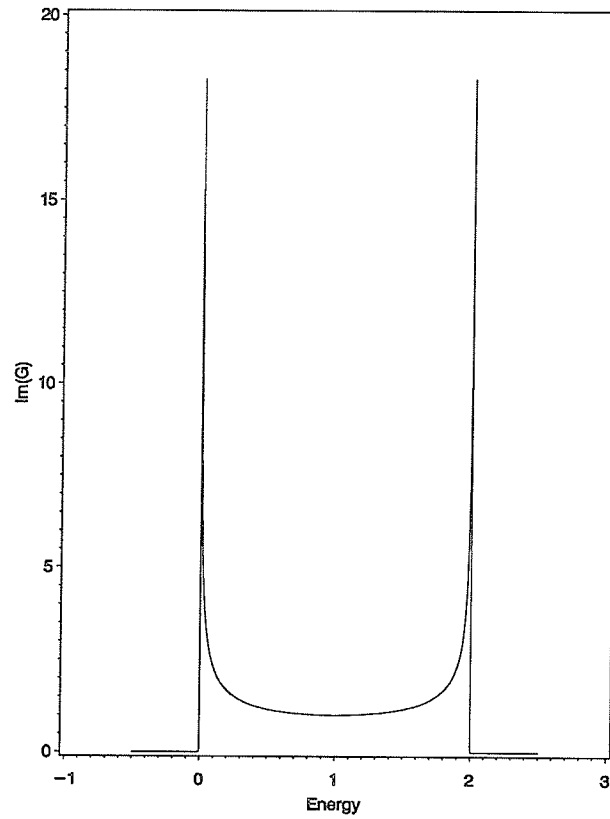


Figure 4.2: Imaginary part of the Green's function for one magnon excitations on an infinite chain. Energy in units of α_1 .

For the uniform semi-infinite chain, the Green's function is

$$\begin{aligned}
 G(E_c) &= \frac{1}{E_c - a - G_\infty(E_c)} \\
 &= \frac{1}{2b^2} \left[E_c - a \mp \sqrt{(E_c - a)^2 - 4b^2} \right] \quad (4.23)
 \end{aligned}$$

which has real and imaginary parts as shown below, for the arbitrary values of a and b of 4 (units of α_1) and $\frac{a}{2}$, respectively.

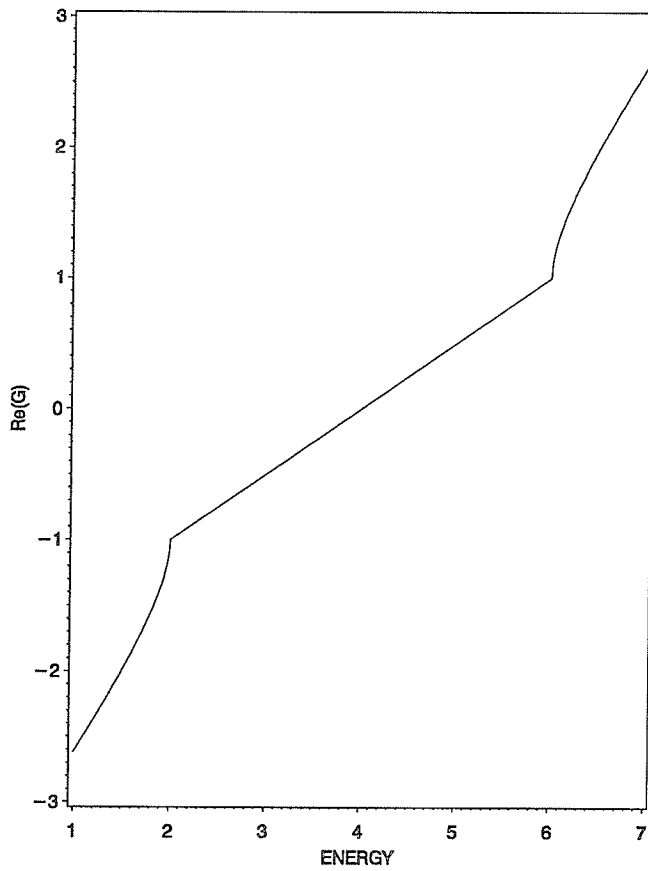


Figure 4.3: Real part of the density of states for constant coefficients. The value of $a = 4$ and $b = \frac{a}{2}$ in units of α_1 .

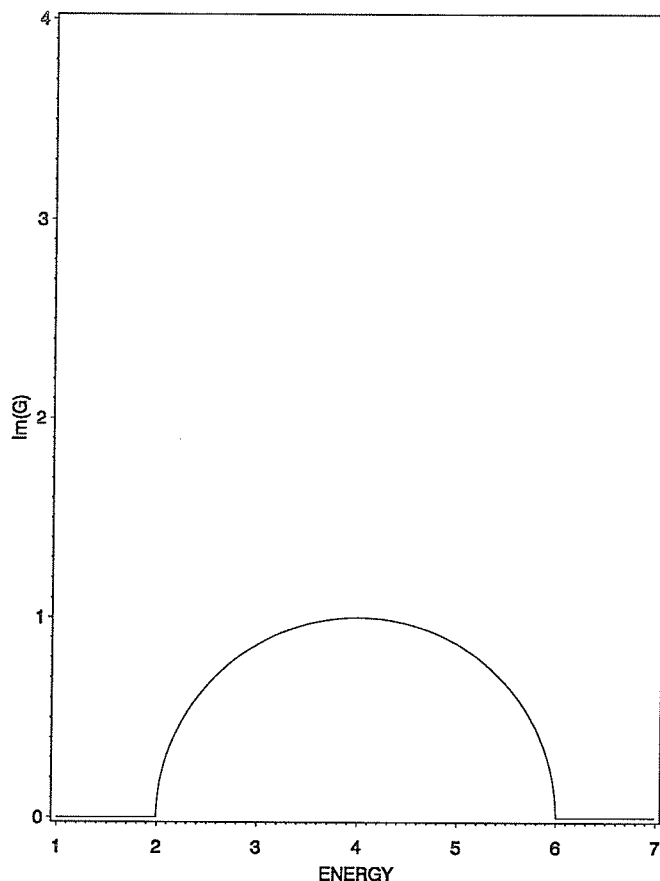


Figure 4.4: Imaginary part of the density of states for constant coefficients. The value of $a = 4$ and $b = \frac{a}{2}$ in units of α_1 .

4.3.2 Oscillating Coefficients

The asymptotic behaviour of the coefficients contain information about the general features of the scattering state band. C. Hodges [25] showed that internal Van Hove singularities led to oscillations in the coefficients but they eventually decay to give constant values of a_i and b_i if the recursion process was carried out far enough. The coefficients will always converge to constant values when there is a single band. However, multiple bands give rise to non-decaying oscillations of the coefficients. This has been extensively studied in the past, [26]–[29]. The analysis given below approaches the problem somewhat differently than in [26]–[29] and only the specific

case of a single gap is considered. However, the references given above provide a general analysis for multiple gaps.

Consider the asymptotic region in the continued fraction when the coefficients oscillate between exactly two a and b pairs, say, $a_1, b_2, a_2, b_1, a_1, b_2, a_2, \dots$. Then the Green's function can be represented by

$$G = \frac{1}{E - a_1 - G_\infty} \quad (4.24)$$

where

$$\begin{aligned} G_\infty &= \frac{b_2^2}{E - a_2 - \frac{b_1^2}{E - a_1 - \frac{b_2^2}{\dots}}} \\ &= \frac{b_2^2}{E - a_2 - \frac{b_1^2}{E - a_1 - G_\infty}} \\ &= \frac{1}{2(E - a_2)} \left\{ (E - a_1)(E - a_2) + b_2^2 - b_1^2 \right. \\ &\quad \left. \pm \sqrt{[(E - a_1)(E - a_2) + b_2^2 - b_1^2]^2 - 4b_2^2(E - a_1)(E - a_2)} \right\} \quad (4.25) \end{aligned}$$

Now, consider only the square root term

$$\begin{aligned} &[(E - a_1)(E - a_2) + b_2^2 - b_1^2]^2 - 4b_2^2(E - a_1)(E - a_2) = \\ &(E - a_1)^2(E - a_2)^2 - 2(E - a_1)(E - a_2)(b_1^2 + b_2^2) + (b_1^2 - b_2^2)^2 \quad (4.26) \end{aligned}$$

which can be factored to $(E - \lambda_1)(E - \lambda_2)(E - \lambda_3)(E - \lambda_4)$, where

$$\lambda_1 = \frac{1}{2} \left[a_1 + a_2 - \sqrt{(a_1 - a_2)^2 + 4(b_1 + b_2)^2} \right] \quad (4.27)$$

$$\lambda_2 = \frac{1}{2} \left[a_1 + a_2 - \sqrt{(a_1 - a_2)^2 + 4(b_1 - b_2)^2} \right] \quad (4.28)$$

$$\lambda_3 = \frac{1}{2} \left[a_1 + a_2 + \sqrt{(a_1 - a_2)^2 + 4(b_1 - b_2)^2} \right] \quad (4.29)$$

$$\lambda_4 = \frac{1}{2} \left[a_1 + a_2 + \sqrt{(a_1 - a_2)^2 + 4(b_1 + b_2)^2} \right] \quad (4.30)$$

with $\lambda_1 \leq \lambda_2 \leq \lambda_3 \leq \lambda_4$. To find the regions where the density of states is non-zero, the imaginary part of G is taken with $E = E + i\varepsilon$. Then the square root term can be expanded (for $\varepsilon \ll 1$) to give an imaginary part which is proportional to ε when $E < \lambda_1$, $\lambda_2 < E < \lambda_3$ or $E > \lambda_4$, so that in the limit of $\varepsilon \rightarrow 0$, the density of states is also 0. However, when $\lambda_1 \leq E \leq \lambda_2$ or $\lambda_3 \leq E \leq \lambda_4$ there is a term independent of ε in the expansion which gives a non-zero density of states for these regions. Hence, the λ_i may be identified with the E_i of two bands extending from $(E_1, E_2) = (\lambda_1, \lambda_2)$ and $(E_3, E_4) = (\lambda_3, \lambda_4)$ with a gap when $\lambda_2 \neq \lambda_3$. The graphical representation of the Green's function is shown below, taking the arbitrary values $a_1 = 4$, $a_2 = 6$, $b_1 = 1$ and $b_2 = 2$ (units of α_1).

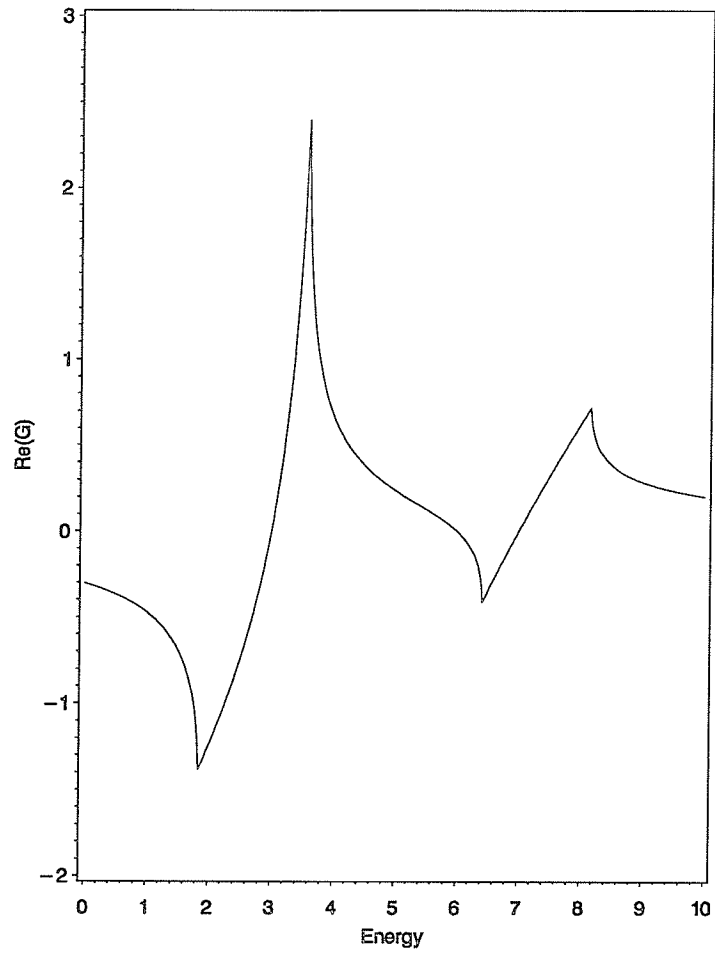


Figure 4.5: Real part of the density of states for alternating coefficients. The value of $a_1 = 4$ and $a_2 = 6$, $b_1 = 1$, $b_2 = 2$ in units of α_1 .

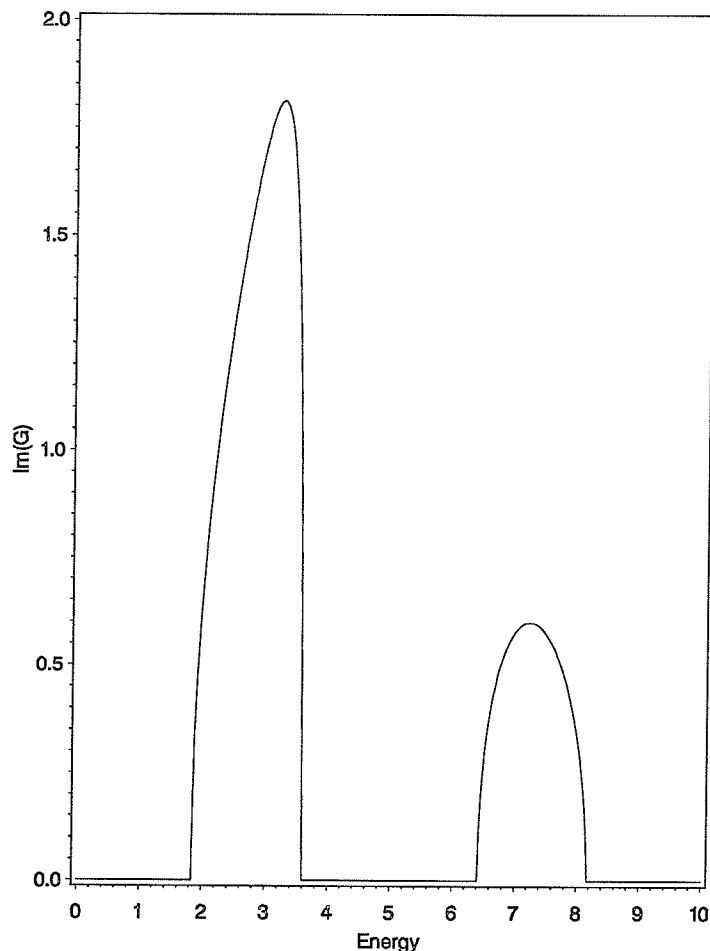


Figure 4.6: Imaginary part of the density of states for alternating coefficients. The value of $a_1 = 4$ and $a_2 = 6$, $b_1 = 1$, $b_2 = 2$ in units of α_1 .

In general, a sequence of a_i and b_i which has a more complicated pattern of oscillations produces more gaps in the scattering state continuum, but the oscillations and/or the Green's function is always characterized by an integral of the form $I = \int \frac{dt}{\sqrt{X(t)}}$ where $X(t) = \prod_{i=1}^{2n} (E_i - t)$ for n scattering state bands bounded by (E_1, E_2) , (E_3, E_4) , \dots , (E_{2n-1}, E_{2n}) . The integral is characteristic of a general class of periodic functions, Abelian or hyperelliptic functions, to which the usual trigonometric functions are but a special case.

The process of finding the periodic function from the energy spectrum is related to what is known as the Jacobi inversion problem and is treated generally by

M. Toda [28]. The method of solution for the inversion problem can be applied to extract the observed periods of the oscillations in the coefficients. This requires taking linear combinations of integrals, I , over various energy ranges.

There exist relations between the coefficients and the energy limits of the bands which can be used to show that the amplitude of the oscillations are related to the width of the gaps [29]. (Multiple gaps generate a sequence which will appear as several different oscillations superimposed on one another with the amplitude of each oscillation varying with the corresponding width of each gap.) For the case of one gap the oscillations in the coefficients are related to the simplest of the Abelian functions which are elliptic functions, and if the gaps are small, the amplitude of the oscillations are also small and the elliptic functions can be accurately approximated by trigonometric functions [29]. The calculation of the integrals requires knowledge of the energies of the edges of each band and fortunately, the asymptotic behaviour of the coefficients have little effect upon the energies of all the band edges and the bound states. The exact form of the termination equation only influences the shape and number of states within any bands. Therefore, the Green's function or density of states can be calculated by first approximating the tail of the continued fraction. Then, the energies for the band edges and bound states can be found to calculate a more accurate tail for the continued fraction. This in turn is used to find a Green's function which is a better representation of the density of states. The scattering state band did not actually have any gaps for any of the cases which we consider but the theory surrounding oscillations in the asymptotic values of the coefficients was useful in the understanding of a peculiar numerical effect which was observed. This is elaborated in the next section when we consider a specific example of the $S = \frac{1}{2}$ model.

4.4 Spin 1/2

The spin $\frac{1}{2}$ case is unique since all Hamiltonians of the form (1.4) are integrable regardless of the value of α_i , $i > 1$. Therefore, the solutions are well known and can be expressed analytically. The solutions must take the form used in the Bethe Ansatz, providing a means for a direct comparison between results obtained through the recursion method and exact results.

The application of the recursion method to this system requires the selection of an initial state which corresponds to a vertex on the Hamiltonian diagram, Fig. 3.1. Since the x and y coordinates represent the separation of the magnons, clearly the edges and the apex at the left are unphysical as this has x and/or y equal to zero and corresponds to a single spin being raised by more than one. When the parameters which describe the Hamiltonian ($\varepsilon_0, \varepsilon_1, \dots, \varepsilon_4, \varepsilon, v_0, v_1, v, u, w$) are evaluated, the unphysical layer completely decouples from the rest. Graphically, this unphysical Hamiltonian takes the form shown below

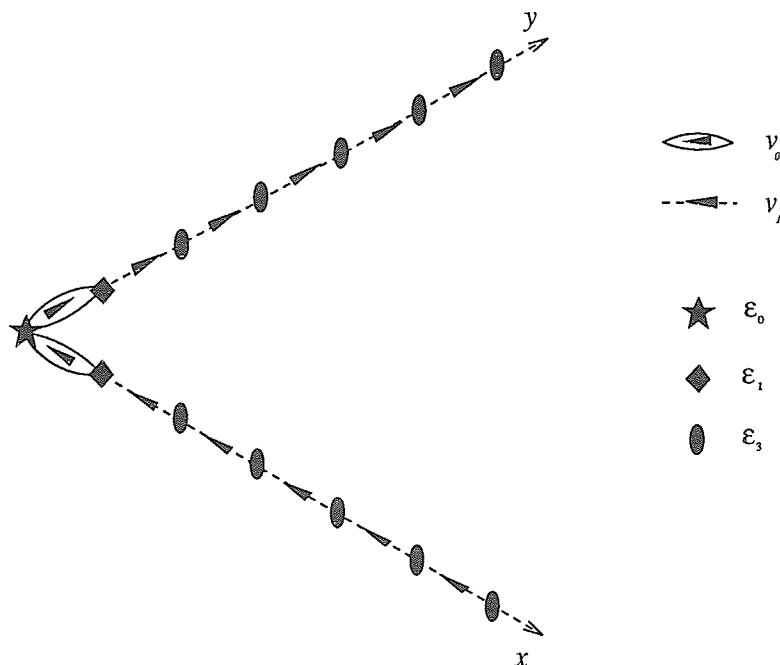


Figure 4.7: Graphical representation of the unphysical part of the Hamiltonian for $S = \frac{1}{2}$.

If the unphysical nature of these states are ignored and the recursion method applied using the states $u_0 = |0,0\rangle$ (a symmetric state) and $u_0 = \frac{1}{\sqrt{2}}(\zeta^*|1,0\rangle - \zeta|0,1\rangle)$ (anti-symmetric state), then the recursion coefficients converge extremely rapidly to constants and the Green's functions are given by

$$G_{\text{symm}} = \frac{4\sigma(E-1) - 1}{4\sigma(E-1)(E-3) - (E-3) + 6\sigma} \quad (4.31)$$

$$G_{\text{anti}} = \frac{4\sigma}{4\sigma(E-1) - 1} \quad (4.32)$$

where $\sigma = \frac{1}{2} \left[E - 3 \pm \sqrt{(E-4)(E-2)} \right]$. These functions have poles at $E = 2$ and $E = \frac{7}{8}$ respectively. Both of which are completely independent of the wavevector, K . This latter energy corresponds to one of the solutions found by Millet and Kaplan [22]. For the physical states it is known that there is a single bound state below the scattering state band which has a dispersion relation given by $E = \frac{\alpha_1}{3}(1 - \cos Ka)$. There is also a single connected scattering state band bounded by $E = \frac{\alpha_1}{2} \left[3 - \sqrt{4 \cos(Ka) + 5} \right]$ and $E = 3\alpha_1 \left[1 - \cos \left(\frac{K + 2\pi}{3} \right) \right]$. This band is comprised of two types of scattering states as described previously. There is a large degree of overlap between the two-bound one-free and the three-free continua, but the lower edges of both continua are quite close to each other while the upper edge of the two-bound one-free continuum (the smaller one) is far from any of the edges. This internal edge appears as a Van Hove singularity in the density of states.

When the recursion method is applied to any state contained within the physical part of the Hamiltonian the resulting coefficients rapidly converge (~ 20) to nearly constant values. However, the singularities in the continuum may produce visible oscillations which are still noticeable after a large number of iterations. It is therefore necessary to continue the method well beyond 20 iterations and, as the resulting states are normalized, the individual contribution of some of the kets will approach machine zero. This computer limitation has significant effects on the re-

sulting coefficients in the form of anomalously large deviations from the values to which the coefficients converge. These deviations can be demonstrated to be strictly numerical in origin by calculating the recursion coefficients at various precisions. For example, using single precision calculations in Fortran 77 the anomalous deviations repeat fairly regularly with a period of approximately 34 iterations and the first appears at the 38th iteration. The a_i are plotted below to 285 iterations at $K = \pi$ (Fig. 4.8).

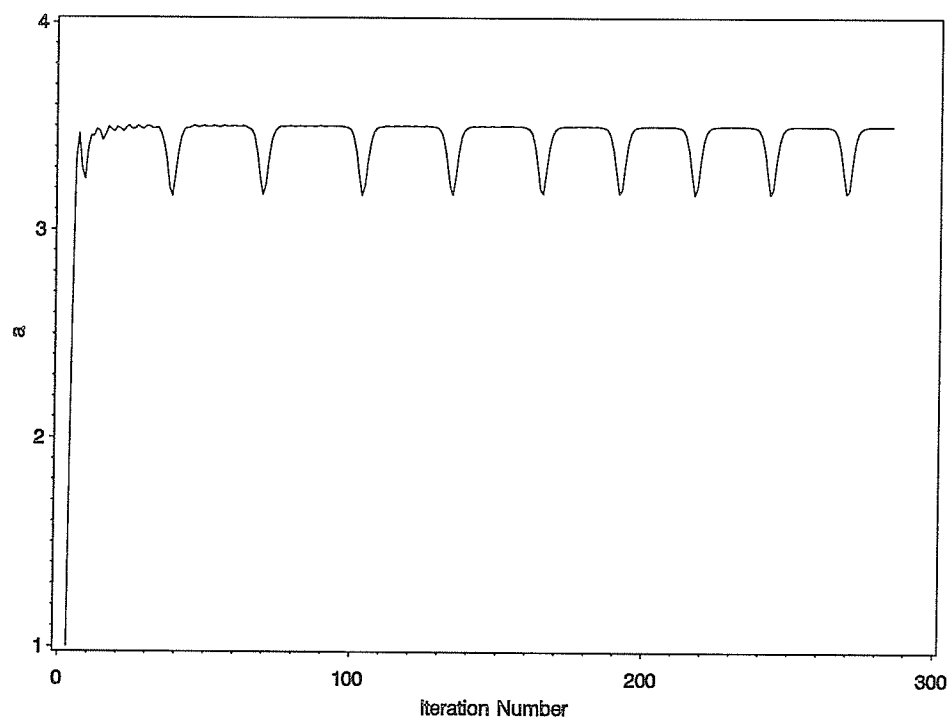


Figure 4.8: Single precision a_i recursion coefficients for $S = \frac{1}{2}$ at $K = \pi$.

By changing to double precision, the first deviation does not appear until the 77th iteration and the period of repetition is almost exactly double at 67 (see Fig. 4.9).

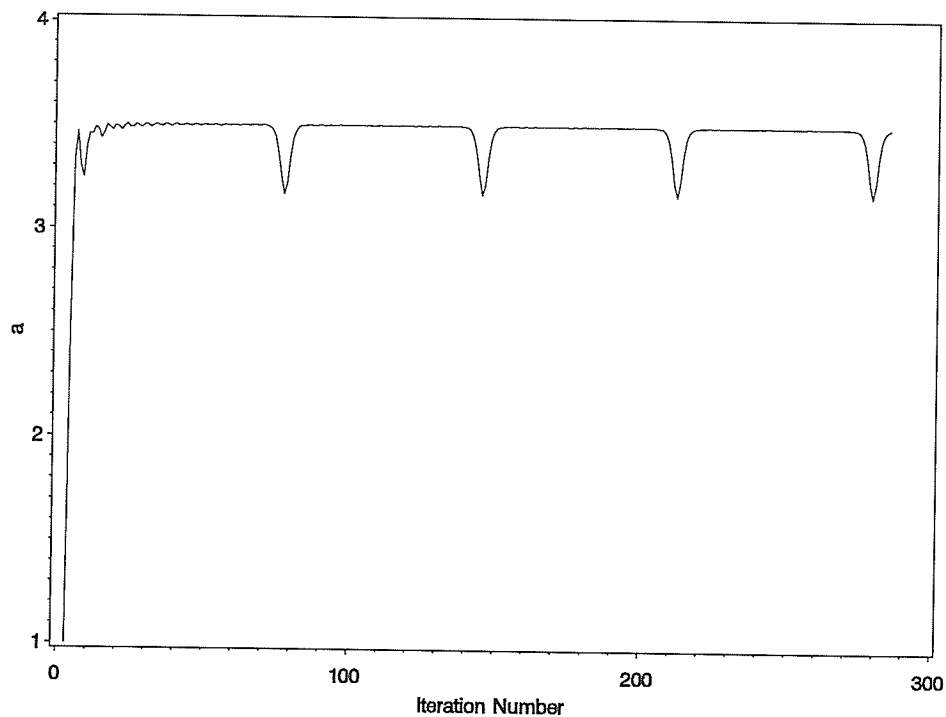


Figure 4.9: Double precision a_i recursion coefficients for $S = \frac{1}{2}$ at $K = \pi$.

Performing the calculation at quadruple precision moves the first deviation to the 152nd iteration. But due to limitations of the computer system used to provide the quadruple precision calculation, it was not possible to generate enough coefficients to determine a period.

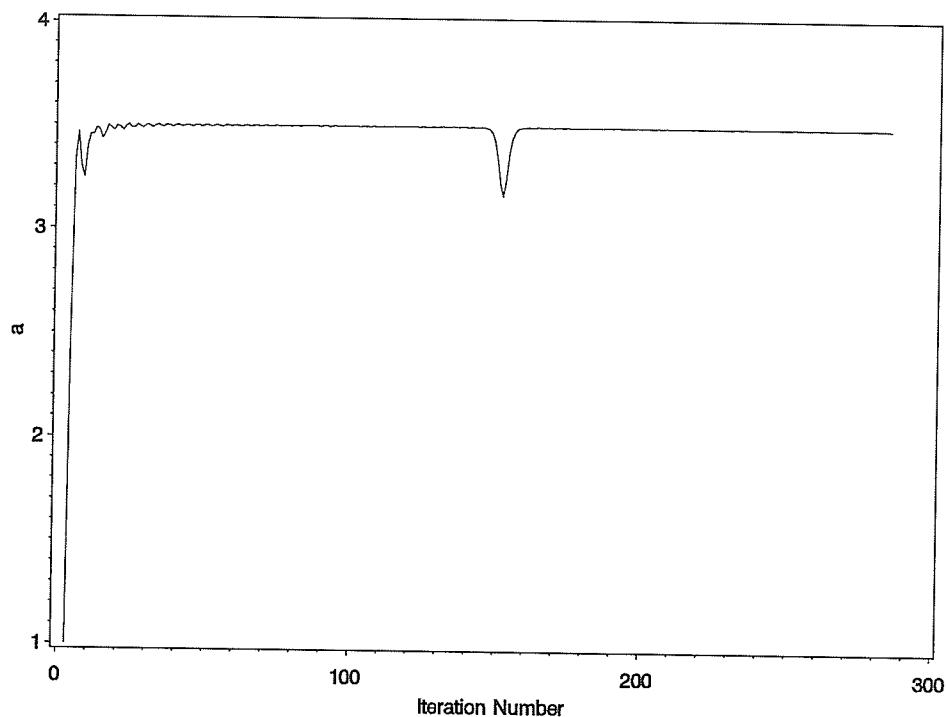


Figure 4.10: Quadruple precision a_i recursion coefficients for $S = \frac{1}{2}$ at $K = \pi$.

There is also a slight accumulation to the error, as can be seen in the single precision calculation. There is a slight decrease in the periods.

Aside from the small decrease in the period, the periodicity in the coefficients is quite consistent. It appears to be an unusual case of oscillations in the coefficients, which indicates a gap in the band. The exact solutions do not exhibit any such gap, however we can imagine one if the bound state is treated not as a delta function, but as having a very narrow but finite width equal to the smallest number that the computer cannot distinguish from zero for each precision. This interpretation is supported by the appearance of the coefficients in the graphs, above. As was given earlier, the behaviour of the coefficients are described by hyperelliptic (or Abelian) functions and in the limit of narrow bands these functions tend to have relatively abrupt peaks or valleys separated by wide flat regions (as shown in Toda [28]). The paper by Turchi et al. [29] gives an example of the analysis of a band with one gap. Following the same procedure, a similar analysis can be performed for this limit of a

very narrow band. The oscillations are characterized by a differential equation which contains a term of the form $\frac{dt}{\sqrt{X(t)}}$, which is also characteristic of an elliptic function

(when X is quartic in t). The function $X(t) = \prod_{i=1}^4 (E_i - t)$ requires knowledge of the energies of the edges for each band and at $K = \pi$ the energies for the scattering state band is 1 and 6 (units of α_1) and there is a bound state at $\frac{2}{3}$. Taking the double precision case and the machine accuracy to be approximately 10^{-14} , the energy bands extend from $(E_1, E_2) = (\frac{2}{3} - \frac{10^{-14}}{2}, \frac{2}{3} + \frac{10^{-14}}{2})$ and $(E_3, E_4) = (1, 6)$. One of the periods for the elliptic function can be taken to be

$$\begin{aligned}
K &= 2 \int_{E_2}^{E_3} \frac{dt}{\sqrt{X(t)}} \\
&= \frac{2 \cdot 2}{\sqrt{(E_4 - E_2)(E_3 - E_1)}} \mathcal{K}(q) \\
&= 2 \cdot 25.4816
\end{aligned} \tag{4.33}$$

where \mathcal{K} is the complete elliptic integral of the first kind and

$$q = \sqrt{\frac{(E_3 - E_2)(E_4 - E_1)}{(E_4 - E_2)(E_3 - E_1)}} \sim 1 \tag{4.34}$$

The second period can be related to $J = \int_E^{E'} \frac{dt}{\sqrt{X(t)}}$. There are two equivalent choices for $[E, E']$ up to a multiple of $\frac{K}{2}$, ie. $(-\infty, E_1]$ and $[E_4, \infty)$, so let

$$\begin{aligned}
J_1 &= \int_{-\infty}^{E_1} \frac{dt}{X(t)} \\
&= \frac{2}{\sqrt{(E_4 - E_2)(E_3 - E_1)}} \mathcal{F}(\mu, q) \\
&= 25.0985
\end{aligned} \tag{4.35}$$

$$\begin{aligned}
J_2 &= \int_{E_4}^{\infty} \frac{dt}{X(t)} \\
&= \frac{2}{\sqrt{(E_4 - E_2)(E_3 - E_1)}} \mathcal{F}(\nu, q) \\
&= 0.383119
\end{aligned} \tag{4.36}$$

taking

$$\begin{aligned}
\sin(\mu) &= \sqrt{\frac{E_4 - E_2}{E_4 - E_1}} \sim 1 \\
\sin(\nu) &= \sqrt{\frac{E_3 - E_1}{E_4 - E_1}} \sim \frac{1}{4}
\end{aligned} \tag{4.37}$$

and \mathcal{F} is the elliptic function of the first kind.

As the two J_1 and J_2 are equivalent it is easier to use small wavevectors and we shall take $J = J_2$. The period of the index for the recursion coefficients, n , is given by

$$\begin{aligned}
2nJ &= lK, \quad l \in \mathcal{Z} \\
n &= \frac{lK}{2J}
\end{aligned} \tag{4.38}$$

And using the smallest positive l , $n = 67$ (for the nearest integer) which is in agreement with the observed period.

The calculation can be generalized to an arbitrary band width, γ centred on an energy E so that $E_1 = E - \frac{\gamma}{2}$, $E_2 = E + \frac{\gamma}{2}$ and the other two band energies are E_3 and E_4 . Then

$$\begin{aligned}
K &= 2 \int_{E + \frac{\gamma}{2}}^{E_3} \frac{dt}{\sqrt{X(t)}} \\
&= \frac{2 \cdot 2}{\sqrt{(E_4 - E_2)(E_3 - E_1)}} \mathcal{K}(q)
\end{aligned} \tag{4.39}$$

and

$$\begin{aligned}
q &= \sqrt{\frac{(E_3 - E_2)(E_4 - E_1)}{(E_4 - E_2)(E_3 - E_1)}} \\
&= \sqrt{\left[\frac{1 + \frac{\gamma}{2(E_4 - E)}}{1 - \frac{\gamma}{2(E_4 - E)}} \right] \left[\frac{1 - \frac{\gamma}{2(E_3 - E)}}{1 + \frac{\gamma}{2(E_4 - E)}} \right]} \\
&= \left\{ \left[1 + \frac{\gamma}{E_4 - E} + \frac{\gamma^2}{2(E_4 - E)^2} + \frac{\gamma^3}{4(E_4 - E)^3} + \dots \right] \times \right. \\
&\quad \left. \left[1 - \frac{\gamma}{E_3 - E} + \frac{\gamma^2}{2(E_3 - E)^2} - \frac{\gamma^3}{4(E_3 - E)^3} + \dots \right] \right\}^{\frac{1}{2}} \quad (4.40)
\end{aligned}$$

Assuming $\gamma \ll E_3, E_4$

$$q = \sqrt{1 - \gamma \left[\frac{E_4 - E_3}{(E_4 - E)(E_3 - E)} \right]} \quad (4.41)$$

To be specific we can take the smallest of J_1 or J_2 to be

$$J = J_2 = \frac{2}{\sqrt{(E_4 - E - \frac{\gamma}{2})(E_3 - E + \frac{\gamma}{2})}} \mathcal{F}(\nu, q) \quad (4.42)$$

and

$$\sin(\nu) = \sqrt{\frac{E_3 - E + \frac{\gamma}{2}}{E_4 - E + \frac{\gamma}{2}}} \quad (4.43)$$

Then the period of the oscillations is related to

$$\frac{K}{2J} = \frac{\mathcal{K}(q)}{\mathcal{F}(\nu, q)} \quad (4.44)$$

and when $q \sim 1$, $\mathcal{F}(\nu, q) \sim \frac{2}{\pi} \mathcal{K}'(q) \ln \tan(\frac{\nu}{2} + \frac{\pi}{4})$, where q' is the complementary

modulus, defined by $q^2 + q'^2 = 1$. Then

$$\begin{aligned} \frac{K}{2J} &\sim \frac{\pi \mathcal{K}(q)}{2 \ln \tan(\frac{\nu}{2} + \frac{\pi}{4}) \mathcal{K}'(q')} \\ &\sim \frac{\pi}{2 \ln \tan(\frac{\nu}{2} + \frac{\pi}{4})} \left[\frac{\ln(\frac{4}{q'}) + \frac{1}{4}(\ln \frac{4}{q'} - 1)q'^2 + \dots}{\frac{\pi}{2}(1 + \frac{1}{4}q'^2 + \dots)} \right] \end{aligned} \quad (4.45)$$

As well,

$$\frac{1}{\ln \tan(\frac{\nu}{2} + \frac{\pi}{4})} \sim \frac{1}{\ln \tan(\frac{1}{2}\sqrt{\frac{E_3-E}{E_4-E}})} \left[1 + \frac{\gamma \sqrt{\frac{E_3-E}{E_4-E}}}{8 \ln \tan(\sqrt{\frac{E_3-E}{E_4-E}})} \right] \quad (4.46)$$

Since $q \sim 1 \rightarrow q' \sim 0$ and by ignoring all terms of order q'^2 or smaller then, (4.45) along with (4.41) and (4.46) gives

$$\begin{aligned} \frac{K}{2J} &\sim \frac{\ln(\frac{4}{q'})}{\ln \tan(\frac{\nu}{2} + \frac{\pi}{4})} \\ &\sim \frac{1}{\ln \tan(\frac{1}{2}\sqrt{\frac{E_3-E}{E_4-E}})} \left[1 + \frac{\gamma \sqrt{\frac{E_3-E}{E_4-E}}}{8 \ln \tan(\frac{1}{2}\sqrt{\frac{E_3-E}{E_4-E}})} \right] [\ln(4) - \ln(q')] \\ &\propto \gamma - \ln q' - \gamma \ln q' \\ &\propto \gamma \left[1 - \ln(\sqrt{1-q^2}) \right] - \ln(\sqrt{1-q^2}) \\ &\propto -\ln \left\{ 1 - 1 + \gamma \left[\frac{E_4 - E_3}{(E_4 - E)(E_3 - E)} \right] \right\} \\ &\propto -\ln(\gamma) \end{aligned} \quad (4.47)$$

This shows that the period of the anomalous deviations in the coefficients vary with the logarithm of the width of the narrow band (taken to be machine zero).

Another indication that the bound state is not being treated as a delta function can be shown by studying the relations between the coefficients. This was also done by Turchi et. al. [29] and was accomplished by comparing a series expansion of the Green's function from its continued fraction representation with a corresponding

series using the analytic expression for G_{00} . A relation was found between a_i , b_i and the limits of the energy bands. For a single gap, the exact relation is

$$(A^2 + E'A + E'' + 2B^2)^2 = X(-E' - A) \quad (4.48)$$

where A is related to the a_i coefficients but extended to a continuous variable and similarly B is related to b_i . Also,

$$E' = -\frac{1}{2} \sum_{i=1}^{2n} E_i \quad (4.49)$$

$$E'' = \frac{1}{2} \sum_{i < j} E_i E_j - \frac{1}{2} E'^2 \quad (4.50)$$

$$X(x) = \prod_{i=1}^{2n} (E_i - x) \quad (4.51)$$

Equation (4.48) can be viewed as a relation in the phase space of a_i and b_i^2 and is dependent upon the values used for the energies of the band edges. A change to any of the energies could alter its graphical appearance significantly. A plot is shown below for the double precision calculation. The solid line is (4.48), taking $E_1 = \frac{2}{3} - \frac{10^{-14}}{2}$, $E_2 = \frac{2}{3} + \frac{10^{-14}}{2}$, $E_3 = 1$ and $E_4 = 6$ and the two types of symbols represents (a_i, b_i^2) and (a_i, b_{i-1}^2) pairs. Because of the ambiguity of the numbering of the starting coefficient, the relation holds for both sets of pairs. The first 50 coefficients have been ignored as the analysis is valid only in the asymptotic region.

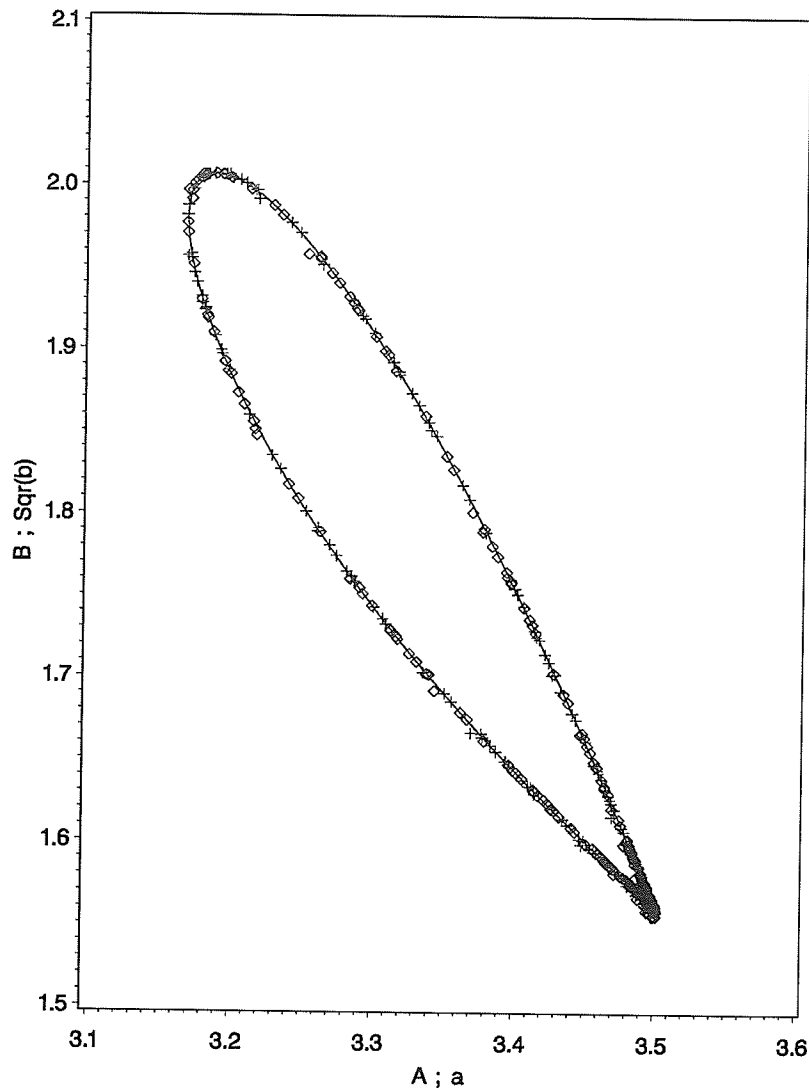


Figure 4.11: Phase space relation between a_i , b_i^2 (given by \diamond) and a_i , b_{i-1}^2 pairs (given by $+$).

The values where the coefficients are essentially constant appear at the lower right corner whereas the points which corresponds to a major deviation is distributed along the rest of the curve.

A final observation which can be obtained from Fig. 4.8–Fig. 4.10 is that the amplitude of the major deviations are essentially constant at 0.33 and the asymptotic value of a_i is 3.5. This in agreement with the predicted values. The asymptotic value of a_i should be the energy which corresponds to the middle of the continuum band, $\frac{1+6}{2} = 3.5$, and the amplitude should extend across the width of the gap,

$1 - \frac{2}{3} = \frac{1}{3}$. When the bound state is below the continuum the deviations, for the a_i coefficients, extend to values less than the asymptotic a . But a bound state above the band would generate a sharp peak rather than the valleys, as in Fig. 4.8–Fig. 4.10, and although these deviations are a numerical effect they can be used to locate the position of bound states if they are separated from the continuum by a large enough gap to produce visible oscillations.

The accuracy that the phase space relation agrees with the data, along with the ability to calculate the period of repetition of the anomalous deviations and the shift of the deviations with changes in the accuracy of the calculations, are convincing arguments for regarding the deviations as simply numerical limitations of the computer system which was used. These limitations result in a non-zero width for the bound state but do not affect the energy of any bound state or band edges. The inclusion of the deviations only alters the magnitude of the density of states slightly and since only the local density of states is considered, this is of little consequence. Therefore, the constant termination can be used while carrying out the recursion calculations to a large number of iterations (to ensure that the asymptotic region has been reached) without concern that the deviations are altering any results. These observations are presented in the next chapter for various Hamiltonians and for several values of S .

Chapter 5

Non-Integrable Models

The recursion method described in the previous chapter was implemented using Fortran 77 and applied to several general systems containing three magnon excitations. The size of the spins on the chain naturally divide into several classes. When $S = \frac{1}{2}$ only the uniform part of the diagrammatic representation of the Hamiltonian (Figure 3.1) defines the behaviour of the system for the physical states. This was described in the previous chapter and agrees completely with the results obtained by Bethe [7]. When $S = 1$, the physical part of the Hamiltonian includes the edges of the diagram (Figure 3.1) but not the single ket, $|x, y\rangle = |0, 0\rangle$. Since there are differences in the effective Hamiltonian between the two cases, qualitative differences in the behaviour of the system is expected. Similarly if $S = \frac{3}{2}$, the effective Hamiltonian changes once more and includes $|0, 0\rangle$. However, if $S > \frac{3}{2}$, the effective Hamiltonian no longer changes and no significant qualitative differences are expected (for three magnon excitations), in terms of the energies of the bound states and continuum edges for corresponding wavevectors. Therefore, only systems with $S = \frac{1}{2}, 1, \frac{3}{2}$ were studied. For each value of the spin, the Hamiltonian may be changed by altering the value of α_2 or α_3 . These parameters can be changed continuously over all non-negative values so that an infinite number of models can be studied. In general, only the behaviour near the integrable models of Takhtajan and Babujian ([10], [11]) are of interest and the values for α_i were kept relatively close to this integrable point.

In order to observe the behaviour of any particular system, a set of 500 recursion coefficients were generated for several fixed values of total wavevector, K , over the non-negative half of the first Brillouin Zone. The results are presented using the reduced zone representation and the Brillouin Zone is symmetric about $K = 0$ so only one-half of the zone is needed to determine the systems' behaviour over the entire zone. Mostly, the values chosen for the total wavevector were (in units of $\frac{\pi}{a}$) $0, \frac{1}{4}, \frac{1}{2}, \frac{3}{4}$ and 1 . Occasionally, it was necessary to use several more choices of wavevectors in certain energy ranges in order to obtain a more complete picture of the behaviour of the system.

The generated set of coefficients were used in calculating the Green's function for any energy range of interest, for the particular wavevector which was used to generate the set of recursion coefficients. Any bound states were clearly identified as such since they virtually appeared as delta functions but most resonant states could not be as easily distinguished from singularities for many of the systems which were studied. The method of classification of peaks into resonances and singularities was highly subjective and mainly involved choosing several relatively large peaks as possible resonances and observing their behaviour as the total wavevector was changed. Since the change in wavevector was always discrete, it could not be certain which peaks correspond to the same structure between different wavevectors and this difficulty was resolved by simply assuming the peaks would move smoothly across the Brillouin Zone.

The size of any resonant peaks is dependent upon the choice of initial ket and a number of different choices were tried for a few models, but it was observed that the structures in the density of states have edges with energies that are essentially independent of the choice of the initial ket. The main exception was those choices of initial ket which have symmetries that mirror a symmetry of the Hamiltonian such as kets with the relative coordinates $x = y$ (ie. kets along the central horizontal axis of the diagram, Figure 3.1) or an antisymmetric combination of kets. This effect

was particularly evident for the $S = \frac{3}{2}$ Heisenberg model where one bound state can be removed by choosing a completely symmetric initial state (see Fig. 5.24). For convenience, the initial state was almost always chosen to be $|x, y\rangle = |1, 0\rangle$ and is a combination of symmetric and antisymmetric kets.

In order to observe the differences between the general models and the integrable ones, the models of Takhtajan and Babujian will be described briefly. The dispersion diagrams for the $S = 1$ and $S = \frac{3}{2}$ are shown below.

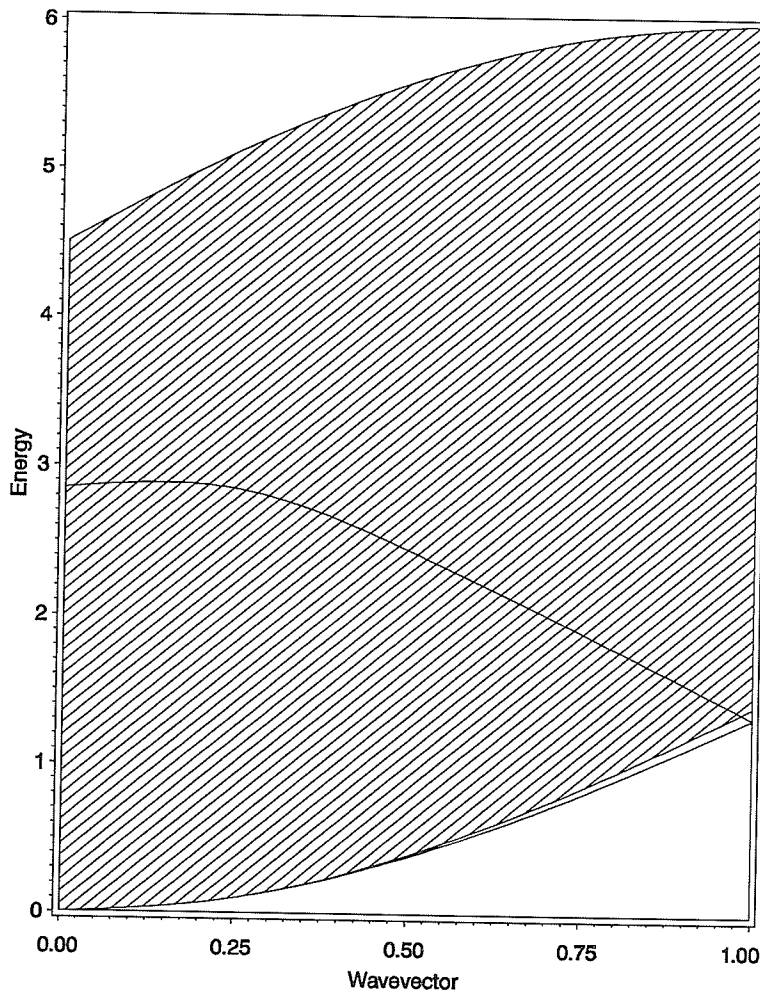


Figure 5.1: Behaviour of three magnon excitations for an integrable model $S = 1$ spin chain. Energy in units of α_1 and K in units of $\frac{\pi}{a}$. The solid lines are bound states, and the shaded region is the scattering state continuum.

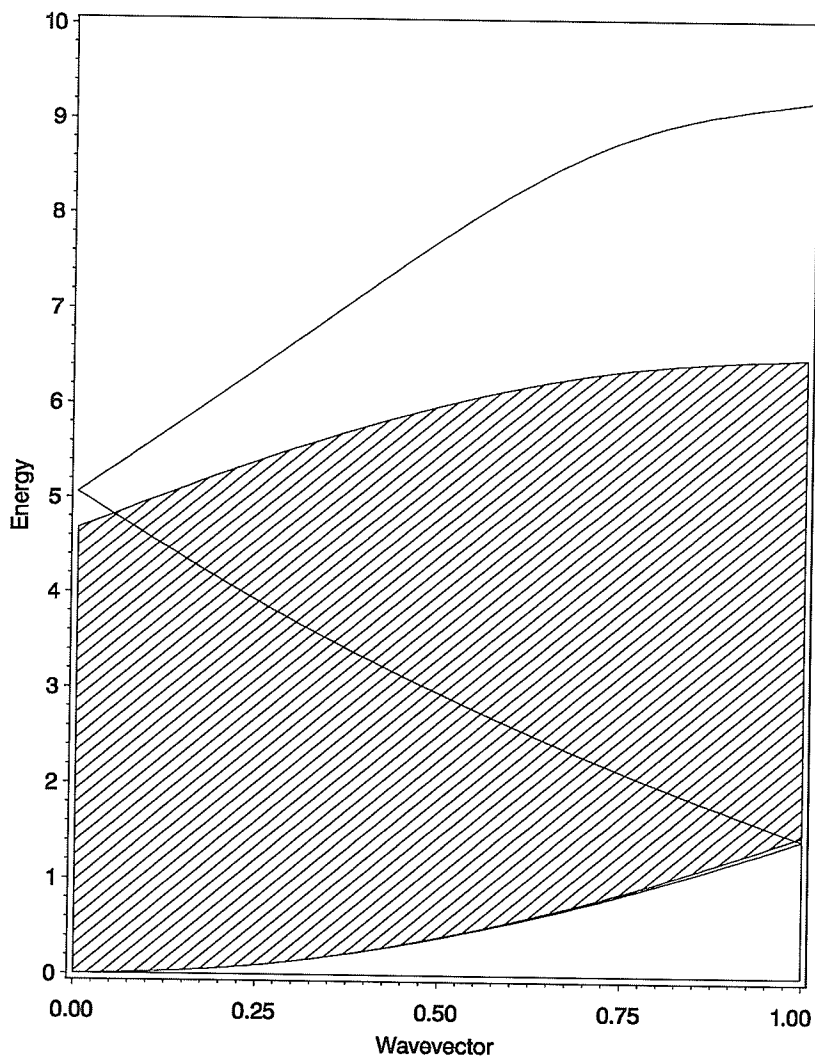


Figure 5.2: Behaviour of three magnon excitations for an integrable model $S = \frac{3}{2}$ spin chain. Energy in units of α_1 and K in units of $\frac{\pi}{a}$. The solid lines are bound states, and the shaded region is the scattering state continuum.

In both the $S = 1$ and the $S = \frac{3}{2}$ cases, the bound state branches meet exactly at the Brillouin zone boundaries and these remain true bound states across the entire Brillouin zone even for the middle branch. (In an extended zone representation it can be seen that the branches do not actually enter the continuum and hence do not become resonances.) The number of branches is determined by the minimum of $2S$ or the number of magnons which are present in the system (in this case 3). These

integrable models appear when the parameters of the Hamiltonian, $g_2 = \frac{4S - 1}{2S - 1}$ and $g_3 = \frac{6S^2 - 6S + 1}{2S^2 - 3S + 1}$.

5.1 Spin 1

When the spin is $\frac{1}{2}$, the model is independent of α_2 and α_3 so that the only available parameter simply results in a scaling of the energy (when only the energy positions of the bound states and the continuum edges are considered). This was mostly described in the previous chapter so we will start with the $S = 1$ case. Consider the Heisenberg model which is quite far from integrability. The density of states for $S = 1$ for each of the five choices of wavevector are shown below, Fig. 5.3 – Fig. 5.11.

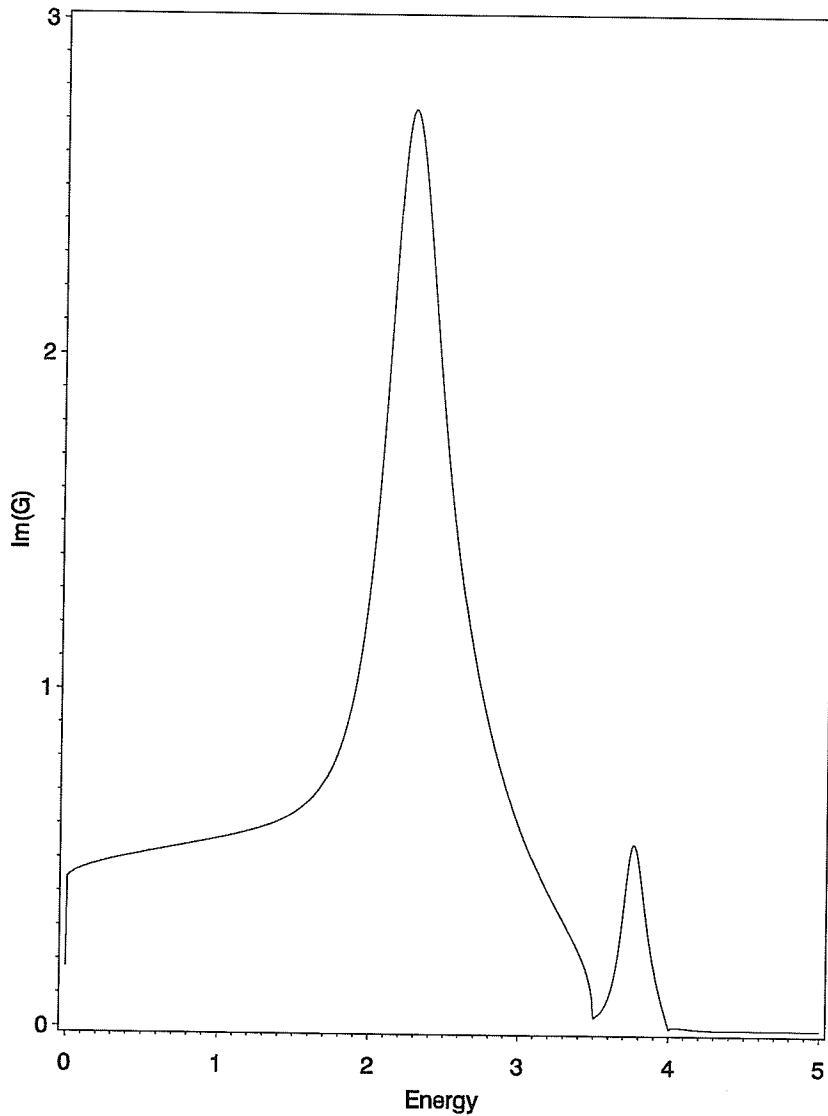


Figure 5.3: Density of states for three magnon excitation Heisenberg model, $S = 1$ spin chain at $K = 0$.

For $K = 0$ there are two peaks (Fig. 5.3, above). The one with the lower energy is a resonance with an energy at approximately $E = 2.25$. The classification of the peak as a resonance was made by observing its behaviour across the Brillouin zone. In Fig. 5.4–Fig. 5.11 the resonance decreases in energy until it leaves the band and becomes a bound state from $K \in [0.96\frac{\pi}{a}, \frac{\pi}{a}]$. The second peak also decreases in energy as K goes to $\frac{\pi}{a}$ but remains inside the band and becomes part of the internal structure. (The peak at $E = 2$ in Fig. 5.10.) There is also a bound state which

appears to remain outside and below the continuum (as can be seen in the other diagrams, Fig. 5.4 – Fig. 5.11) and this bound state is assumed to be at $E = 0$ (the lower edge of the continuum) at $K = 0$.

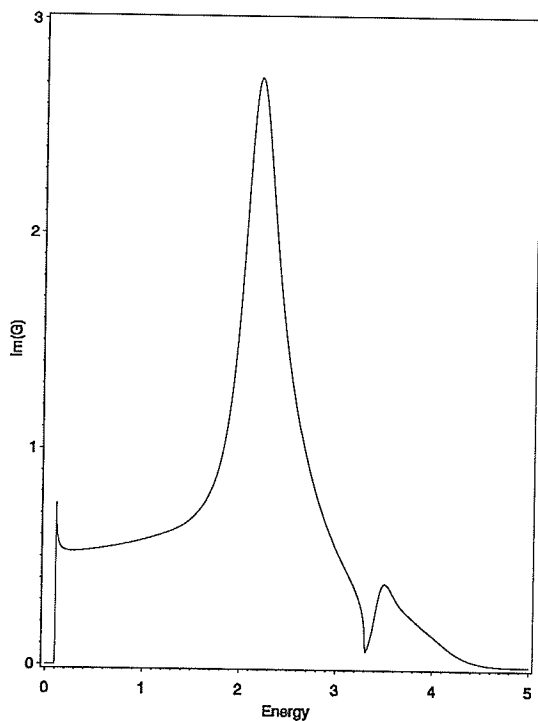


Figure 5.4:
Density of states for three magnon excitations, Heisenberg model $S = 1$ spin chain at $K = \frac{\pi}{4a}$.

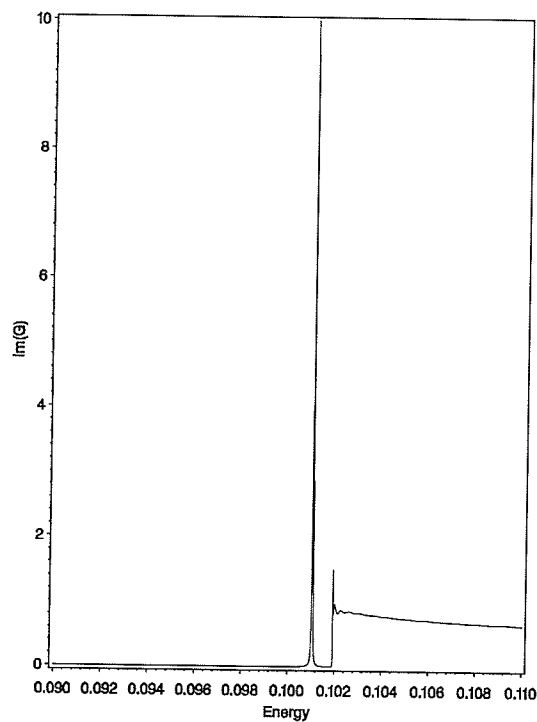


Figure 5.5:
Density of states near the bound state for the Heisenberg model $S = 1$ spin chain at $K = \frac{\pi}{4a}$.

The Green's function for a much smaller energy range for $K = \frac{1}{4}, \dots, 1$ (units of $\frac{\pi}{a}$) is shown in Fig. 5.5, 5.7, 5.9 and 5.11 to show the bound state(s) which are below the continuum more clearly.

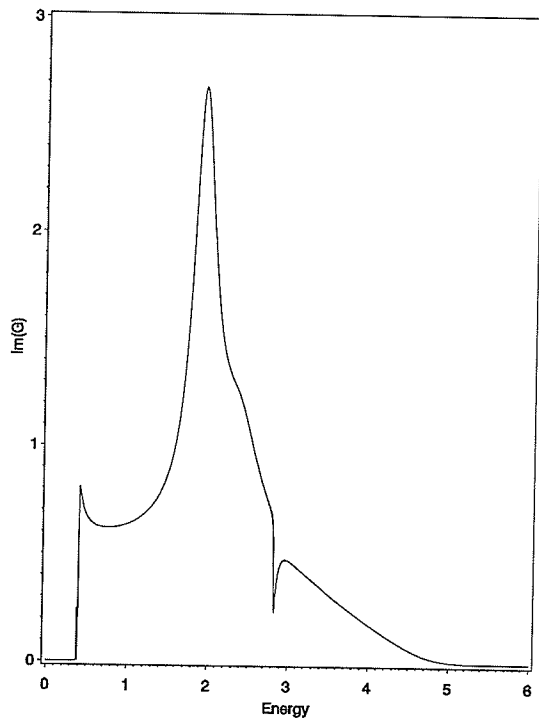


Figure 5.6:
Density of states for three magnon excitations, Heisenberg model $S = 1$ spin chain at $K = \frac{\pi}{2a}$.

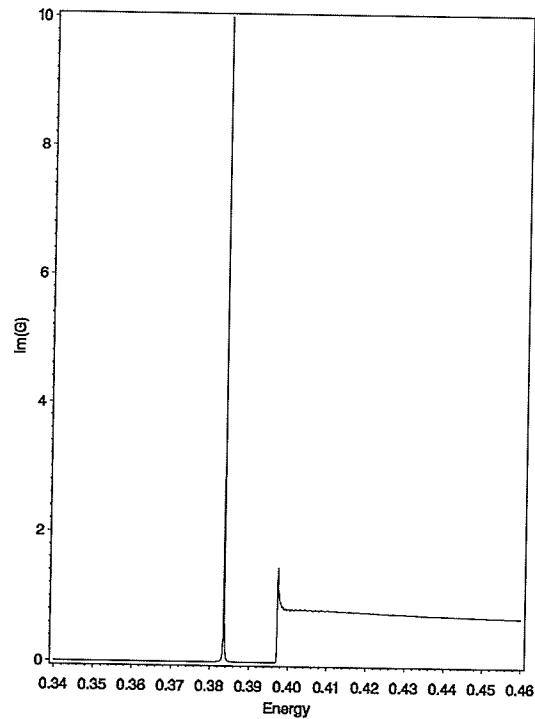


Figure 5.7:
Density of states near the bound state for the Heisenberg model $S = 1$ spin chain at $K = \frac{\pi}{2a}$.

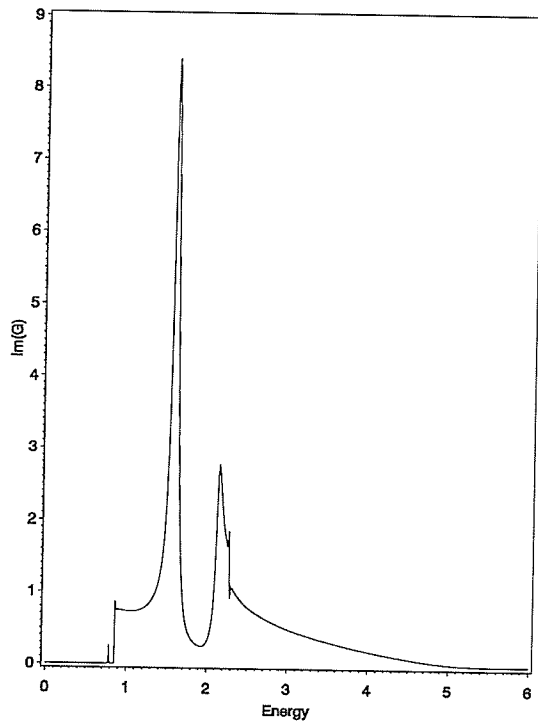


Figure 5.8:
Density of states for three magnon excitations, Heisenberg model $S = 1$ spin chain at $K = \frac{3\pi}{4a}$.

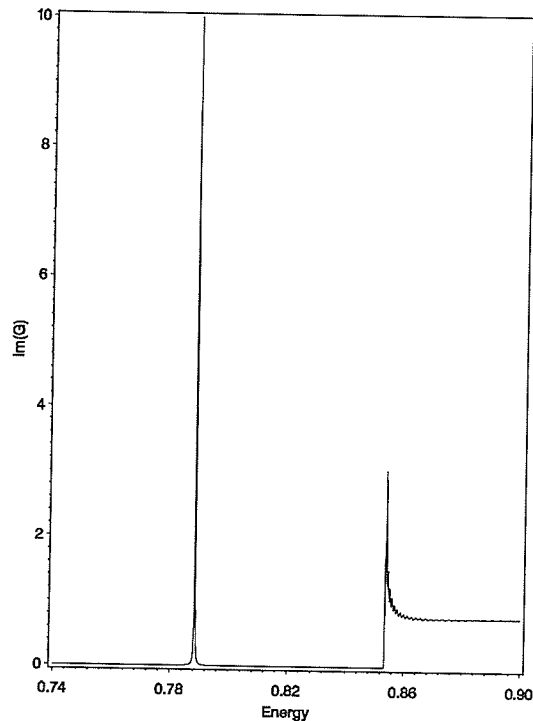


Figure 5.9:
Density of states near the bound state for the Heisenberg model $S = 1$ spin chain at $K = \frac{3\pi}{4a}$.

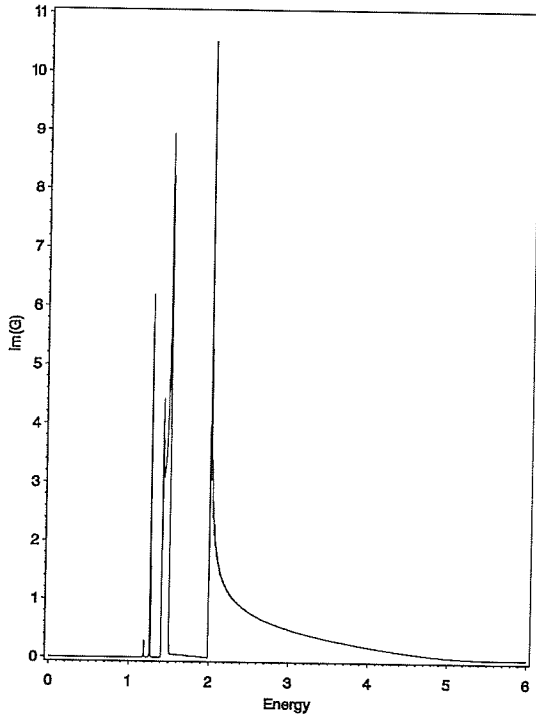


Figure 5.10:
Density of states for three magnon excitation Heisenberg model $S = 1$ spin chain at $K = \frac{\pi}{a}$.

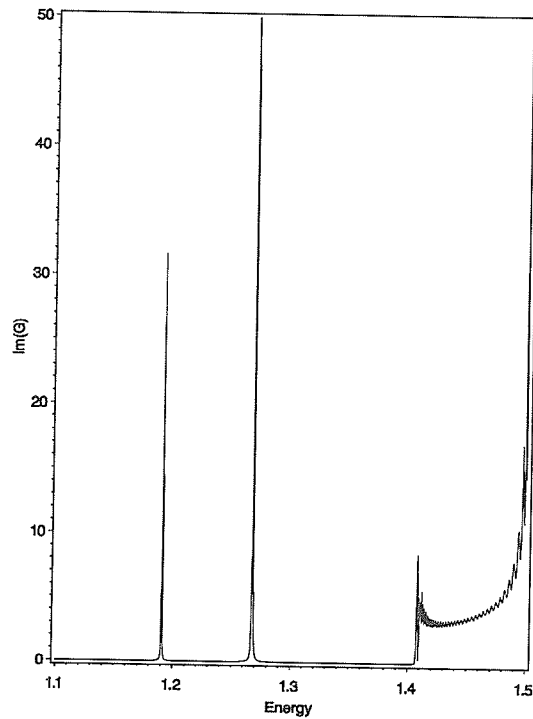


Figure 5.11:
Density of states near the bound state for the Heisenberg model $S = 1$ spin chain at $K = \frac{\pi}{a}$.

Although the recursion procedure was carried to 500 iterations, the coefficients were still not exactly constants but due to constraints with the amount of computer resources which was available (specifically memory) the procedure was stopped and the square root terminator, (4.18), was used for the tail of the Green's function. This had the effect of introducing small oscillations into the density of states which are not visible unless the Green's function is calculated over a very small range of energies. However, the continuum edges can be found very accurately using knowledge of the two magnon spectrum and it is evident that the delta function(s) shown in the diagrams, Fig. 5.4 – Fig. 5.11 are detached from the continuum and not due to these small oscillations within the continuum. This is also suggested by the behaviour of the coefficients for the values of K near the Brillouin zone boundary. For example, the $K = \frac{\pi}{a}$ set of coefficients, Fig. 5.12, show two separate sets of deviations, both of which are due to the limitations of the computer system used to

calculate the coefficients. The computer limitation enables the bound states to act as narrow bands, as described previously (Chapter 4). The smaller amplitude deviations correspond to the bound state which eventually crosses into the continuum to give a resonance, shown in Fig. 5.3, 5.4, 5.6 and 5.8, and the larger deviation corresponds to the bound state which does not enter the continuum for all values of K .

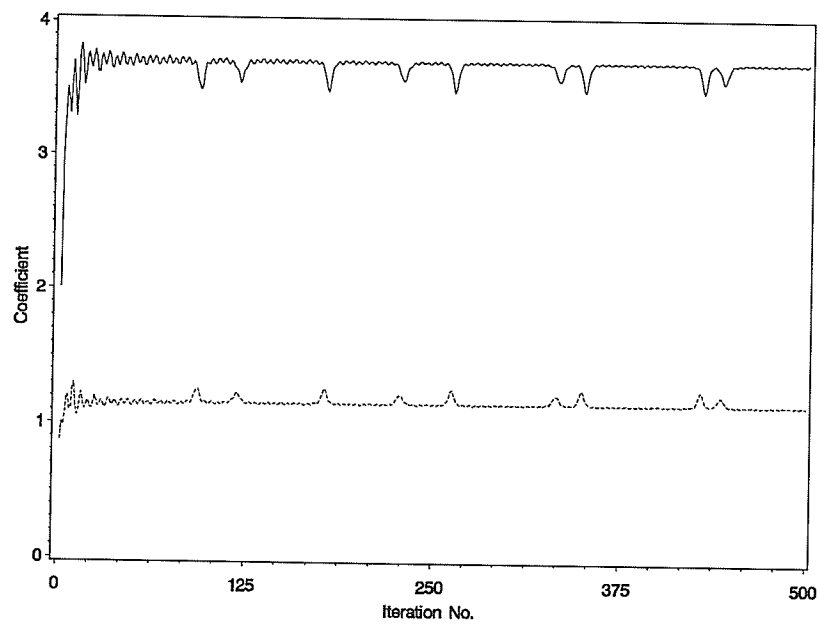


Figure 5.12: Double precision a_i coefficients (solid line) and b_i (dashed line) for a $S = 1$ Heisenberg model spin chain at $K = \frac{\pi}{a}$.

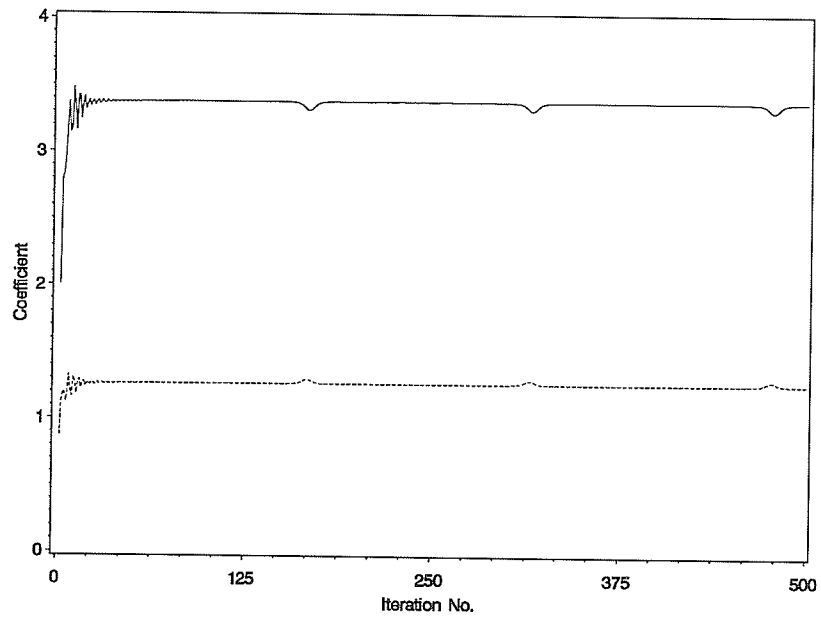


Figure 5.13: Double precision a_i coefficients (solid line) and b_i (dashed line) for a $S = 1$ Heisenberg model spin chain at $K = \frac{3\pi}{4a}$.

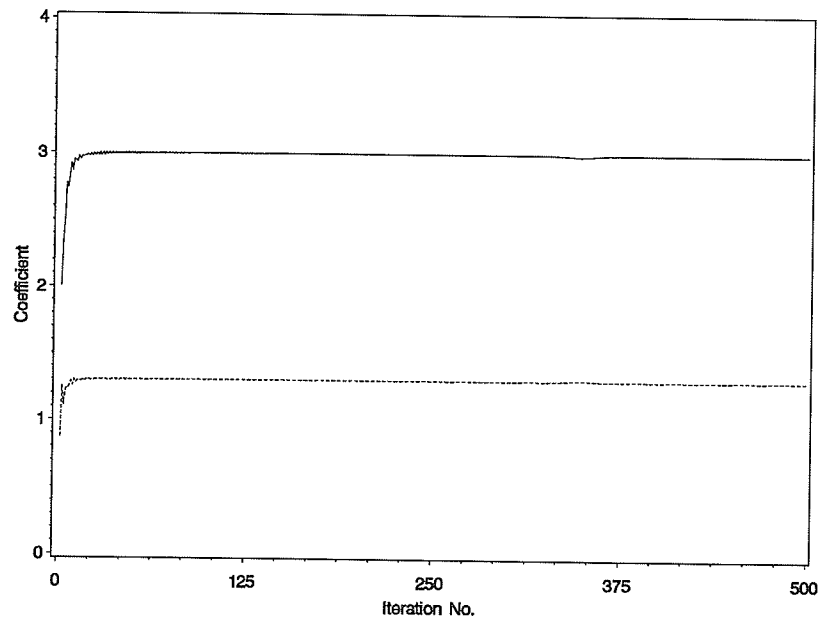


Figure 5.14: Double precision a_i coefficients (solid line) and b_i (dashed line) for a $S = 1$ Heisenberg model spin chain at $K = \frac{\pi}{2a}$.

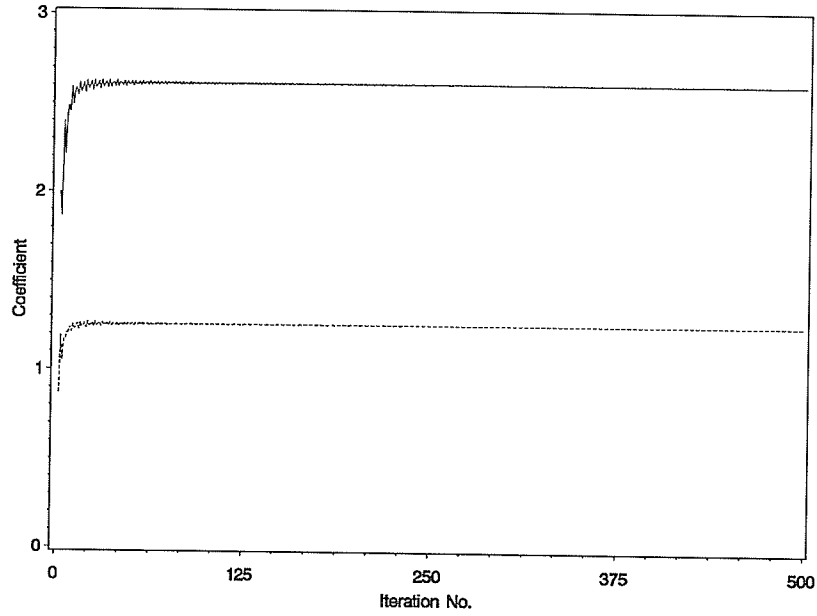


Figure 5.15: Double precision a_i coefficients (solid line) and b_i (dashed line) for a $S = 1$ Heisenberg model spin chain at $K = \frac{\pi}{4a}$.

Fig. 5.13 only shows one deviation since the second bound state is already in the continuum for the value of $K = \frac{3\pi}{4a}$. The coefficients are also shown for $K = \frac{\pi}{2a}$ and $\frac{\pi}{4a}$ simply for comparison to the $K = \frac{\pi}{a}$ and $\frac{3\pi}{4a}$ coefficients. The behaviour of all these features can be summarized by plotting the bound state energies against K across the non-negative half of the Brillouin zone as in Fig. 5.16. The resonance is represented by the dashed line and the bound states by the solid lines. The continuum is indicated by the shaded region.

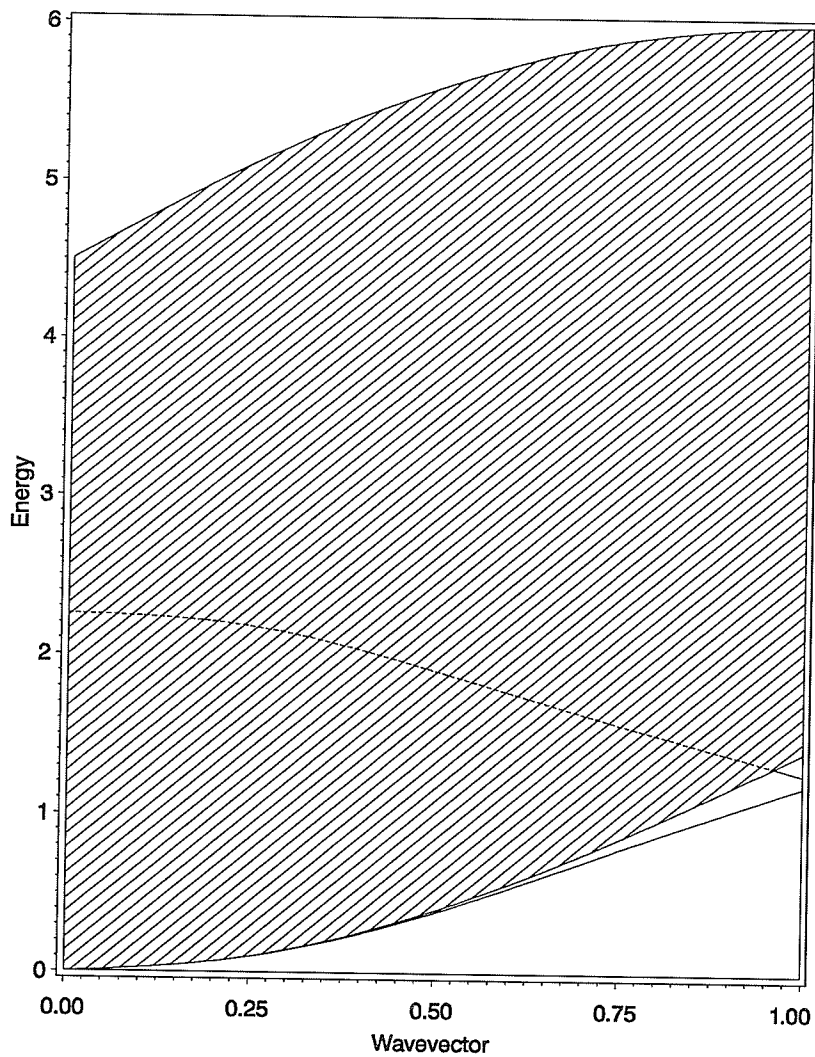


Figure 5.16: Behaviour of three magnon excitations for a Heisenberg model $S = 1$ spin chain. Energy in units of α_1 and K in units of $\frac{\pi}{a}$. The solid lines are bound states, the dashed line are resonances and the shaded region is the scattering state continuum.

As the value of g_2 changes from 1.5 (the value for the Heisenberg model at $S = 1$) to 3 (the value for the integrable model at $S = 1$), the gap between the bound states at the Brillouin zone boundary shrinks until they exactly meet when $g_2 = 3$. The gap appears and grows whether g_2 is changed to a value greater or less than 3. A dispersion diagram is shown in Fig. 5.17 for a value of g_2 which is intermediate between the Heisenberg model and the integrable model.

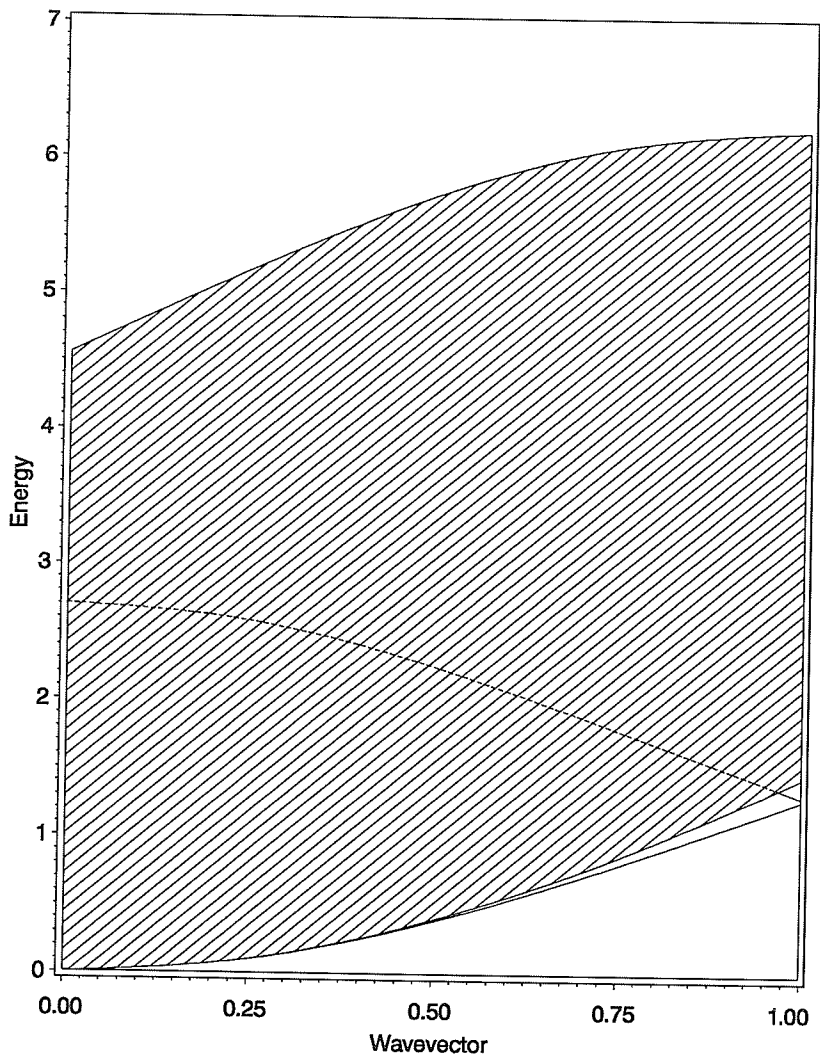


Figure 5.17: Behaviour of three magnon excitations for $g_2 = 2.25$ on a $S = 1$ spin chain. Energy in units of α_1 and K in units of $\frac{\pi}{a}$. The solid lines are bound states, the dashed line are resonances and the shaded region is the scattering state continuum.

The bound state branches are much closer at the Brillouin Zone boundary and the bound state intersects the lower edge of the continuum at $K = 0.969\frac{\pi}{a}$. However the shape of the continuum, in the dispersion diagrams, Fig. 5.16 and Fig. 5.17, does not change significantly. A dispersion diagram is also shown for $g_2 > 3$ in Fig. 5.18.

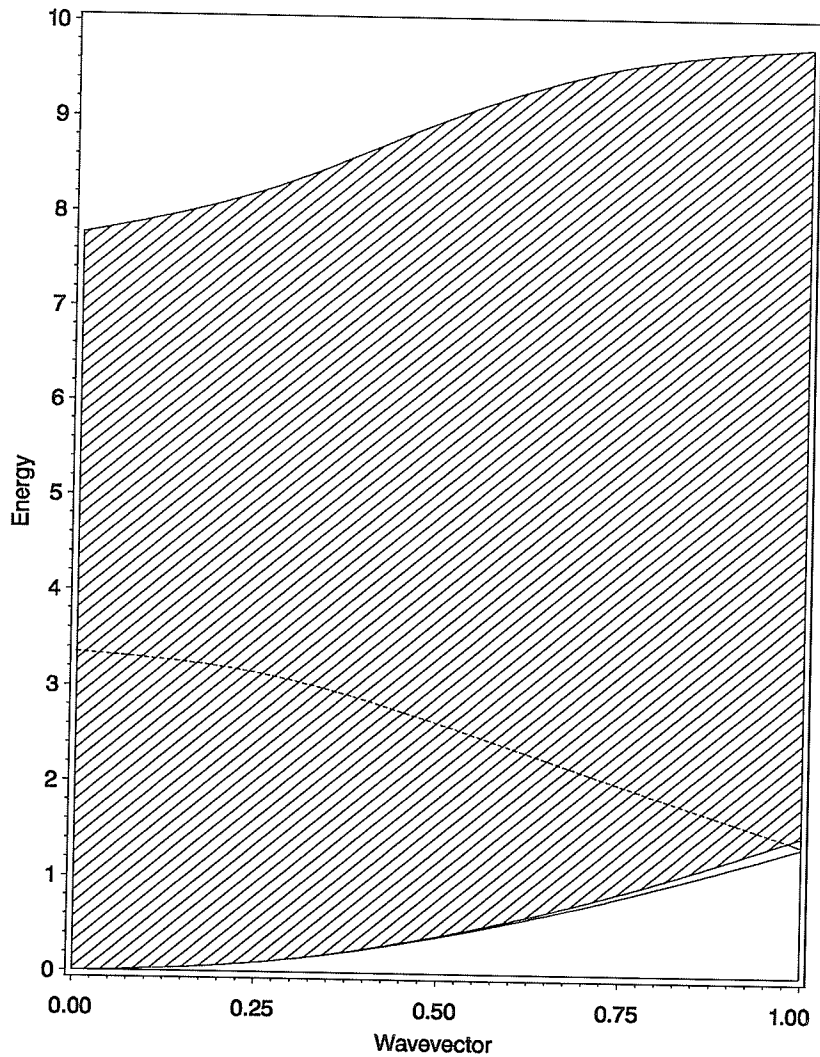


Figure 5.18: Behaviour of three magnon excitations for $g_2 = 4.5$ on a $S = 1$ spin chain. Energy in units of α_1 and K in units of $\frac{\pi}{a}$. The solid lines are bound states, the dashed line are resonances and the shaded region is the scattering state continuum.

For this case the gap is still fairly small (slightly over $\frac{1}{3}$ the size of the gap in the Heisenberg model) and it crosses the lower continuum edge at $K = 0.981 \frac{\pi}{a}$.

One integrable case was mentioned previously but the recursion procedure was needed to obtain any solutions for it. This was the Temperley-Lieb model for $S = 1$ and corresponds to $\alpha_1 = 0$ and $\alpha_2 = \alpha$ (a constant). When the recursion method is applied to this system, a single delta function is seen in the density of states along

with one continuum. Neither the delta function nor the continuum change size or position for all $K \in [0, \pi]$ (ie. independent of K). The delta function has an energy of 0 and the edges of the continuum are at $\frac{\alpha_1}{3}$ and $\frac{5\alpha_1}{3}$. The shape of the density of states for the continuum resembles that for the one magnon case, that is, there are sharp peaks at each continuum edge and there are low values in the middle (see Figure 4.2). Most of the kets decouple for this model (ie. all kets with relative coordinates $x, y \geq 2$ and $|0, 0\rangle$) and all of these are degenerate with an energy of 0 except for the unphysical state, $|0, 0\rangle$. Further, the value of α_1 is 0 for this model so that all the single magnon states are also degenerate with the decoupled physical states. Since the initial ket chosen was not one of the decoupled states, the delta functions which are observed represent the energy from the one magnon states such as the three-free continuum and the free magnon for the two-bound, one-free continuum. The band gives the energy range for the two magnon bound state (from the two-bound, one-free continuum) in agreement with the results of Parkinson [8].

5.2 Spin 3/2

When the spin is increased to $\frac{3}{2}$ both α_2 and α_3 influence the effective Hamiltonian so that the model can be shifted away from integrability by changing either or both. The option of changing α_2 and α_3 simultaneously was not studied in depth except for a few isolated cases. The most notable of these was the Heisenberg model.

First consider a Hamiltonian when g_2 (α_2) is changed from the integrable value of 2.5 for $S = \frac{3}{2}$ but g_3 (α_3) is set to 5.5 (the integrable value at $S = \frac{3}{2}$). As predicted by Haldane [12], [13], gaps appear between the bound state branches at the Brillouin zone boundaries as the model moves away from integrability and the gaps grow the further the model is from the integrable point. However, there are other properties which can be seen. For example, there are always at least two bound state branches for the values of $g_2 \in [1, 5] \forall |K| > 0$. The dispersion diagram for the extremes of this range is given in Fig. 5.19 and in Fig. 5.20, below.

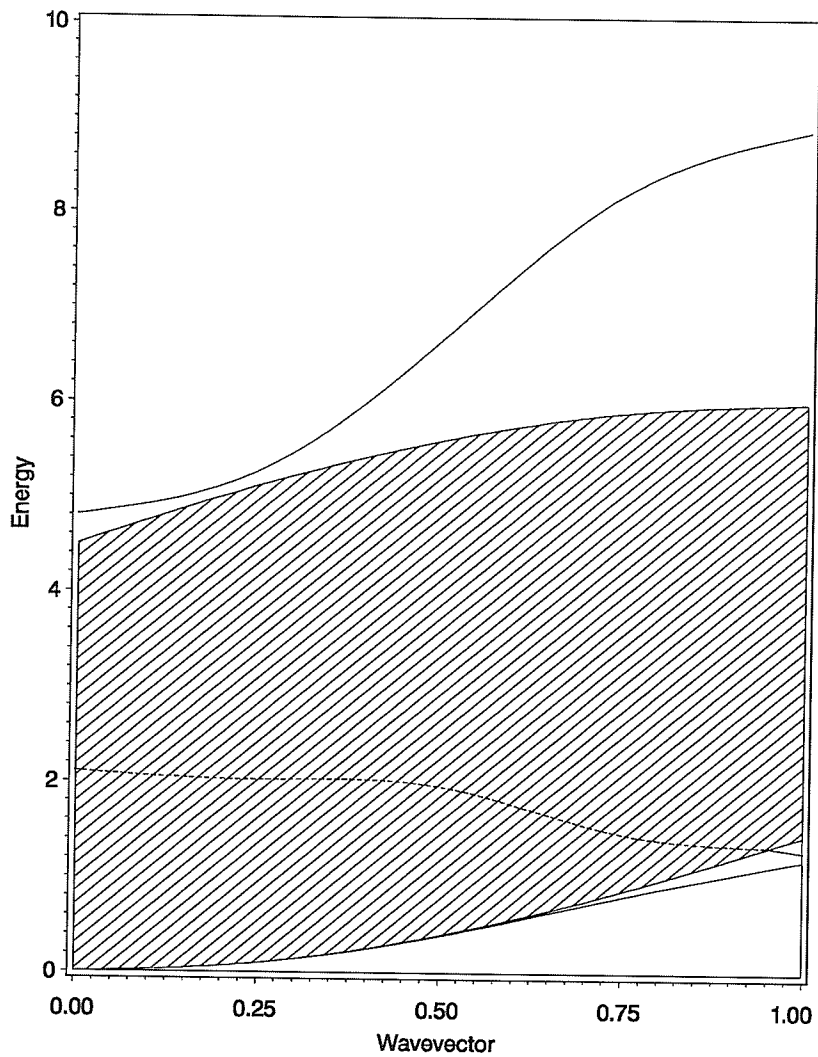


Figure 5.19: Behaviour of three magnon excitations for a model with $g_2 = 1$, $g_3 = 5.5$ (limited integrability) on a $S = \frac{3}{2}$ spin chain. Energy in units of α_1 and K in units of $\frac{\pi}{a}$. The solid lines are bound states, the dashed line are resonances and the shaded region is the scattering state continuum.

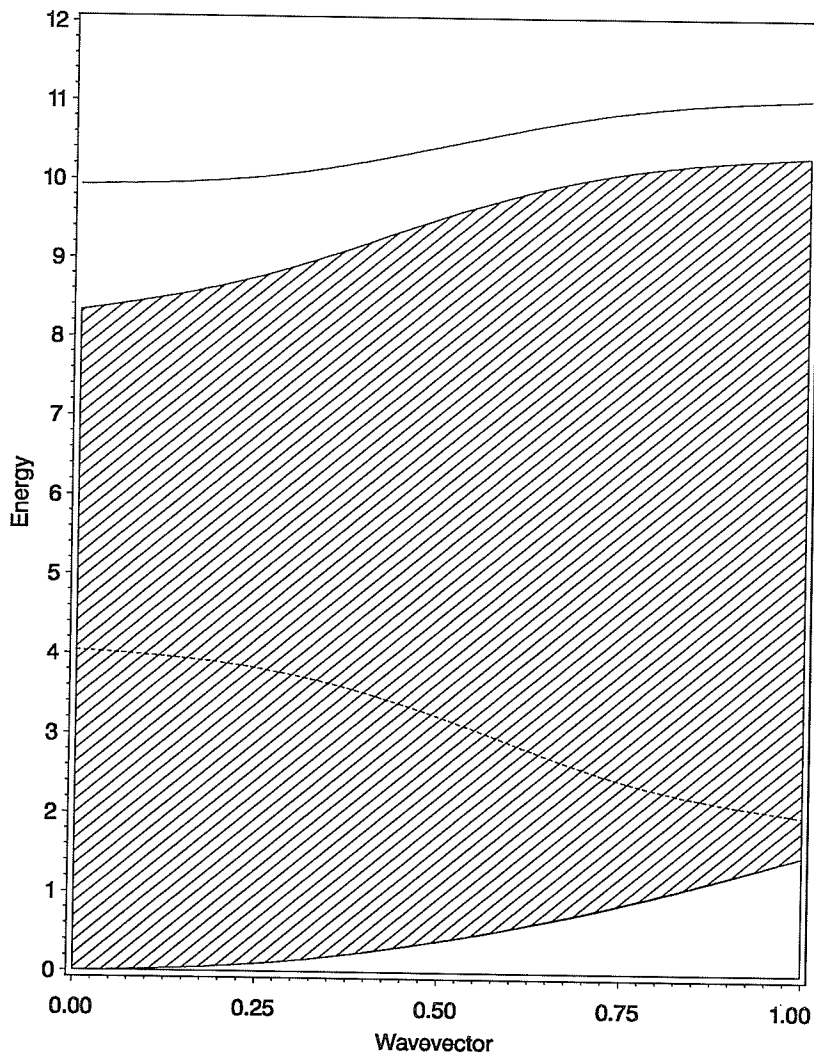


Figure 5.20: Behaviour of three magnon excitations for a model with $g_2 = 5$, $g_3 = 5.5$ (limited integrability) on a $S = \frac{3}{2}$ spin chain. Energy in units of α_1 and K in units of $\frac{\pi}{a}$. The solid lines are bound states, the dashed line are resonances and the shaded region is the scattering state continuum.

One bound state remains below the continuum as in the two magnon case or in the $S = 1$, three magnon case for all $K > 0$, but for the scale used in Fig. 5.18 this bound state is not visible. At $K = 0$ the bound state is coincident with the lower edge of the continuum. The other bound state branch which is always present remains above the continuum for all K . The resonances are somewhat suspect as these models are quite far from the integrable point and when the model is pushed

far from this point the resonance become more and more difficult to distinguish from any singularities internal to the continuum.

Now consider keeping g_2 at 2.5 but varying g_3 . Since g_2 is still at the integrable value, the behaviour of any system containing one or two magnons would be indistinguishable from a model using an integrable Hamiltonian. There has been some speculation that such a Hamiltonian would retain certain integrable characteristics. (See Chubukov and Khveschenko [30]). The Hamiltonian used in that paper is of the same form as (1.4) but is only the most general Hamiltonian up to $S = \frac{3}{2}$, ie. n in (1.4) attains the values 1,2 and 3, so that the Hamiltonian can be represented by

$$\widehat{\mathcal{H}} = -\lambda \left[\sum_i \tilde{\mathcal{S}}_i \cdot \tilde{\mathcal{S}}_{i+1} + \gamma (\tilde{\mathcal{S}}_i \cdot \tilde{\mathcal{S}}_{i+1})^2 + \delta (\tilde{\mathcal{S}}_i \cdot \tilde{\mathcal{S}}_{i+1})^3 \right] \quad (5.1)$$

where the parameters $\lambda = J^{(1)}$ in our notation. Similarly, $\gamma = \frac{J^{(2)}}{J^{(3)}}$ and $\delta = \frac{J^{(3)}}{J^{(1)}}$. In [30] the condition for these models where $g_2 = 2.5$ and g_3 is variable, can be represented by

$$1 + \gamma [1 + 6S(S - 1)] = -\delta(15S^4 - 42S^3 + 35S^2 - 10S^2 + 1) \quad (5.2)$$

To relate our notation to that used in [30] it can be shown that

$$\alpha_1 = \lambda [2S + 4S^2\gamma(S - 1) + 2S^3\delta(3S^2 - 6S + 4)] \quad (5.3)$$

$$\alpha_2 = \lambda [4S - 1 + \gamma(8S^3 - 18S^2 + 8S - 1) + \delta(12S^5 - 51S^4 + 88S^3 - 51S^2 + 12S - 1)] \quad (5.4)$$

$$\alpha_3 = 3\lambda [2S - 1 + \gamma(4S^3 - 14S^2 + 12S - 9) + 3\delta(2S^5 - 13S^4 + 36S^3 - 39S^2 + 18S - 3)] \quad (5.5)$$

When $S = 1$, a solution to equation (5.2) is $\gamma = -1$ and $\delta = 0$ and equations (5.3)–(5.5) give $g_2 = \frac{\alpha_2}{\alpha_1} = 3$. This value of g_2 agrees with the condition for integrability

when the models of Takhtajan [10] and Babujian [11] are written in the α_i notation. However, for $S = \frac{3}{2}$ equation (5.2) gives $\delta = \frac{16 + 88\gamma}{17}$ and $\alpha_1 = \frac{\lambda}{17}(240 + 1116\gamma)$, $\alpha_2 = \frac{30\lambda}{17}(20 + 93\gamma)$ and $\alpha_3 = \frac{6\lambda}{17}(188 + 915\gamma)$. This gives $g_2 = \frac{\alpha_2}{\alpha_1}$ to be 2.5 which agrees with the expected value but g_3 is $\frac{118 + 915\gamma}{2(20 + 93\gamma)}$. This would not be expected to give an integrable Hamiltonian unless $\gamma = -\frac{8}{27}$. ($\gamma = -\frac{8}{27}$ gives the integrable model of Takhtajan and Babujian.) When the recursion procedure is performed on these types of Hamiltonians, ($g_2 = 2.5$ and $g_3 \in [1, 11]$), only when $g_3 = 5.5$ does a fully integrable Hamiltonian result. These resemble the previous case where g_2 was variable and g_3 was fixed, in that when the variable parameter, g_3 , deviates from the integrable point, gaps appear at the Brillouin zone boundaries and change in size in accordance with the magnitude of the difference between g_3 and the integrable value. Also, there was always at least two bound state branches for all the value of g_3 which were used and for all $K > 0$. One of the branches remained below the scattering state continuum and the other above it. Below are the dispersion diagrams for the extreme cases of $g_3 = 1$ and $g_3 = 11$.

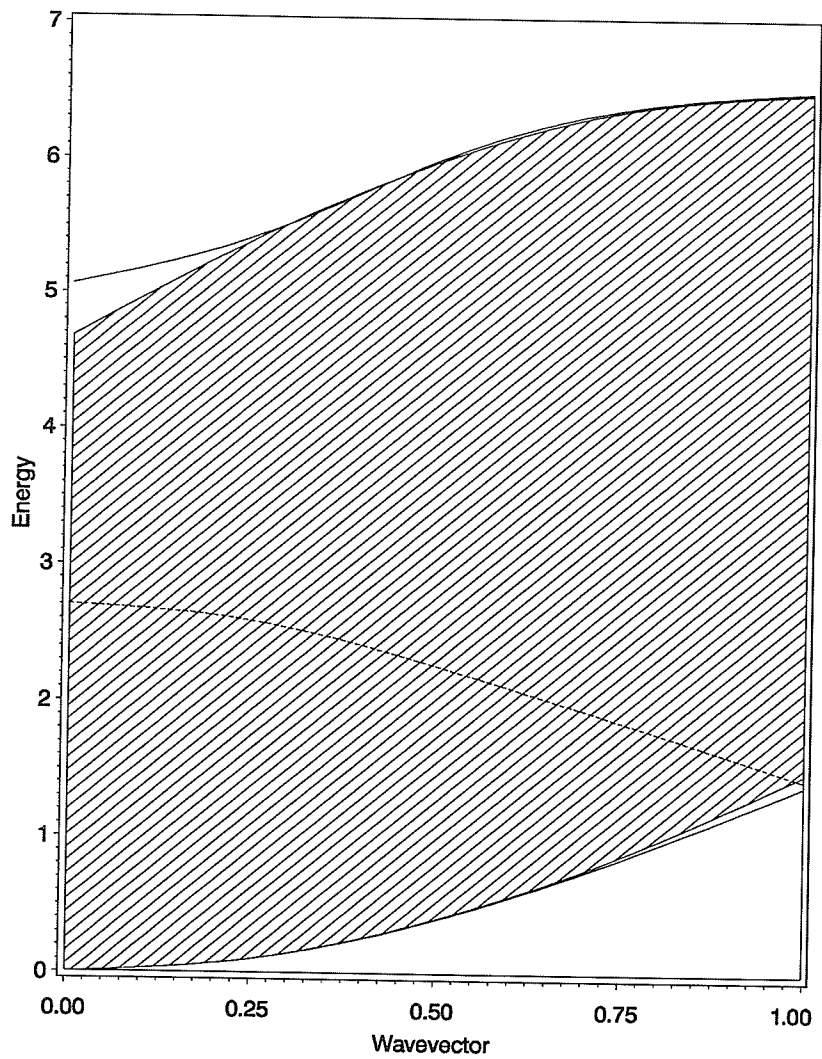


Figure 5.21: Behaviour of three magnon excitations for a partly integrable model with $g_2 = 2.5$, $g_3 = 1$ on a $S = \frac{3}{2}$ spin chain. Energy in units of α_1 and K in units of $\frac{\pi}{a}$. The solid lines are bound states, the dashed line are resonances and the shaded region is the scattering state continuum.

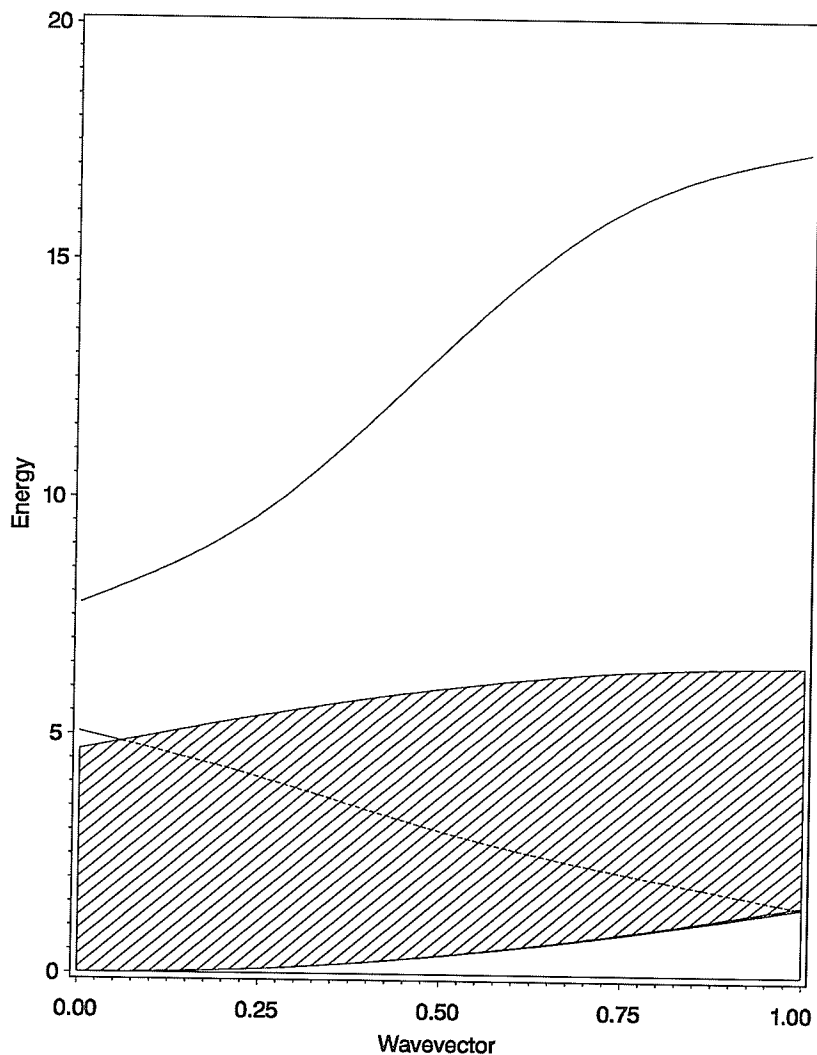


Figure 5.22: Behaviour of three magnon excitations for a partly integrable model with $g_2 = 2.5$, $g_3 = 11$ on a $S = \frac{3}{2}$ spin chain. Energy in units of α_1 and K in units of $\frac{\pi}{a}$. The solid lines are bound states, the dashed line are resonances and the shaded region is the scattering state continuum.

The Heisenberg model is a case where both the g_2 and g_3 differ from integrable values, specifically at $S = \frac{3}{2}$, $g_2 = \frac{5}{3}$ and $g_3 = 2$. For these cases, where g_2 and g_3 change, the upper bound state may enter the continuum and for the Heisenberg model this branch is entirely within the continuum for all K . The resonance line that represents this branch (shown in Fig. 5.23) is somewhat suspect since it has a very peculiar property that it remains at an almost constant energy across the

Brillouin zone.

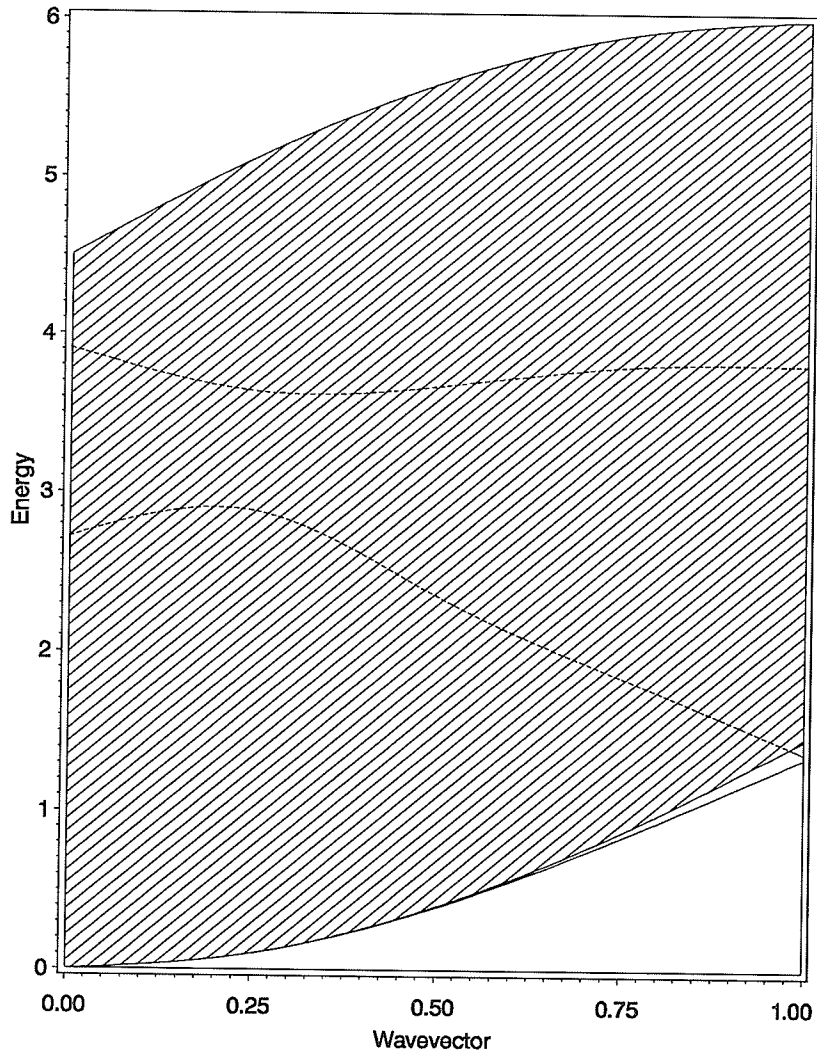


Figure 5.23: Behaviour of three magnon excitations for the Heisenberg model ($g_2 = \frac{5}{3}$, $g_3 = 2$) on a $S = \frac{3}{2}$ spin chain. Energy in units of α_1 and K in units of $\frac{\pi}{a}$. The solid lines are bound states, the dashed line are resonances and the shaded region is the scattering state continuum.

The middle resonance eventually leaves the continuum at $K = 0.98\frac{\pi}{a}$ and becomes a bound state from $0.98\frac{\pi}{a} - \frac{\pi}{a}$. This resonance/bound state was found to contain no symmetric components. Below, Fig. 5.24, is the density of states using a completely

symmetric initial ket, $(x, y) = (0, 0)$, at $K = \frac{\pi}{a}$. Note that the middle bound state branch is missing in comparison with Fig. 5.25.

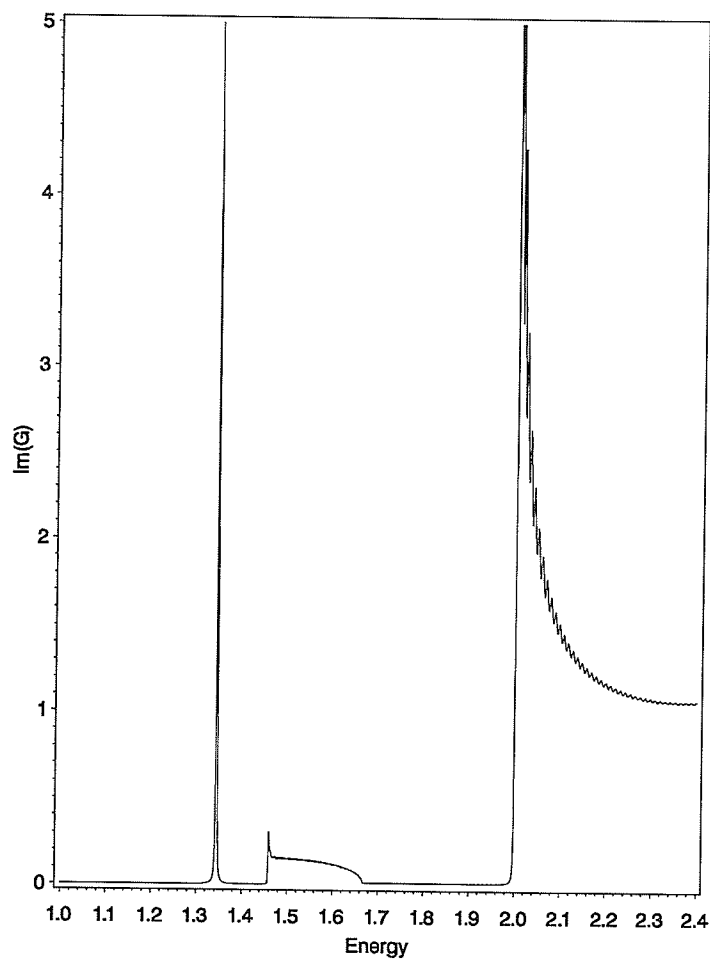


Figure 5.24: Behaviour of three magnon excitations for a Heisenberg model on a $S = \frac{3}{2}$ spin chain at $K = \pi$ using a symmetric initial ket. Energy in units of α_1 .

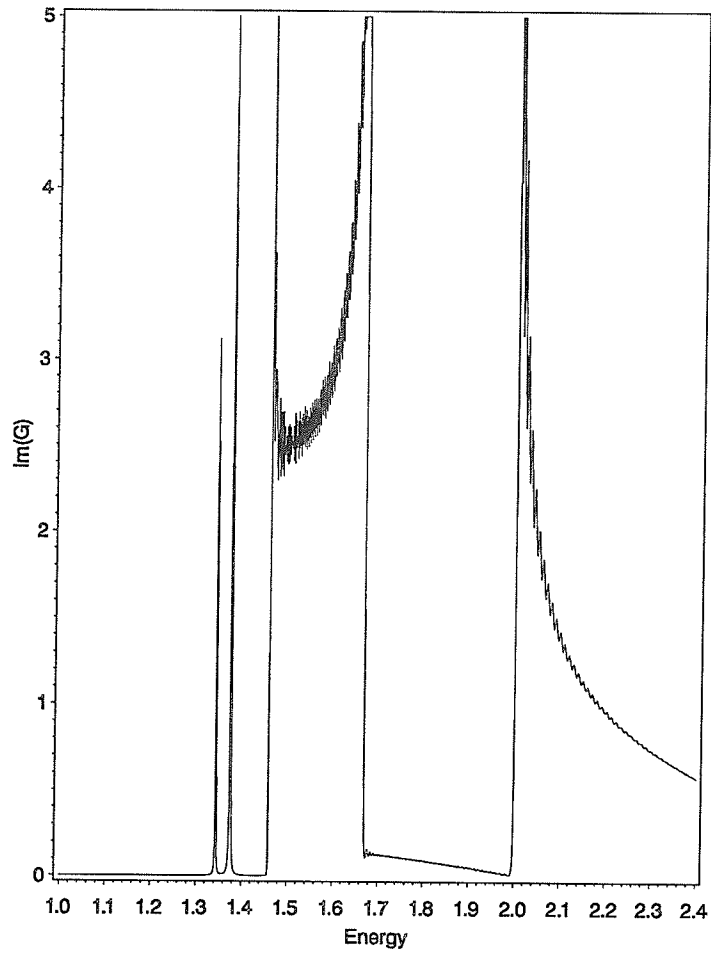


Figure 5.25: Behaviour of three magnon excitations for a Heisenberg model on a $S = \frac{3}{2}$ spin chain at $K = \pi$ using an arbitrary initial ket. Energy in units of α_1 .

For this case, there is also a branch which remains below the continuum for all $K > 0$. The upper branch does not seem to enter the continuum unless both g_2 and g_3 are far enough below the integrable values. For the cases which were studied, this branch does not enter the continuum even if the parameters are quite far above the integrable values, for example Fig. 5.26, below

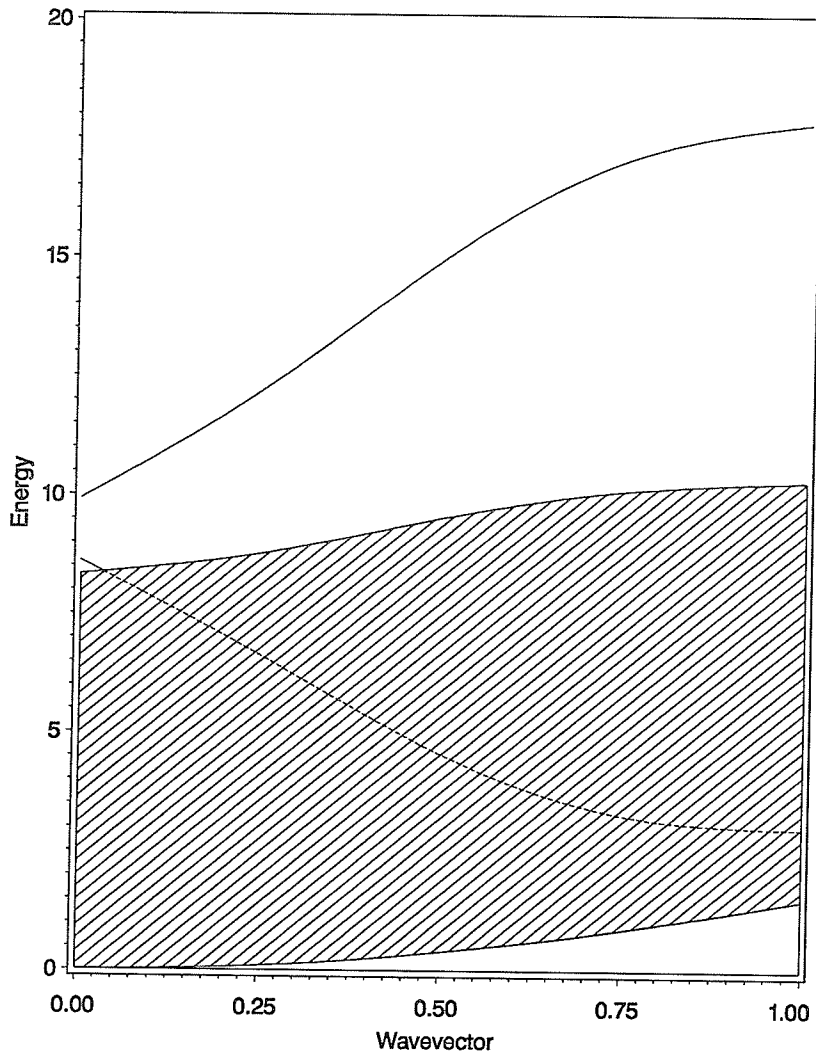


Figure 5.26: Behaviour of three magnon excitations for $g_2 = 5$, $g_3 = 11$ on a $S = \frac{3}{2}$ spin chain. Energy in units of α_1 and K in units of $\frac{\pi}{a}$. The solid lines are bound states, the dashed line are resonances and the shaded region is the scattering state continuum.

and the upper branch remains outside the continuum even if only one parameter is below the integrable value Fig. 5.27 and Fig. 5.28.

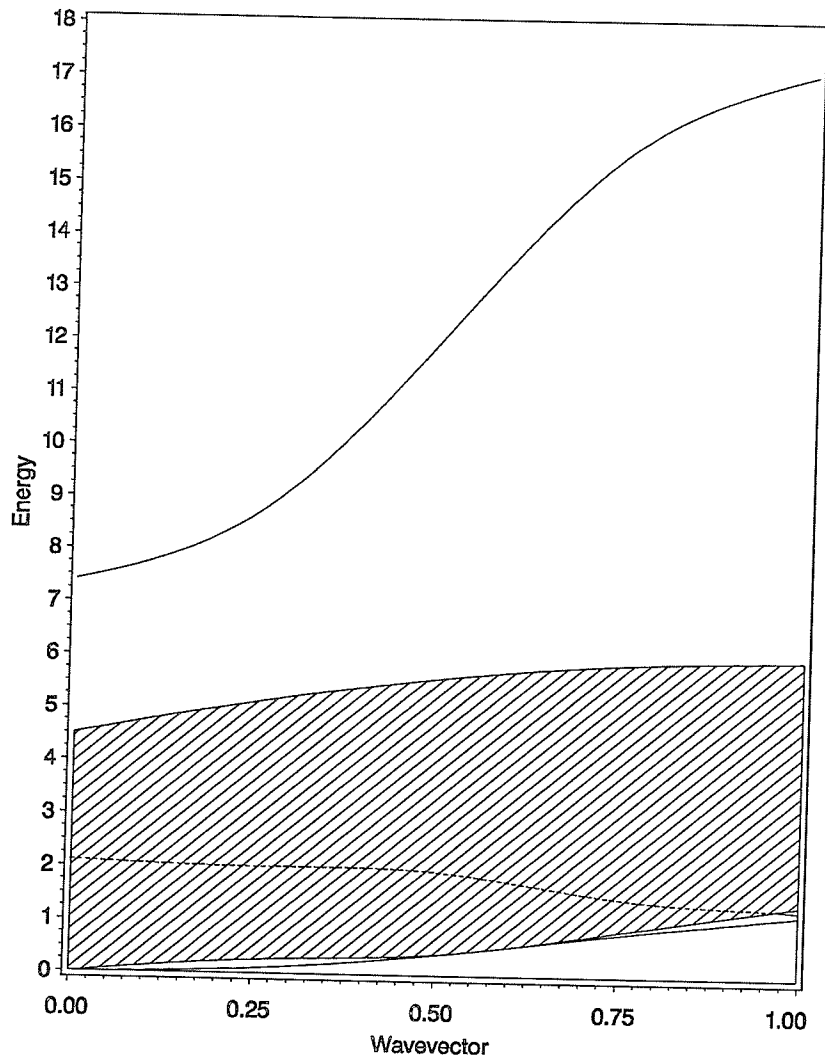


Figure 5.27: Behaviour of three magnon excitations for $g_2 = 1$, $g_3 = 11$ on a $S = \frac{3}{2}$ spin chain. Energy in units of α_1 and K in units of $\frac{\pi}{a}$. The solid lines are bound states, the dashed line are resonances and the shaded region is the scattering state continuum.

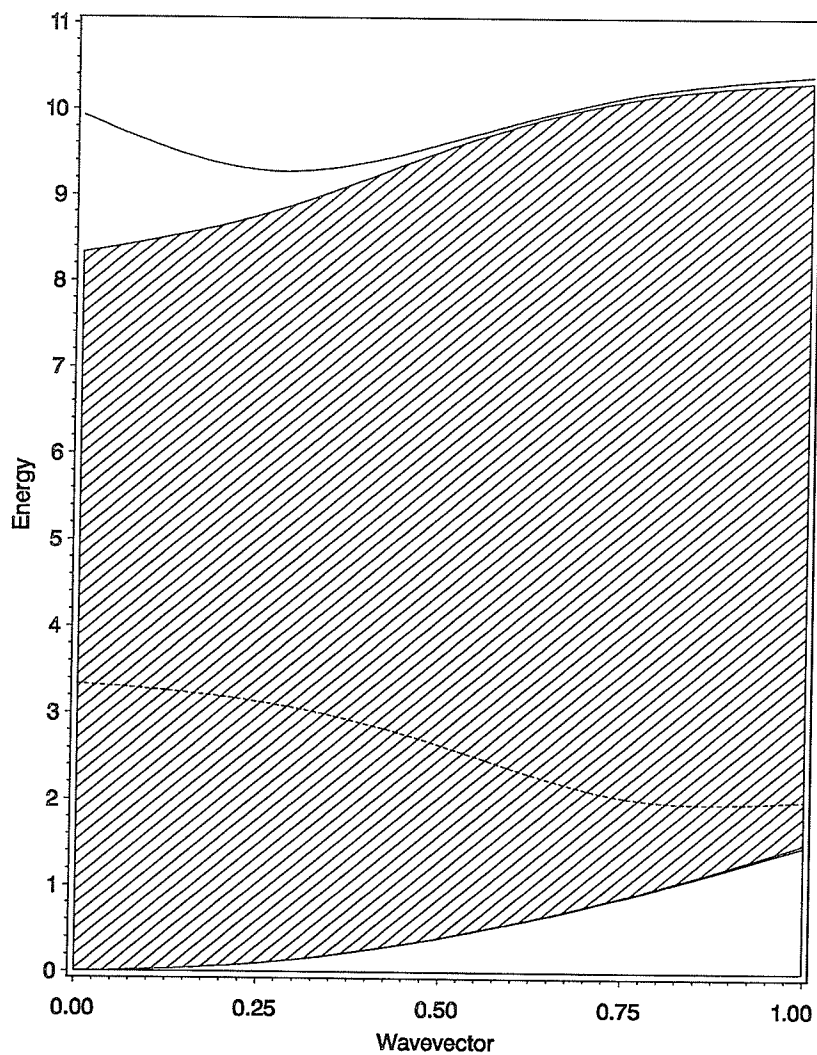


Figure 5.28: Behaviour of three magnon excitations for $g_2 = 5$, $g_3 = 1$ on a $S = \frac{3}{2}$ spin chain. Energy in units of α_1 and K in units of $\frac{\pi}{a}$. The solid lines are bound states, the dashed line are resonances and the shaded region is the scattering state continuum.

Chapter 6

Summary

In summary, the recursion procedure was successfully applied to study three magnon excitations and gave results which were in agreement with the exact results found for the integrable models of Takhtajan and Babujian, Lai-Sutherland and Temperley-Lieb. For the integrable model of Takhtajan and Babujian, a single bound state was found (using the extended zone representation) which was continuous across the minimum of $2S$ and m Brillouin zones and it remained outside the continuum over this entire region. As the models were moved away from integrability, gaps appeared and grew at the Brillouin zone boundaries as predicted by Haldane [12, 13]. The numerical values for the energies of the edges and bound states agree with the results found by Millet and Kaplan, aside from a single non-physical state for $S = \frac{1}{2}$. All the cases studied did not show any integrable properties aside from the models which correspond to those already known. The recursion method can easily be applied to more general Hamiltonians than the form which was used. For example, the Hamiltonian can be extended to include the effects of an external magnetic field or single ion anisotropic effects. Generally, these make relatively minor changes to the Hamiltonian. The most extensive alterations would be to the equations to produce a new set of equations to represent the Hamiltonian [ie. the equations appearing in the appendix and (3.6)–(3.25)]. However, the alterations to the programs which implement the recursion method are very trivial.

The extensions needed to describe m magnons systems for $m > 3$ is also clear.

The effects of the Hamiltonian when the magnons are less than one lattice spacing away from each other would be the most time consuming part to address. This is also the information necessary for the appearance of m -magnon bound states. The continua of such an extended system can be obtained from the $m - 1$ system and since the equations governing a system with 1,2 or 3 magnons is known, the range of energies that the continua states can attain for a m magnon system can be easily found. The Hamiltonian of such a system can be represented by a hyper-tetrahedron of dimension of $m - 1$ with the origin at one apex and the edges as well as the sides correspond to special situations within the system (ie. 2, 3, 4, \dots , $m - 1$ magnons on the same site with the remaining magnons greater than nearest neighbours from each of the others. Only the apex corresponds to m magnons on the same site). The next layer corresponds to where each magnon is at most one lattice spacing apart from the rest. The rest of the Hamiltonian defines the behaviour of the three free continuum.

Extensions for models which use greater than nearest neighbours are also possible. The recursion method itself is independent of this kind of modification and the calculation of the equations which define the system is the most difficult part to modify. Essentially the derivations in the appendix and equations (3.6)–(3.25) must be recalculated without restricting the Hamiltonian to having only nearest neighbour interactions. However, there are practical limitations to the extent which the model can be extended. The recursion process usually is performed for a very large number of iterations and some of these limitations can already be seen in the anomalously large deviations from the expected average value of the recursion coefficients. These deviations were used to assist in finding some bound states and were converted from a hindrance to an asset. Unfortunately, there are also storage and memory allocation limitations.

In the present implementation of the recursion method, arrays were used to keep track of the current vector, u_i , the next vector, u_{i+1} and the previous vector,

u_{i-1} . The size of the vectors increased on the order $O(n^2)$ with the iteration number, n and for a three dimensional Hamiltonian or four magnon excitations, the vectors would increase as $\sum \sum n$ or $O(n^3)$. Therefore, assuming the maximum amount of storage to be constant, then the maximum number of iterations is decreased by approximately the $\frac{2}{3}$ power of n . For the three magnon case, the maximum number of iterations was approximately 590. Then the maximum number of iterations for a four magnon system is roughly 70. However, the true maximum number of iterations may be significantly different depending upon the machine's memory allocation methods. It may be possible to sidestep these memory difficulties by storing the vectors in a secondary mass storage system (ie. disk) but for a multi-user, pre-emptive multitasking operating system such as Unix, the resulting amount of disk access would probably make the calculation agonizingly slow. Finally, the calculation of each vector element is not trivial and the modifications to the Hamiltonian would make the calculations even more intensive but there is the consolation that the calculations are readily amenable to systems which are able to perform the numerical operations in parallel.

In conclusion, extending the solution to more extensive situations is not particularly difficult but very tedious and the extension to greater number of magnons soon result in rapidly diminishing returns which require some creative solutions. However, the difficulties are only practical implementation dependent problems which may be solved as newer hardware becomes available.

Appendix

Three Magnon Excitation Equations

From Chapter 3, the orthonormal set of three spin deviations are taken to be

$$|i, j, k\rangle = C_{ijk} S_i^+ S_j^+ S_k^+ |0\rangle \quad (\text{A.1})$$

where C_{ijk} is a constant satisfying

$$C_{ijk} = \begin{cases} \frac{1}{\sqrt{8S^3}}, & i \neq j \neq k \\ \frac{1}{\sqrt{8S^2(2S-1)}}, & 2 \text{ of } \{i, j, k\} \text{ the same} \\ \frac{1}{\sqrt{24S(2S-1)(S-1)}}, & i = j = k \end{cases} \quad (\text{A.2})$$

and with the indices $i \leq j \leq k$ for the entire set of states.

To find the effect of $\widehat{\mathcal{H}}$ on these states, several different cases must be considered, depending upon whether the indices are equal, nearest neighbours or otherwise. Consider first the situation where $i+1 < j$, $j+1 < k$, ie. when the three deviations are separated by more than nearest neighbours. By using the commutation relations of S_i^\pm and S_i^z , along with the definition of the states, $|i, j, k\rangle$, we find

$$\left. \begin{aligned} \widetilde{\mathcal{P}}_l |i, j, k\rangle &= S^2 |i, j, k\rangle, & k \neq l \\ \widetilde{\mathcal{P}}_l |i, j, l\rangle &= S(S-1) |i, j, l\rangle + S |i, j, l+1\rangle, & k = l \\ \widetilde{\mathcal{P}}_l |i, j, l+1\rangle &= S |i, j, l\rangle + S(S-1) |i, j, l+1\rangle, & k = l+1 \end{aligned} \right\} \quad (\text{A.3})$$

These equations have the same structure as for the one-magnon excitations, (2.2) so the matrix representation of $\widetilde{\mathcal{P}}_l^n$ for only these states must have the form

as in (2.4). The equations must have this structure since $\tilde{\mathcal{P}}_l$ commutes with \mathcal{S}_i^+ and \mathcal{S}_j^+ , for the states which satisfy the restrictions on the indices (above). This is also true for states of the form $|i, l, j\rangle$ and $|l, i, j\rangle$. Using these results, the pair Hamiltonian is given by

$$\begin{aligned}
& i+1 < j, j+1 < k \\
\widehat{\mathcal{H}}_l |i, j, k\rangle = & \begin{cases} 0, & i, j, k \neq l, l+1 \\ \frac{\alpha_1(S)}{2} |l, j, k\rangle - \frac{\alpha_1(S)}{2} |l+1, j, k\rangle, & i = l \\ \frac{\alpha_1(S)}{2} |l+1, j, k\rangle - \frac{\alpha_1(S)}{2} |l, j, k\rangle, & i = l+1 \\ \frac{\alpha_1(S)}{2} |i, l, k\rangle - \frac{\alpha_1(S)}{2} |i, l+1, k\rangle, & j = l \\ \frac{\alpha_1(S)}{2} |i, l+1, k\rangle - \frac{\alpha_1(S)}{2} |l, l, k\rangle, & j = l+1 \\ \frac{\alpha_1(S)}{2} |i, j, l\rangle - \frac{\alpha_1(S)}{2} |i, j, l+1\rangle, & k = l \\ \frac{\alpha_1(S)}{2} |i, j, l+1\rangle - \frac{\alpha_1(S)}{2} |i, j, l+1\rangle, & k = l+1 \end{cases} \quad (\text{A.4})
\end{aligned}$$

where all terms involving E_0 are absorbed into a shift in the zero of energy. This shift of energy is used for all that follows as well.

The full Hamiltonian gives

$$\begin{aligned}
\widehat{\mathcal{H}} |i, j, k\rangle = & 3\alpha_1(S) |i, j, k\rangle - \frac{\alpha_1(S)}{2} |i-1, j, k\rangle - \frac{\alpha_1(S)}{2} |i+1, j, k\rangle \\
& - \frac{\alpha_1(S)}{2} |i, j-1, k\rangle - \frac{\alpha_1(S)}{2} |i, j+1, k\rangle - \frac{\alpha_1(S)}{2} |i, j, k-1\rangle \\
& - \frac{\alpha_1(S)}{2} |i, j, k+1\rangle \quad (\text{A.5})
\end{aligned}$$

Next, consider the case when two deviations are on the same site or nearest neighbours and the remaining deviation is further than nearest neighbours from either of the other two. States of the form $|i, l, l\rangle$ and $|i, l, l+1\rangle$, belong to this

class and we find

$$\begin{aligned}
& i \neq l, l+1 \\
\tilde{\mathcal{P}}_l |i, l, l\rangle &= S(S-2)|i, l, l\rangle + \sqrt{S(2S-1)}|i, l, l+1\rangle \\
\tilde{\mathcal{P}}_l |i, l, l+1\rangle &= \sqrt{S(2S-1)}[|i, l, l\rangle + |i, l+1, l+1\rangle] + (1-S)^2|i, l, l+1\rangle \\
\tilde{\mathcal{P}}_l |i, l+1, l+1\rangle &= \sqrt{S(2S-1)}|i, l, l+1\rangle + S(S-2)|i, l+1, l+1\rangle
\end{aligned} \tag{A.6}$$

These equations form an additional block in the full matrix and has the same form as given for the two-magnon interactions, (2.15)–(2.16). Therefore, the matrix representation of $\tilde{\mathcal{P}}_l$ for these states, has the form of (2.21) and $\tilde{\mathcal{P}}_l^n$ is given by (2.22) when using the vector

$$\begin{pmatrix} |i, l, l\rangle \\ |i, l, l+1\rangle \\ |i, l+1, l+1\rangle \end{pmatrix} \tag{A.7}$$

The effect of the pair Hamiltonian on these states gives

$$\widehat{\mathcal{H}}_l |i, j, j+1\rangle = \begin{cases} 0, & i \neq l, l+1 \quad j \neq l-1, l, l+1 \\ \frac{\alpha_1}{2} |l, j, j+1\rangle - \frac{\alpha_1}{2} |l+1, j, j+1\rangle, & i = l+1 \\ \frac{\alpha_1}{2} |l+1, j, j+1\rangle - \frac{\alpha_1}{2} |l, j, j+1\rangle, & i = l \\ \frac{\alpha_1}{2} |i, l-1, l\rangle - \frac{\alpha_1}{2} |i, l-1, l+1\rangle, & j = l-1 \\ -\frac{\sqrt{S(2S-1)}}{4S-1} \alpha_2 [|i, l, l\rangle + |i, l+1, l+1\rangle] + \\ \quad \frac{2S-1}{4S-1} \alpha_2 |i, l, l+1\rangle, & j = l \\ \frac{\alpha_1}{2} |i, l+1, l+2\rangle - \frac{\alpha_1}{2} |i, l, l+2\rangle, & j = l+1 \end{cases} \tag{A.8}$$

$$\widehat{\mathcal{H}}_l |i, j, j\rangle = \begin{cases} 0, & i, j \neq l, l+1 \\ \frac{\alpha_1}{2} |l, j, j\rangle - \frac{\alpha_1}{2} |l+1, j, j\rangle, & i = l \\ \frac{\alpha_1}{2} |l+1, j, j\rangle - \frac{\alpha_1}{2} |l, j, j\rangle, & i = l+1 \\ \frac{1}{2} \left[\alpha_1 + \frac{2S\alpha_2}{4S-1} \right] |i, l, l\rangle - \frac{\sqrt{S(2S-1)}}{4S-1} \alpha_2 |i, l, l+1\rangle - \\ \quad \frac{1}{2} \left[\alpha_1 - \frac{2S\alpha_2}{4S-1} \right] |i, l+1, l+1\rangle, & j = l \\ \frac{1}{2} \left[\alpha_1 + \frac{2S\alpha_2}{4S-1} \right] |i, l+1, l+1\rangle - \frac{\sqrt{S(2S-1)}}{4S-1} \alpha_2 |i, l, l+1\rangle \\ \quad - \frac{1}{2} \left[\alpha_1 - \frac{2S\alpha_2}{4S-1} \right] |i, l, l\rangle, & j = l+1 \end{cases} \quad (\text{A.9})$$

and for the total Hamiltonian

$$\begin{aligned} \widehat{\mathcal{H}} |i, j, j+1\rangle &= 2\alpha_1(S) |i, j, j+1\rangle - \frac{\alpha_1(S)}{2} |i-1, j, j+1\rangle - \frac{\alpha_1(S)}{2} |i+1, j, j+1\rangle \\ &\quad - \frac{\alpha_1(S)}{2} |i, j-1, j+1\rangle - \frac{\alpha_1(S)}{2} |i, j, j+2\rangle + \frac{2S-1}{4S-1} \alpha_2(S) |i, j, j+1\rangle \\ &\quad - \frac{\sqrt{S(2S-1)}}{4S-1} \alpha_2(S) |i, j, j\rangle - \frac{\sqrt{S(2S-1)}}{4S-1} \alpha_2(S) |i, j+1, j+1\rangle, \\ &\quad i < j-1 \end{aligned} \quad (\text{A.10})$$

$$\begin{aligned} \widehat{\mathcal{H}} |i, j, j\rangle &= 2\alpha_1(S) |i, j, j\rangle - \frac{\alpha_1(S)}{2} |i-1, j, j\rangle - \frac{\alpha_1(S)}{2} |i+1, j, j\rangle \\ &\quad + \frac{2S\alpha_2(S)}{4S-1} |i, j, j\rangle - \frac{1}{2} \left[\alpha_1(S) - \frac{2S\alpha_2(S)}{4S-1} \right] |i, j-1, j-1\rangle \\ &\quad - \frac{1}{2} \left[\alpha_1(S) - \frac{2S\alpha_2(S)}{4S-1} \right] |i, j+1, j+1\rangle - \frac{\sqrt{S(2S-1)}}{4S-1} \alpha_2(S) |i, j-1, j\rangle \\ &\quad - \frac{\sqrt{S(2S-1)}}{4S-1} \alpha_2(S) |i, j, j+1\rangle, \quad i < j-1 \end{aligned} \quad (\text{A.11})$$

The operator, $\widetilde{\mathcal{P}}_l$, also generates equations of the same form as (A.6) for the states $|l, l, j\rangle$, $|l-1, l, j\rangle$, and $|l-1, l, l+1\rangle$. The pair Hamiltonian, for these

states are given by

$$\widehat{\mathcal{H}}_l |i-1, i, j\rangle = \begin{cases} 0, & i \neq l-1, l, l+1 \quad j \neq l, l+1 \\ \frac{\alpha_1}{2} |i-1, i, l\rangle - \frac{\alpha_1}{2} |i-1, i, l+1\rangle, & j = l \\ \frac{\alpha_1}{2} |i-1, i, l+1\rangle - \frac{\alpha_1}{2} |i-1, i, l\rangle, & j = l+1 \\ \frac{\alpha_1}{2} |l-1, l, j\rangle - \frac{\alpha_1}{2} |l-1, l+1, j\rangle, & i = l \\ -\frac{\sqrt{S(2S-1)}}{4S-1} \alpha_2 [|l, l, j\rangle + |l+1, l+1, j\rangle] + \\ \quad \frac{2S-1}{4S-1} \alpha_2 |l, l+1, j\rangle, & i = l+1 \\ \frac{\alpha_1}{2} |l+1, l+2, j\rangle - \frac{\alpha_1}{2} |l, l+2, j\rangle, & i = l+2 \end{cases} \quad (\text{A.12})$$

$$\widehat{\mathcal{H}}_l |i, i, j\rangle = \begin{cases} 0, & i, j \neq l, l+1 \\ \frac{\alpha_1}{2} |i, i, l\rangle - \frac{\alpha_1}{2} |i, i, l+1\rangle, & j = l \\ \frac{\alpha_1}{2} |i, i, l+1\rangle - \frac{\alpha_1}{2} |i, i, l\rangle, & j = l+1 \\ \frac{1}{2} \left[\alpha_1 + \frac{2S\alpha_2}{4S-1} \right] |l, l, j\rangle - \frac{\sqrt{S(2S-1)}}{4S-1} \alpha_2 |l, l+1, j\rangle - \\ \quad \frac{1}{2} \left[\alpha_1 - \frac{2S\alpha_2}{4S-1} \right] |l+1, l+1, j\rangle, & i = l \\ \frac{1}{2} \left[\alpha_1 + \frac{2S\alpha_2}{4S-1} \right] |l+1, l+1, j\rangle - \frac{\sqrt{S(2S-1)}}{4S-1} \alpha_2 |l, l+1, j\rangle \\ \quad - \frac{1}{2} \left[\alpha_1 - \frac{2S\alpha_2}{4S-1} \right] |l, l, j\rangle, & i = l+1 \end{cases} \quad (\text{A.13})$$

$$\widehat{\mathcal{H}}_l |i-1, i, i+1\rangle = \begin{cases} 0, & i \neq l-1, l, l+1, l+2 \\ -\frac{\sqrt{S(2S-1)}}{4S-1} \alpha_2 (|l-1, l, l\rangle + |l-1, l+1, l+1\rangle) \\ \quad + \left(\frac{2S-1}{4S-1} \right) \alpha_2 |l-1, l, l+1\rangle, & i = l \\ -\frac{\sqrt{S(2S-1)}}{4S-1} \alpha_2 (|l-1, l-1, l+1\rangle + |l-1, l+1, l+1\rangle) \\ \quad + \left(\frac{2S-1}{4S-1} \right) \alpha_2 |l, l+1, l+2\rangle, & i = l+1 \end{cases} \quad (\text{A.14})$$

Which gives, for the total Hamiltonian,

$$\begin{aligned} \widehat{\mathcal{H}} |i, i, j\rangle &= 2\alpha_1(S) |i, i, j\rangle - \frac{\alpha_1(S)}{2} |i, i, j-1\rangle - \frac{\alpha_1(S)}{2} |i, i, j+1\rangle \\ &+ \frac{2S\alpha_2(S)}{4S-1} |i, i, j\rangle - \frac{1}{2} \left[\alpha_1(S) - \frac{2S\alpha_2(S)}{4S-1} \right] |i-1, i-1, j\rangle \end{aligned}$$

$$\begin{aligned}
& -\frac{1}{2} \left[\alpha_1(S) - \frac{2S\alpha_2(S)}{4S-1} \right] |i+1, i+1, j\rangle - \frac{\sqrt{S(2S-1)}}{4S-1} \alpha_2(S) |i-1, i, j\rangle \\
& - \frac{\sqrt{S(2S-1)}}{4S-1} \alpha_2(S) |i, i+1, j\rangle, \quad i < j-1
\end{aligned} \tag{A.15}$$

$$\begin{aligned}
\widehat{\mathcal{H}} |i-1, i, j\rangle &= 2\alpha_1(S) |i-1, i, j\rangle - \frac{\alpha_1(S)}{2} |i-1, i, j-1\rangle - \frac{\alpha_1(S)}{2} |i-1, i, j+1\rangle \\
& - \frac{\alpha_1(S)}{2} |i-2, i, j\rangle - \frac{\alpha_1(S)}{2} |i-1, i+1, j\rangle + \left[\frac{2S-1}{4S-1} \alpha_2(S) \right] |i-1, i, j\rangle \\
& - \frac{\sqrt{S(2S-1)}}{4S-1} \alpha_2(S) |i-1, i-1, j\rangle - \frac{\sqrt{S(2S-1)}}{4S-1} \alpha_2(S) |i, i, j\rangle, \\
& \quad j > i+1
\end{aligned} \tag{A.16}$$

$$\begin{aligned}
\widehat{\mathcal{H}} |i-1, i, i+1\rangle &= \alpha_1(S) |i-1, i, i+1\rangle - \frac{\alpha_1(S)}{2} |i-1, i, i+1\rangle \\
& - \frac{\alpha_1(S)}{2} |i-1, i, i+2\rangle + 2 \left[\frac{2S-1}{4S-1} \right] \alpha_2(S) |i-1, i, i+1\rangle \\
& - \frac{\sqrt{S(2S-1)}}{4S-1} \alpha_2(S) |i-1, i-1, i+1\rangle - \frac{\sqrt{S(2S-1)}}{4S-1} \alpha_2(S) |i, i, i+1\rangle \\
& - \frac{\sqrt{S(2S-1)}}{4S-1} \alpha_2(S) |i-1, i, i\rangle - \frac{\sqrt{S(2S-1)}}{4S-1} \alpha_2(S) |i-1, i+1, i+1\rangle
\end{aligned} \tag{A.17}$$

As for the two-magnon case, the Hamiltonian is block diagonal and the blocks can be classified by the number of magnons which are nearest neighbours at one time. The two smallest blocks were considered above and correspond to three free non-interacting magnons and to a system of two interacting magnons combined with a single free magnon, respectively.

The final block of the Hamiltonian which needs to be considered is for the states $|l, l, l\rangle$, $|l, l, l+1\rangle$ and $|l, l+1, l+1\rangle$ (ie. when all three magnons interact with each other). The effect of $\tilde{\mathcal{P}}_l$ on these states are given by

$$\begin{aligned}
\tilde{\mathcal{P}}_i |l, l, l\rangle &= S(S-3) |l, l, l\rangle + \sqrt{3S(S-1)} |l, l, l+1\rangle \\
\tilde{\mathcal{P}}_i |l, l, l+1\rangle &= \sqrt{3S(S-1)} |l, l, l\rangle + (S^2 - 3S + 2) |l, l, l+1\rangle \\
&\quad + (2S-1) |l, l+1, l+1\rangle \\
\tilde{\mathcal{P}}_i |l, l+1, l+1\rangle &= (2S-1) |l, l, l+1\rangle + (S^2 - 3S + 2) |l, l+1, l+1\rangle \\
&\quad + \sqrt{3S(S-1)} |l+1, l+1, l+1\rangle \\
\tilde{\mathcal{P}}_i |l+1, l+1, l+1\rangle &= \sqrt{3S(S-1)} |l, l+1, l+1\rangle + S(S-3) |l+1, l+1, l+1\rangle
\end{aligned} \tag{A.18}$$

and for the matrix representation, restricted to these four basis states is

$$\tilde{\mathcal{P}}_i = \begin{bmatrix} S(S-3) & \sqrt{3S(S-1)} & 0 & 0 \\ \sqrt{3S(S-1)} & S^2 - 3S + 2 & 2S-1 & 0 \\ 0 & 2S-1 & S^2 - 3S + 2 & \sqrt{3S(S-1)} \\ 0 & 0 & \sqrt{3S(S-1)} & S(S-3) \end{bmatrix} \tag{A.19}$$

then

$$\tilde{\mathcal{P}}_i^n = -\frac{1}{2} \begin{bmatrix} \rho_{11} & \rho_{12} & \rho_{13} & \rho_{14} \\ \rho_{12} & \rho_{22} & \rho_{23} & \rho_{13} \\ \rho_{13} & \rho_{23} & \rho_{22} & \rho_{12} \\ \rho_{14} & \rho_{13} & \rho_{12} & \rho_{11} \end{bmatrix} \tag{A.20}$$

where

$$\begin{aligned}
\rho_{11} &= 3S(S-1) \left[\frac{S^{2n}-S^n(S-2)^n}{S(4S-3)} + \frac{S^{2n}-(S^2-4S+1)^n}{(S-1)(4S-1)} + \frac{S^{2n}-(S^2-6S+3)^n}{3(S-1)(4S-3)} \right] \\
\rho_{12} &= \sqrt{3S(S-1)} \left[S \frac{S^{2n}-S^n(S-2)^n}{S(4S-3)} - (S-1) \frac{S^{2n}-(S^2-4S+1)^n}{(S-1)(4S-1)} \right. \\
&\quad \left. - 3(S-1) \frac{S^{2n}-(S^2-6S+3)^n}{3(S-1)(4S-3)} \right] \\
\rho_{13} &= \sqrt{3S(S-1)} \left[-S \frac{S^{2n}-S^n(S-2)^n}{S(4S-3)} - (S-1) \frac{S^{2n}-(S^2-4S+1)^n}{(S-1)(4S-1)} \right. \\
&\quad \left. + 3(S-1) \frac{S^{2n}-(S^2-6S+3)^n}{3(S-1)(4S-3)} \right] \\
\rho_{14} &= -3S(S-1) \left[\frac{S^{2n}-S^n(S-2)^n}{S(4S-3)} - \frac{S^{2n}-(S^2-4S+1)^n}{(S-1)(4S-1)} + \frac{S^{2n}-(S^2-6S+3)^n}{3(S-1)(4S-3)} \right] \\
\rho_{22} &= S^2 \frac{S^{2n}-S^n(S-2)^n}{S(4S-3)} + (S-1)^2 \frac{S^{2n}-(S^2-4S+1)^n}{(S-1)(4S-1)} + 9(S-1)^2 \frac{S^{2n}-(S^2-6S+3)^n}{3(S-1)(4S-3)} \\
\rho_{23} &= -S^2 \frac{S^{2n}-S^n(S-2)^n}{S(4S-3)} + (S-1)^2 \frac{S^{2n}-(S^2-4S+1)^n}{(S-1)(4S-1)} - 9(S-1)^2 \frac{S^{2n}-(S^2-6S+3)^n}{3(S-1)(4S-3)}
\end{aligned} \tag{A.21}$$

and the pair Hamiltonian gives

$$\begin{aligned}
\widehat{\mathcal{H}}_l |l, l+1, l+1\rangle &= -\frac{\sqrt{3S(S-2)}}{2} \left[\frac{\alpha_1(S)}{4S-3} + \frac{\alpha_2(S)}{4S-1} - \frac{\alpha_3(S)}{4S-3} \right] |l, l, l\rangle \\
&\quad - \frac{1}{2} \left[\frac{S\alpha_1(S)}{4S-3} - \frac{(S-1)\alpha_2(S)}{4S-1} + \frac{3(S-1)\alpha_3(S)}{4S-3} \right] |l, l, l+1\rangle \\
&\quad + \frac{1}{2} \left[\frac{S\alpha_1(S)}{4S-3} + \frac{(S-1)\alpha_2(S)}{4S-1} + \frac{3(S-1)\alpha_3(S)}{4S-3} \right] |l, l+1, l+1\rangle \\
&\quad + \frac{\sqrt{3S(S-2)}}{2} \left[\frac{\alpha_1(S)}{4S-3} + \frac{\alpha_2(S)}{4S-1} - \frac{\alpha_3(S)}{4S-3} \right] |l+1, l+1, l+1\rangle
\end{aligned} \tag{A.22}$$

By using the above equation along with the results from equation (A.3)

$$\begin{aligned}
\widehat{\mathcal{H}}_l |i-1, i, i\rangle &= 0, \quad i > l+2, i < l \\
\widehat{\mathcal{H}}_l |l+1, l+2, l+2\rangle &= \frac{\alpha_1}{2} |l+1, l+2, l+2\rangle - \frac{\alpha_1}{2} |l, l+2, l+2\rangle
\end{aligned} \tag{A.23}$$

and the results from equation (A.6),

$$\begin{aligned}
\widehat{\mathcal{H}}_l |l-1, l, l\rangle &= \frac{1}{2} \left[\alpha_1 + \frac{2S\alpha_2}{4S-1} \right] |l-1, l, l\rangle - \frac{\sqrt{S(2S-1)}}{4S-1} \alpha_2 |l-1, l, l+1\rangle \\
&\quad - \frac{1}{2} \left[\alpha_1 - \frac{2S\alpha_2}{4S-1} \right] |l-1, l+1, l+1\rangle
\end{aligned} \tag{A.24}$$

the total effect of the full Hamiltonian on a state of the form $|i-1, i, i\rangle$ is

$$\begin{aligned}
\widehat{\mathcal{H}}|i-1, i, i\rangle = & -\frac{\alpha_1(S)}{2}|i-2, i, i\rangle - \\
& \frac{\sqrt{3S(S-1)}}{2} \left[\frac{\alpha_1(S)}{4S-3} + \frac{\alpha_2(S)}{4S-1} - \frac{\alpha_3(S)}{4S-3} \right] |i-1, i-1, i-1\rangle \\
& -\frac{1}{2} \left[\frac{S\alpha_1(S)}{4S-3} + \frac{(1-S)\alpha_2(S)}{4S-1} - \frac{3(1-S)\alpha_3(S)}{4S-3} \right] |i-1, i-1, i\rangle + \\
& \frac{\sqrt{3S(S-1)}}{2} \left[\frac{\alpha_1(S)}{4S-3} - \frac{\alpha_2(S)}{4S-1} - \frac{\alpha_3(S)}{4S-3} \right] |i, i, i\rangle - \\
& \frac{\sqrt{S(2S-1)}}{4S-1} \alpha_2(S) |i-1, i, i+1\rangle - \frac{1}{2} \left[\alpha_1(S) - \frac{2S\alpha_2(S)}{4S-1} \right] |i-1, i+1, i+1\rangle \\
& + \frac{1}{2} \left[\frac{3(3S-2)\alpha_1(S)}{4S-3} + \frac{(3S-1)\alpha_2(S)}{4S-1} - \frac{3(1-S)\alpha_3(S)}{4S-3} \right] |i-1, i, i\rangle \quad (\text{A.25})
\end{aligned}$$

Similarly, (A.3) also gives

$$\begin{aligned}
\widehat{\mathcal{H}}_l|i, i, i+1\rangle & = 0, \quad i \neq l-1, l, l+1 \\
\widehat{\mathcal{H}}_l|l-1, l-1, l\rangle & = \frac{\alpha_1}{2}|l-1, l-1, l\rangle - \frac{\alpha_1}{2}|l-1, l-1, l+1\rangle \quad (\text{A.26})
\end{aligned}$$

while (A.6) gives

$$\begin{aligned}
\widehat{\mathcal{H}}_l = & \frac{1}{2} \left[\alpha_1 + \frac{2S\alpha_2}{4S-1} \right] |l+1, l+1, l+2\rangle - \frac{\sqrt{S(2S-1)}}{4S-1} \alpha_2 |l, l+1, l+2\rangle \\
& - \frac{1}{2} \left[\alpha_1 - \frac{2S\alpha_2}{4S-1} \right] |l, l, l+2\rangle \quad (\text{A.27})
\end{aligned}$$

and from (A.18)

$$\begin{aligned}
\widehat{\mathcal{H}}_l|l, l, l+1\rangle = & \frac{1}{2} \left[\frac{S\alpha_1}{4S-3} + \frac{(S-1)\alpha_2}{4S-1} + \frac{3(S-1)\alpha_3}{4S-3} \right] |l, l, l+1\rangle + \\
& \frac{\sqrt{3S(S-1)}}{2} \left[\frac{\alpha_1}{4S-3} - \frac{\alpha_2}{4S-1} - \frac{\alpha_3}{4S-3} \right] |l, l, l\rangle - \frac{1}{2} \left[\frac{S\alpha_1}{4S-3} - \frac{(S-1)\alpha_2}{4S-1} + \frac{3(S-1)\alpha_3}{4S-3} \right] |l, l+1, l+1\rangle \\
& - \frac{\sqrt{3S(S-1)}}{2} \left[\frac{\alpha_1}{4S-3} + \frac{\alpha_2}{4S-1} - \frac{\alpha_3}{4S-3} \right] |l+1, l+1, l+1\rangle \quad (\text{A.28})
\end{aligned}$$

These result in

$$\begin{aligned}
\widehat{\mathcal{H}}|i, i, i+1\rangle &= -\frac{\alpha_1(S)}{2}|i, i, i+2\rangle - \\
&\frac{\sqrt{3S(S-1)}}{2} \left[\frac{\alpha_1(S)}{4S-3} + \frac{\alpha_2(S)}{4S-1} - \frac{\alpha_3(S)}{4S-3} \right] |i, i+1, i+1\rangle \\
&-\frac{1}{2} \left[\frac{S\alpha_1(S)}{4S-3} + \frac{(1-S)\alpha_2(S)}{4S-1} - \frac{3(1-S)\alpha_3(S)}{4S-3} \right] |i, i+1, i+1\rangle + \\
&\frac{\sqrt{3S(S-1)}}{2} \left[\frac{\alpha_1(S)}{4S-3} - \frac{\alpha_2(S)}{4S-1} - \frac{\alpha_3(S)}{4S-3} \right] |i, i, i\rangle - \\
&\frac{\sqrt{S(2S-1)}}{4S-1} \alpha_2(S) |i-1, i, i+1\rangle - \frac{1}{2} \left[\alpha_1(S) - \frac{2S\alpha_2(S)}{4S-1} \right] |i-1, i-1, i+1\rangle \\
&+\frac{1}{2} \left[\frac{3(3S-2)\alpha_1(S)}{4S-3} + \frac{(3S-1)\alpha_2(S)}{4S-1} - \frac{3(1-S)\alpha_3(S)}{4S-3} \right] |i, i, i+1\rangle \quad (\text{A.29})
\end{aligned}$$

Continuing this process,

$$\widehat{\mathcal{H}}_l |i, i, i\rangle = 0, \quad i \neq l, l+1 \quad (\text{A.30})$$

From (A.3). There is no relevant equations from (A.6), but (A.18) gives

$$\begin{aligned}
\widehat{\mathcal{H}}_l |l+1, l+1, l+1\rangle &= \\
&-\frac{3}{2}S(S-1) \left[\frac{\alpha_1}{S(4S-3)} + \frac{\alpha_2}{(4S-1)(S-1)} + \frac{\alpha_3}{3(S-1)(4S-3)} \right] |l+1, l+1, l+1\rangle \\
&-\frac{\sqrt{3S(S-1)}}{2} \left[\frac{\alpha_1}{4S-3} + \frac{\alpha_2}{4S-1} - \frac{\alpha_3}{4S-3} \right] |l, l, l+1\rangle + \\
&\frac{\sqrt{3S(S-1)}}{2} \left[\frac{\alpha_1}{4S-3} - \frac{\alpha_2}{4S-1} - \frac{\alpha_3}{4S-3} \right] |l, l+1, l+1\rangle - \\
&\frac{3}{2}S(S-1) \left[\frac{\alpha_1}{S(4S-3)} - \frac{\alpha_2}{(4S-1)(S-1)} + \frac{\alpha_3}{3(S-1)(4S-3)} \right] |l, l, l\rangle
\end{aligned} \quad (\text{A.31})$$

$$\begin{aligned}
\widehat{\mathcal{H}}_l |l, l, l\rangle &= \frac{3}{2}S(S-1) \left[\frac{\alpha_1}{S(4S-3)} + \frac{\alpha_2}{(4S-1)(S-1)} + \frac{\alpha_3}{3(S-1)(4S-3)} \right] |l, l, l\rangle \\
&+\frac{\sqrt{3S(S-1)}}{2} \left[\frac{\alpha_1}{4S-3} - \frac{\alpha_2}{4S-1} - \frac{\alpha_3}{4S-3} \right] |l, l, l+1\rangle - \\
&\frac{\sqrt{3S(S-1)}}{2} \left[\frac{\alpha_1}{4S-3} + \frac{\alpha_2}{4S-1} - \frac{\alpha_3}{4S-3} \right] |l, l+1, l+1\rangle \\
&\frac{3}{2}S(S-1) \left[\frac{\alpha_1}{S(4S-3)} + \frac{\alpha_2}{(4S-1)(S-1)} + \frac{\alpha_3}{3(S-1)(4S-3)} \right] |l+1, l+1, l+1\rangle
\end{aligned} \quad (\text{A.32})$$

so that

$$\begin{aligned}
\widehat{\mathcal{H}}|i, i, i\rangle = & \\
& 3S(S-1) \left[\frac{\alpha_1(S)}{2(4S-3)} + \frac{\alpha_2(S)}{S(S-1)(4S-1)} + \frac{\alpha_3(S)}{3(S-1)(4S-3)} \right] |i, i, i\rangle - \\
& \frac{3}{2}S(S-1) \left[\frac{\alpha_1(S)}{S(4S-3)} - \frac{\alpha_2(S)}{(S-1)(4S-1)} + \frac{\alpha_3(S)}{3(S-1)(4S-3)} \right] |i-1, i-1, i-1\rangle \\
& - \frac{3}{2}S(S-1) \left[\frac{\alpha_1(S)}{S(4S-3)} - \frac{\alpha_2(S)}{(S-1)(4S-1)} + \frac{\alpha_3(S)}{3(S-1)(4S-3)} \right] |i+1, i+1, i+1\rangle \\
& + \frac{\sqrt{3S(S-1)}}{2} \left[\frac{\alpha_1(S)}{4S-3} - \frac{\alpha_2(S)}{4S-1} - \frac{\alpha_3(S)}{4S-3} \right] (|i-1, i, i\rangle + |i, i, i+1\rangle - \\
& |i-1, i-1, i\rangle - |i, i+1, i+1\rangle) \tag{A.33}
\end{aligned}$$

These final set of equations that specify the effect of the total Hamiltonian on the complete set of orthonormal states are (A.5), (A.10), (A.11), (A.15)–(A.17), (A.25), (A.29) and (A.33).

Bibliography

- [1] W. Heisenberg, *Z. Phys.* 49, 619 (1928).
- [2] S. V. Tyablikov, *Methods in Quantum Theory of Magnetism*, Plenum Press, N.Y., 1967.
- [3] J. B. Torrance Jr. and M. Tinkham, *Phys. Rev. Series 2* 187, 587 (1969).
- [4] R. Hoogerbeets, A. J. van Duynveldt, A. C. Phaff, C. H. W. Swüste and W. J. M. de Jonge, *J. Phys. C* 17, 2595 (1987).
- [5] D. N. Haines and J. E. Drumheller, *Phys. Rev. Lett.* 58, 2702 (1987).
- [6] P. A. M. Dirac, *Proc. Roy. Soc.* 112A, 661 (1929).
- [7] H. A. Bethe, *Z. Phys.* 71, 205 (1931).
- [8] J. B. Parkinson, *J. Phys. C* 21, 3793 (1988).
- [9] M. T. Batchelor, M. N. Barber, *J. Phys. A* 23, L15 (1990).
- [10] L. A. Takhtajan, *Phys. Lett.* 87A, 479 (1982).
- [11] H. M. Babujian, *Phys. Lett.* 90A, 479 (1982).
- [12] F. D. M. Haldane, *J. Phys. C* 15, L831 (1982)
- [13] F. D. M. Haldane, *J. Phys. C* 15, L1309 (1982)
- [14] B. W. Southern, T. S. Liu and D. A. Lavis, *Phys. Rev. B* 39, 12 160 (1989).

- [15] B. Sutherland, Phys. Rev. B 12, 3795 (1975).
- [16] R. Haydock, *The Recursive Solution of the Schrödinger Equation*, Solid State Physics Vol. 35, Academic Press, Inc., 1980.
- [17] C. K. Majumdar, Phys Rev. B 1, 287 (1970).
- [18] C. K. Majumdar, J. Math. Phys. 13, 705 (1972).
- [19] S. K. Mukhopadhyay and C. K. Majumdar, J. Math. Phys. 17, 478 (1976).
- [20] J. E. Van Himbergen, Physica 86A, 93 (1977).
- [21] L. D. Faddeev, JETP 12, 1014 (1961).
- [22] Peter J. Millet and Harvey Kaplan, Phys. Rev. B 10, 3923 (1974).
- [23] Robert M. White, *Quantum Theory of Magnetism*, McGraw Hill Inc., 1970.
- [24] E. N. Economou, *Green's Functions in Quantum Physics, Second Edition*, Springer-Verlag, 1979, 1983.
- [25] C. H. Hodges, Le Journal De Physique - Lettres 38, L187 (1977).
- [26] A. Magnus, *Recurrence Coefficients for Orthogonal Polynomials on Connected and Non-connected Sets*, Padé Approximation and Its Applications; Proceedings, Antwerp 1979, Lecture Notes in Mathematics 765, Springer-Verlag (1979).
- [27] J. Nuttall and S. R. Singh, J. Approx. Theory 21, 1 (1977).
- [28] M. Toda, *Theory of Non-Linear Lattices*, Springer Series in Solid-State Sciences 20, Springer-Verlag (1981).
- [29] P. Turchi, F. Ducastelle, and G. Tréglia, J. Phys. C 15, 2891 (1982).
- [30] A. V. Chubukov and D. V. Khveschenko, J. Phys. C 20, L505 (1987).